

THESIS

ESTIMATING EMISSION RATES OF VOLATILE ORGANIC COMPOUNDS
FROM OIL AND NATURAL GAS OPERATIONS IN THE PICEANCE BASIN

Submitted by

Landan Patrick MacDonald

Department of Atmospheric Science

In partial fulfillment of the requirements

For the Degree of Master of Science

Colorado State University

Fort Collins, Colorado

Fall 2015

Master's Committee:

Advisor: Jeffrey R. Pierce

Co-Advisor: Jeffrey L. Collett Jr.

Jay M. Ham

Copyright by Landan Patrick MacDonald 2015

All Rights Reserved

ABSTRACT

ESTIMATING EMISSION RATES OF VOLATILE ORGANIC COMPOUNDS FROM OIL AND NATURAL GAS OPERATIONS IN THE PICEANCE BASIN

Oil and natural gas production has been steadily increasing in Colorado for the past 10 years. Garfield County is partially located above the natural gas rich Piceance Basin. Horizontal drilling techniques provide increased access to subsurface gas deposits while hydraulic fracturing is employed to increase the permeability of the tight gas formations by pumping pressurized fluids into the ground to allow more cost-effective oil and gas extraction. Once fractured, the fluid is allowed to flow back to the surface to be captured before the well is considered producing.

Our team conducted field measurements from 2013 to 2015 in Garfield County to determine emission rates of methane, hazardous air pollutants, and ozone precursors at 18 oil and gas operations. Drilling and well completion operations were targeted because they are understudied relative to production. We estimate the emission rates of methane and 58 additional VOCs (focusing on benzene, toluene, and ethane) for three common operations. We found benzene had mean emission rates of 0.72, 0.23, and 0.055 g s^{-1} for drilling, hydraulic fracturing, and flowback operations respectively. We calculated mean methane emission rates of 6.2, 29, and 64 g s^{-1} for drilling, hydraulic fracturing, and flowback operations respectively. We use the estimated methane emission rates from drilling and well completion operations to compare to typical well lifetime emissions during a 30 year production phase and find that drilling and well completion operations may be contributing from 0.1 to 10% of total well pad emissions. These results are based on a limited sampling size (18 sites)

and limited overall measurement time (4.25 hours of total measurement time included in results). It is possible we did not perform measurements for long enough periods of time at enough sites. This study is beginning to fill the information gap by focusing on drilling and well completion operations.

AERMOD is an atmospheric dispersion model used for new source apportionment. We compared our measured concentration fields to AERMOD predicted concentration fields by replicating fieldwork locations and conditions. Meteorological conditions were taken from an on-site meteorological station for use in the dispersion model. Comparing to the measurements, we found there was a low log-mean bias (-0.007) with a large amount of scatter ($r = 0.0007$). Additionally, we use AERMOD and data from the NCEP North American Regional Reanalysis database to predict the distribution of concentrations experienced throughout for various meteorological conditions in Garfield County at various distances surrounding oil and gas wells. We normalized these predicted concentration fields by emission rate and created cumulative distribution functions.

ACKNOWLEDGEMENTS

The collection of field data was imperative for this thesis. Thanks to Arsineh Hecobian for organizing and coordinating all field measurements. Recognition also goes to the rest of the field work team: Andrea Clements, Kira Shonkwiler, Bradley Wells, Yury Desyaterik, Noel Hilliard, and Yong Zhou. The operation of the gas chromatography system was done by Yong Zhou, Andrea Clements, and Noel Hilliard. Thanks also to Jay Ham, the co-PI of the oil and gas project.

Working with the Pierce group provided continuous motivation for the past four years. Special thanks goes to my office-mate John (Jack) Kodros for the laughs. Thanks also goes to Bonne Ford, Stephen D'Andrea, Kimiko Sakamoto, Robin Stevens, William Lassman, and Anna Hodshire.

Finally, a very special acknowledgement goes to my advisers: Jeff Pierce and Jeff Collett. Their guidance and support throughout the past two years was a source of inspiration. Thank you so much Jeff ²!

TABLE OF CONTENTS

Abstract	ii
Acknowledgements	iv
List of Tables	viii
List of Figures	x
Chapter 1. Introduction	1
1.1. Motivation	1
1.2. Outline	8
Chapter 2. Oil and Natural Gas Extraction in Garfield County	10
2.1. Drilling	11
2.2. Hydraulic Fracturing	14
2.3. Flowback	17
2.4. Production	19
2.5. Combination Sites	19
Chapter 3. Methods	20
3.1. Tracer Ratio Method	20
3.2. Field Measurements	22
3.3. VOC analysis by Gas Chromatography	29
3.4. Emission Ratios	30
3.5. AERMOD	31
Chapter 4. Data Processing	38

4.1. Picarro Data.....	38
4.2. Canister Data.....	42
Chapter 5. Data Analysis Results.....	43
5.1. Methane Concentrations.....	43
5.2. Selected VOC Concentrations.....	44
5.3. Emissions Estimate: Methane.....	48
5.4. Emissions Estimates: VOCs.....	61
5.5. Emission Ratios.....	65
5.6. Analysis of Integrated Emissions over Process Lifetime.....	68
Chapter 6. Dispersion Modeling Results.....	70
6.1. Replication of Field Measurements.....	70
6.2. Dispersion Modeling Under Various Meteorological Conditions.....	72
6.3. Modeling of all Sites.....	75
Chapter 7. Conclusions.....	77
Chapter 8. Future Work.....	79
Bibliography.....	81
Appendix A. Fieldwork Sites.....	99
Appendix B. Information About VOCs.....	100
Appendix C. All VOC Emission Rates.....	103
Appendix D. Correlation Coefficient Cutoff.....	112
Appendix E. Comparing Picarro and Canister Acetylene.....	115

Appendix F. Atmospheric Stability Dependence.....	117
Appendix G. Comparison of Methane Emission Rate Distributions.....	119
Appendix H. Flowback Gaussian Fit.....	120

LIST OF TABLES

2.1	List of hydraulic fracturing fluid additives.....	15
3.1	Tracer Ratio Method bias summary.....	21
3.2	List of instruments on the meteorological station.....	25
3.3	List of instruments in the mobile plume tracker.....	26
3.4	List of canister triggering system components.....	29
3.5	AERMOD meteorological inputs.....	32
5.1	Emission rate distributions for methane.....	50
5.2	Emission rate distributions for methane during canister periods.....	61
5.3	Benzene emission rates distributions.....	63
5.4	Toluene emission rates distributions.....	64
5.5	Ethane emission rates distributions.....	65
5.6	Ethane emission ratio distributions.....	67
5.7	Benzene emission ratio distributions.....	67
5.8	Toluene emission ratio distributions.....	68
A.1	Fieldwork sites.....	99
B.1	List of alkanes analyzed by GC system.....	100
B.2	List of alkenes analyzed by GC system.....	101
B.3	List of aromatic compounds analyzed by GC system.....	102

G.1 Comparison of Methane Emission rate distributions..... 119

LIST OF FIGURES

1.1	Natural gas production by source in US	1
1.2	Map of oil and gas shale basins in the US	2
1.3	Number of active wells in Colorado as a function of time	3
1.4	Spatial density of active oil and gas wells in Colorado	4
2.1	Map of Piceance Basin	11
2.2	Sedimentary formations in Piceance Basin	12
2.3	Drilling schematic	13
2.4	Hydraulic fracturing schematic	16
2.5	Flowback schematic	18
2.6	Schematic of a vapor recovery unit	18
3.1	Fieldwork overview	22
3.2	Diagram of tracer release system	23
3.3	Manifold schematic	24
3.4	Diagram of mobile plume tracker	26
3.5	Picarro light intensity schematic	28
4.1	Acetylene time series with smoothing	39
4.2	Methane background correction	40
4.3	Acetylene mixing ratio PDF	42
5.1	Methane mixing ratio distributions by operation type	44

5.2	VOC mixing ratio distributions by operation type without background correction	45
5.3	VOC mixing ratio distributions by operation type with background correction....	48
5.4	Methane emission rate distributions by operation type	49
5.5	Methane emission rate of flowback sub-operations	51
5.6	Methane emission rate distributions for flowback operations separated by measurement day	52
5.7	Methane emission rate distributions for drilling operations separated by measurement day	53
5.8	Methane emission rate of hydraulic fracturing sub-operations	55
5.9	Methane emission rate distributions for hydraulic fracturing operations separated by measurement day	56
5.10	Comparison of methane emission rates to other studies	59
5.11	Methane emission rate distributions during canister sampling times	60
5.12	VOC emission rate distributions	62
5.13	Benzene, toluene emission rate 1:1 plot	64
5.14	VOC emission ratio distributions	66
5.15	Contribution of methane emissions from drilling and well completion	69
6.1	Comparison of measurements to AERMOD	71
6.2	Mixing ratio field predicted by AERMOD	73
6.3	Mixing ratio distributions predicted by AERMOD	74
6.4	Predicted concentration distributions normalized by emission rate	76

C.1	Alkane emission rate distributions during drilling	103
C.2	Alkane emission rate distributions during hydraulic fracturing	104
C.3	Alkane emission rate distributions during flowback	105
C.4	Alkene emission rate distributions during drilling	106
C.5	Alkene emission rate distributions during hydraulic fracturing	107
C.6	Alkene emission rate distributions during flowback	108
C.7	Aromatic emission rate distributions during drilling	109
C.8	Aromatic emission rate distributions during hydraulic fracturing	110
C.9	Aromatic emission rate distributions during flowback	111
D.1	Correlation coefficient cutoff	112
D.2	Emission rate distribution after correlation coefficient cutoff	113
E.1	Comparison of Picarro and canisters	116
F.1	Atmospheric stability dependence	117
H.1	Flowback emission rate distribution bimodal fit	120

CHAPTER 1

INTRODUCTION

1.1. MOTIVATION

Energy development is deeply rooted to the economic potential of society[1]. Americans use infrastructure that relies upon massive amounts of energy. Oil and natural gas resources were used to fulfill 53% of this requirement in 2014[2]. Figure 1.1 shows the sources of natural gas produced in the United States of America (US). The white line signifies the year this information was published (2013).

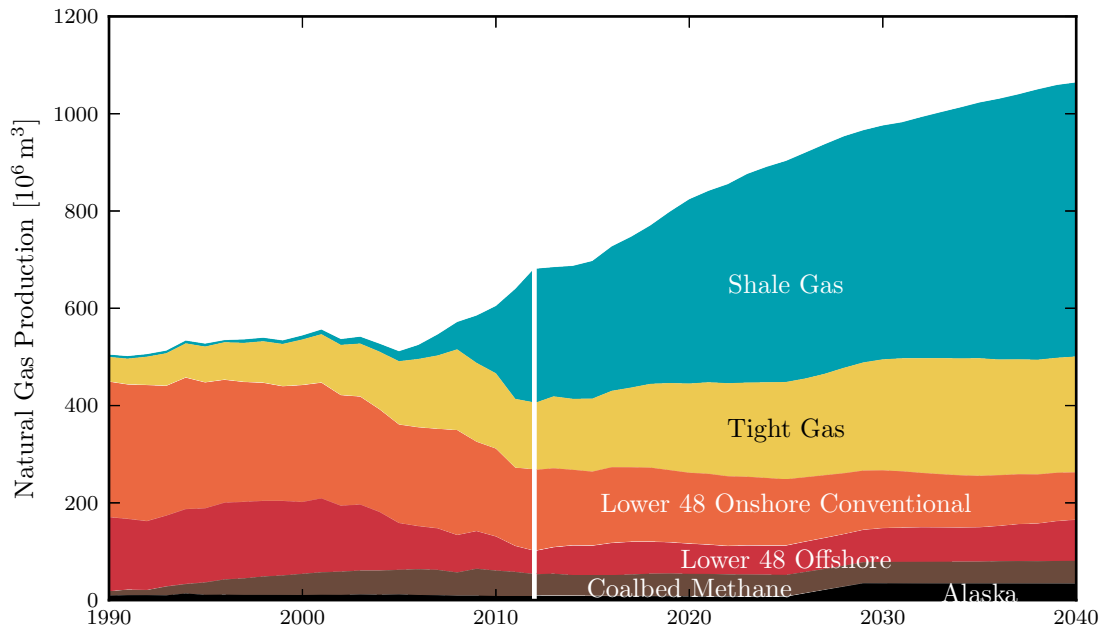


FIGURE 1.1. Natural gas production by source in the US. The white line separates historical record from future projections. This information was taken from the U.S. Energy Information Administration[3].

Since 2010, shale and tight gas combined have become the dominant source of new natural gas production in the US, overtaking conventional gas wells. Shale and tight gas formations

store gas in extremely low permeability sedimentary reservoirs. The decomposition of organic matter within the sedimentary formations produces methane[4] along with other alkanes, alkenes, and aromatics. This mixture is known as natural gas.

Unconventional oil and gas extraction is a term used to describe the extraction of petroleum products via directional drilling and hydraulic fracturing of the shale/tight gas formations[5]. This type of extraction has been increasing in popularity in the US as the number of untapped conventional oil and gas sites grows thin. Methods of unconventional oil and gas extraction were originally developed decades ago[6] but it is only recently that these extraction techniques were more widely implemented and became of concern to those living in communities near unconventional oil and gas sites. Figure 1.2 shows the oil and gas basins in the United States.

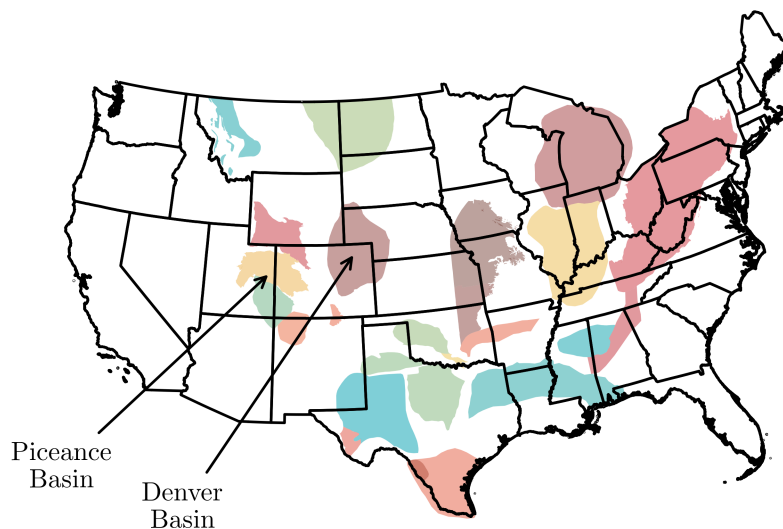


FIGURE 1.2. Map of oil and gas shale basins in the US. The Denver Basin is marked because many studies have examined the emissions from oil and gas operations in this region. The Piceance Basin is the location of the field study discussed in this thesis.

The map shows there are six different basins that are located within the administrative limits of the State of Colorado. Of note are the Piceance Basin (tight gas formation) located on the west of Colorado and the Denver Basin (shale gas formation) to the east. The data analysis of field measurements for this thesis was performed for the Piceance tight gas basin exclusively.

The oil and gas basins in Colorado are home to large increases in active wells since the turn of the 21st century. Figure 1.3 shows the number of active oil and gas wells in Colorado as a function of time. This plot was made using information from the Colorado Oil and Gas Conservation Commission (COGCC), which stores daily records of every oil and gas well in the State of Colorado.

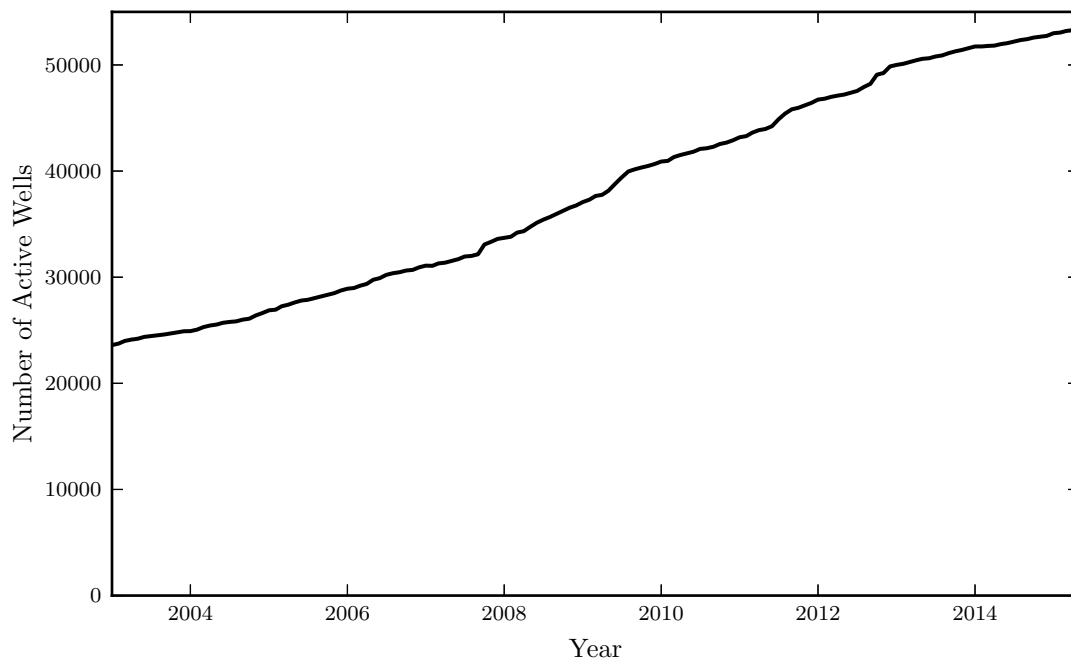


FIGURE 1.3. Number of active oil and gas wells in Colorado as a function of time. This information was provided by the Colorado Oil and Gas Conservation Commission (COGCC) obtained on 5/15/2015[7].

In 2002, there were approximately 22 000 active wells present in Colorado. As of May 4, 2015, this number increased to a total of 53 444 active wells[7]. This represents an average net increase of approximately 2700 wells per year. With tight/shale gas production expected to increase, the number of active wells in Colorado is expected to continue to rise over the long term, especially as commodity prices recover from current lows.

The spatial density of wells in Colorado is shown in Figure 1.4. A two dimensional spatial histogram was performed on this data using a bin size of 0.02° (~ 2 km) latitude and 0.04° (~ 4 km) longitude.

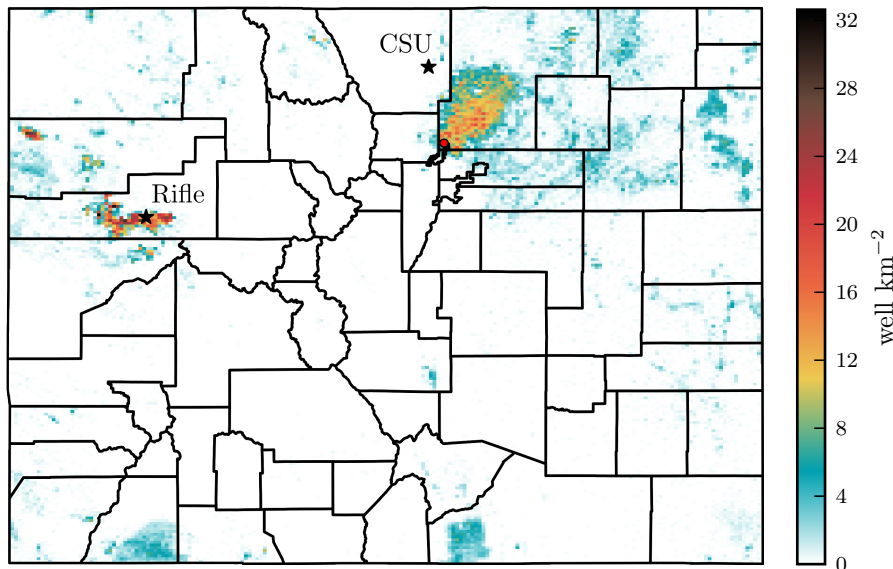


FIGURE 1.4. Spatial density of active oil and gas wells in Colorado using latitude and longitude bins of 0.02° and 0.04° respectively. Rifle, CO was home-base during fieldwork. The red-dot shows the location of the Boulder Atmospheric Observatory (BAO). This information was provided by the COGCC obtained on 5/15/2015[7].

The black star to the west in the Figure indicates the town of Rifle, Colorado located within Garfield County. This was home-base for field work operations. The black star to the east indicates the location of Colorado State University (CSU). To the east of CSU is an expansive oil and gas field located mostly within Weld County (part of the Denver Basin). As

of May 4, 2015, there were 22 411 active wells in Weld County with the majority of the wells in the production phase. In Garfield County, there were half the number of wells as Weld County in a quarter of the area (with the majority of the wells also in production phase). There have been extensive measurements campaigns in Weld County, many at the Boulder Atmospheric Observatory (BAO), a 300 m measurement tower, indicated on the map with a red dot. The results from these studies are compared to the results from this thesis for context.

It is predicted that the US will become a net exporter of oil and natural gas by the year 2019[2]. Unconventional extraction of oil and gas will become the primary means by which the US can supply this demand. The oil and gas industry has had positive effects on surrounding communities, specifically the work-force employed by this industry. Weber et al. (2012) showed that total employment as well as wage and salary income in Colorado boom-counties (such as Weld and Garfield) have seen increases relative to non-boom counties[8]. The potential negative effects from this extraction technique must also be quantified, including any adverse impacts on air quality.

Methane (CH_4) emissions are cause for concern in the US. Methane is a highly potent greenhouse gas (GHG), which just like carbon dioxide (CO_2), contributes to the gradual warming of Earth's atmosphere; methane is a factor of 28 more potent than CO_2 as a GHG over a 100 year time-scale[9]. Although natural gas is hailed as a cleaner alternative to traditional fossil fuels, if enough methane leaks into the atmosphere the potential benefits of this fuel can be offset. Alvarez et al. (2012) determined if cumulative methane leak rates remained *below* 3.2%, natural gas offers climate *benefits* compared to coal-fired power plants for all timeframes[10].

Larsen et al. (2015) found that about 1.3% of the total natural gas produced in the US leaks into the atmosphere[11]. Mitchell et al. (2015) measured leak rates of less than 1% for 114 gathering and production facilities[12]. Allen et al. (2013) estimated that 0.42% of methane leaked during completion and production phases of oil and gas wells[13], slightly less than Environmental Protection Agency's (EPA) estimate of 0.47%[14]. Pétron et al. (2012) reported that there was an overall 2.3 to 7.7% leakage rate of methane from the Denver Basin[15]. Other studies have quantified the mixing ratios of methane surrounding oil and gas operations. While not actually quantifying leak rates, Phillips et al. (2013) mapped urban natural gas pipeline leaks in Boston, MA and found mixing ratios that spanned from background (2.07 ppmv) to 28.6 ppmv suggesting a wide range of pipeline leak rates[16]. Many of the reported methane leak rates did not include measurements of well drilling and completion operations. One part of this thesis aims to quantify methane emission rates from oil and gas sites in Garfield County during these understudied processes. Emission rates provide information that is independent of meteorological conditions and distance from the source, which are used to estimate total emissions as well as predicted downwind concentrations under any meteorological condition.

Oil and gas sites have also been shown to emit a wide variety of non-methane-volatile organic compounds (NM-VOCs). Benzene emissions have been of particular concern because of its importance as an air toxic. Exposure to Hazardous Air Pollutants (HAPs), such as benzene, can cause acute health issues in most living organisms. The emission of benzene can have direct and indirect effects on humans and ecosystems. Benzene is a known carcinogen[17], can cause birth defects, and can affect respiratory function[18]. Benzene mixing ratios have been measured to be up to 10 ppbv when sampling from a few hundred

feet away from oil and gas sites in Garfield County[19]. Esswein et al. (2014) showed that oil and gas workers are at risk of being exposed to high concentrations of benzene that exceed many occupational exposure limits[20]. Swarthout et al. (2013) measured mixing ratios of benzene at BAO ranging from 39 to 869 pptv that were attributed to oil and gas wells in the Denver Basin[21]. Gilman et al. (2013) also measured benzene mixing ratios downwind of the Denver Basin at BAO and recorded a mean concentration of 290 pptv, of which the oil and natural gas industry contributed 32% using a multivariate regression analysis that assumed VOC concentrations can be described by a function of the concentrations of propane and ethyne[22]. Warneke et al. (2014) used a proton transfer reaction mass spectrometer (PTR-MS) to measure time series of benzene concentrations in the Uinta Basin, Utah. This study observed benzene mixing ratios over 10 ppbv for extended periods of time[23]. Finally, McKenzie et al. (2013) collected 24 samples within a few hundred feet of four well completion operations in Garfield County and found a median mixing ratio of about 1 ppbv of benzene. These measurements were used to assess health impacts for a 30 year well lifetime[19].

Ozone (O_3) is a pollutant that is regulated by the EPA[24] and repeated exposure to it can have adverse health effects for humans and biota. A review published by the EPA indicated acute exposures to high ozone levels can cause inflammation, lung morphology changes, coughing, breathing discomfort, throat irritation, and wheezing on humans[25]. Oil and gas extraction and production activities can emit VOCs and nitrogen oxide species (NO_x) which can react to form ozone. These chemical species are therefore known as ozone precursors. Schnell et al. (2009) discovered that ozone formation is not strictly associated with summertime events. Ozone mixing ratios were found to be over 100 ppbv for several time periods in Upper Green River Basin (UGRB) of Wyoming. These mixing ratios were

attributed to wintertime inversions forming at night and trapping ozone precursors. The solar flux during the following day caused the formation of ozone[26]. Field et al. (2015) also found that ozone mixing ratios were at or above the 75 ppbv EPA 8-hour NAAQS during several occurrences in the UGRB. Positive Matrix Factorization (PMF) analysis revealed that combustion from traffic, fugitive natural gas, and fugitive condensate were important factors that lead to the high ozone periods[27]. Edwards et al. (2013) measured mixing ratios of ozone well above the NAAQS in the Uintah Basin, Utah for several days. These high concentrations were attributed directly to the oil and gas operations in that region where wintertime inversions trapped the pollutants[28]. Gilman et al. (2013) reported that oil and gas operations in Northeastern Colorado produce significant amounts ozone precursors[22]. As of July 20, 2012 the Denver Metropolitan Area and the Northern Front Range were classified as a “marginal” nonattainment area by the EPA[29].

1.2. OUTLINE

This thesis is part of a field study that has quantified the emission rates of many VOCs during various stages of well drilling and completion. We used sophisticated instruments to quantify concentrations of VOCs and performed a tracer ratio method technique to estimate their emission rates. The measured concentrations provide information of instantaneous health and environmental risks. One goal of this thesis is to quantify the emission rates of VOCs from various completion activities. Emission rates have benefits over concentration data because they are independent of meteorological conditions and distance from the source. As such, they can be a more useful quantity for emission inventories and dispersion modeling. There are no other scientific studies that have measured emission rates of VOCs from all

drilling and completion stages of unconventional oil and gas wells. We calculated Probability Distribution Functions (PDFs) for VOC emission rates separated by operation type.

We used the emission rate distributions as inputs in dispersion models to predict concentration fields downwind of the oil and gas sites. Using information about emissions from a particular stage of new well development, downwind concentration fields of VOCs were predicted under various meteorological conditions and compared to observations for field study measurement periods.

The following Chapter gives a detailed description on oil and gas operations in Garfield County. Chapter 3 outlines the methods used to determine emission rates from field data as well as a description of the dispersion model. Chapter 4 describes the data analysis performed. Chapters 5 and 6 present the results of the field measurements and the model predicted concentrations respectively. Finally, Chapter 7 summarizes the findings and Chapter 8 discusses future work.

CHAPTER 2

OIL AND NATURAL GAS EXTRACTION IN GARFIELD COUNTY

Funding from Garfield County and several industry partners was provided to CSU to investigate emission rates of air toxics, ozone precursors, and methane from new gas well development in Garfield County. We present the results from a total of 18 experiments focusing primarily on three different operation types: drilling, hydraulic fracturing, and flowback. The emissions from these well drilling and completion operations were studied as they have received little prior attention despite drawing considerable public interest.

The drilling and completion of each new unconventional oil and gas well requires several steps which are outlined below. New well completion techniques can vary between basin, operator, and subcontractor. This field study examined the emissions under a suite of different conditions to obtain a representative distribution of these sources. I will now provide a detailed overview of each of these operations.

2.1. DRILLING

Garfield County is situated above the natural gas rich Piceance Basin where natural gas is trapped within shale/tight gas sedimentary formations below the surface. Figure 2.1 shows the Piceance Basin (in red) straddling Utah and Colorado with the outline of Garfield county plotted over the formation.

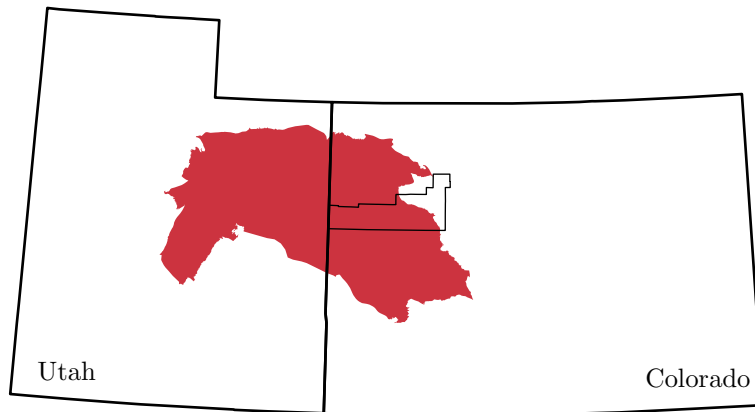


FIGURE 2.1. Map of the Piceance Basin. This basin straddles Colorado and Utah. The County of Garfield is also plotted over the basin to show the location of fieldwork.

In Colorado, the natural-gas rich sedimentary formations of the Piceance basin are located several kilometers beneath the surface. Figure 2.2 shows a vertical cross section of the Piceance Basin indicating some of the different sedimentary formations (adapted from the United States Geological Survey (USGS)[30]). The Williams Fork formation colored in orange is of specific interest to the oil and gas industry. This formation is part of the Mesaverde tight gas sands which are estimated to contain over 8 trillion cubic meters of natural gas[31].

The presence of hydrocarbons in the Piceance basin has been known for several decades. On September 10, 1969, Project Rulison began with the detonation of a 40 kiloton nuclear

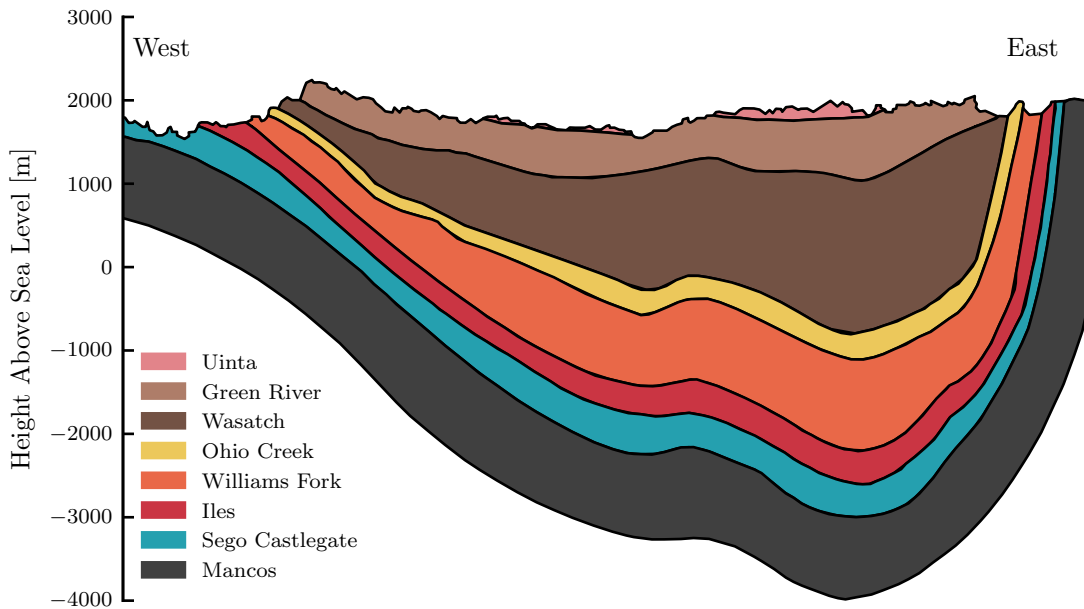


FIGURE 2.2. A schematic of the sedimentary layers within the Piceance Basin. The Williams Fork formation (orange) is a tight gas formation that is fractured to extract natural gas. This Figure was adapted from the USGS[30].

explosive 1500 m below the surface. The goal was to create a large cavity for the hydrocarbons to be easily extracted[32]. This project was a failure but nearly 40 years later with more advanced technology natural gas is extracted from this region on a regular basis. When a new well location has received a permit from the COGCC, well pads ranging from 4000 to 97 000 m² in size are prepared[33] where all machinery associated with the well drilling and completion is stored. Vertical drilling begins by using a rotating pipe with a drill bit on the end. As the pipe is forced deeper in the ground, more drill-pipe is added in 30 ft increments[34]. Drilling mud is transported to the surface on the outside of the drill pipe – this fluid is a combination of the drill cuttings and the fluid pumped down the boreholes to facilitate drilling and keeping the drill bit cool and clean. The borehole has many casing

layers to prevent leakage of oil and gas substances in the adjacent aquifers as shown in Figure 2.3[35].

Horizontal drilling is then performed within the target sedimentary formation to locate and maximize access to the natural gas. Figure 2.3 includes a simple schematic of the horizontal drilling. In this Figure, the rig has drilled into a tight gas formation (indicated by the gray region of the underground layer). The natural gas is stored within sandstone lenses that must be located during the drilling phase, which range in vertical thickness from 0.5 to 29 ft and width from 40 to 2790 ft[34].

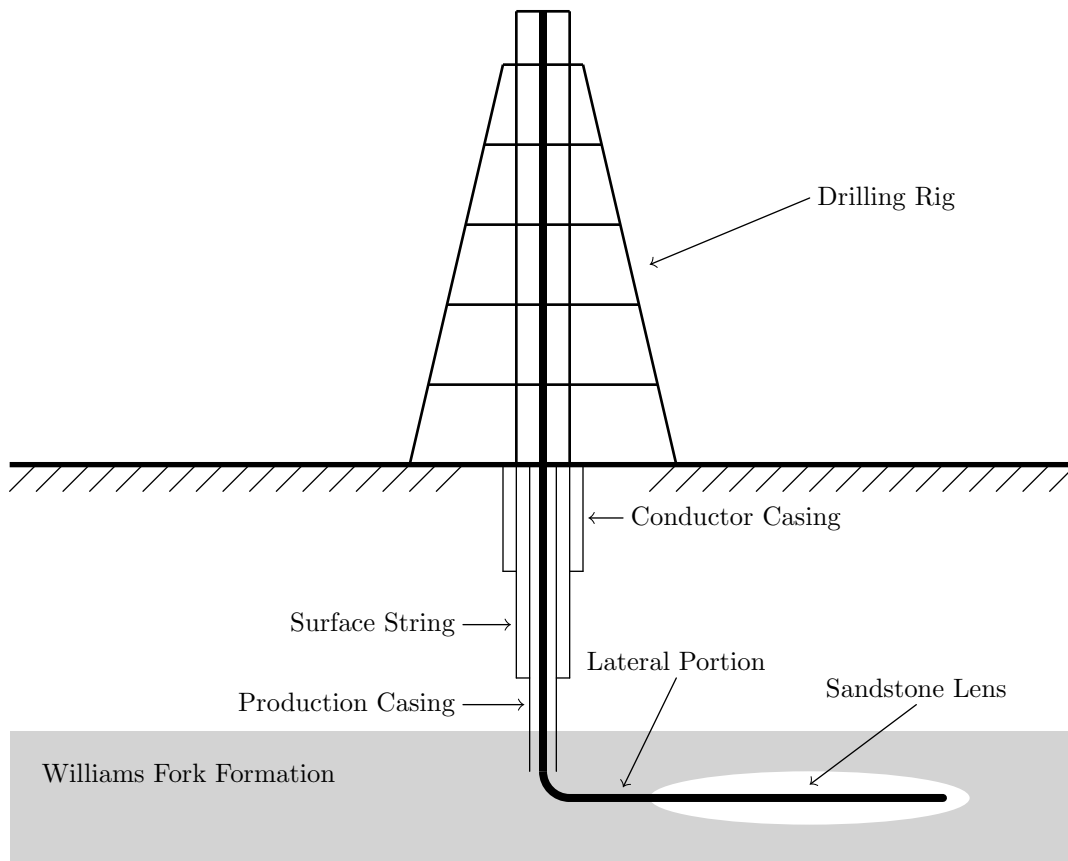


FIGURE 2.3. Schematic of a drilling operation for tight gas formations in Garfield County. The rig drills vertically into the Williams Fork formation while inserting protective casings. Horizontal drilling is then performed in the lateral section while locating sandstone lenses.

Drilling into tight gas formations can release natural gas that is trapped within the sedimentary material especially when a pocket of high pressure gas is encountered. Drilling into the Earth’s surface is an energy intensive process that is powered by large generators located on the well pad. These generators emit exhaust from the combustion of fossil fuels. For the sites measured in Garfield County, drilling can span 2 to 7 days per well. Additionally, recovered drilling mud, which is processed and stored on the pad, may contain hydrocarbons which are emitted to the atmosphere during its processing, transportation, and storage phases.

2.2. HYDRAULIC FRACTURING

Drilling provides a means to access the tight gas formation. Once drilling is completed, gas can escape the formation at a very low rate. Because of this, the formation must be fractured in order to release the trapped natural gas more effectively. Hydraulic fracturing is an advanced engineering process that uses a specialized fluid mixture to create fissures in the formation[5]. The increased permeability of the rock allows for gases trapped inside to be collected[28]. Computer simulations are performed in advance to maximize the effectiveness of each hydraulic fracturing phase. These simulations can help prevent the fractures from propagating into another formation which would waste resources and cause natural gas to escape[36].

Once seismic testing and computer simulation has been performed, fractures are initialized using small explosive devices detonated in precise regions. This process is referred to as “perforation”[37]. Next, fluid is pumped into the cavity at extremely high pressures, a process known as hydraulic fracturing or “fracking”. Hydraulic fracturing is the process of fracturing rock by use of pressurized fluid. The hydraulic fracturing fluid that is pumped

down consists of mostly water and sand. The sand is referred to as the proppant. The rest of the composition varies between operator and subcontractor. It is generally thought that the remaining fraction of the fracking fluid consists of the substances given in Table 2.1[38].

TABLE 2.1. List hydraulic fracturing fluid compounds. Adapted from the U.S. Department of Energy [38].

Additive Type	Main Compound(s)	Purpose
(15%)Acid Diluted	Hydrochloric acid or muriatic acid	Help dissolve minerals and initiate cracks in the rock
Biocide	Glutaraldehyde	Eliminates bacteria in the water that produce corrosive byproducts
Breaker	Ammonium persulfate	Allows a delayed break down of the gel polymer chains
Corrosive Inhibitor	N,n-dimethyl formamide	Prevents the corrosion of the pipe
Crosslinker	Borate salts	Maintains fluid viscosity as temperature increases
Friction Reducer	Polyacrylamide	Minimized friction between the fluid and the pipe
	Mineral oil	
Gel	Guar gum or hydroxyethyl cellulose	Thickens the water in order to suspend the sand
Iron Control	Citric acid	Prevents precipitation of metal oxides
KCl	Potassium chloride	Creates a brine carrier fluid
Oxygen scavenger	Ammonium bisulfite	Removes oxygen from the water to protect the pipe from corrosion
pH Adjusting Agent	Sodium or potassium carbonate	Maintains the effectiveness of other components, such as crosslinkers
Scale Inhibitor	Ethylene glycol	Prevents scale deposits in the pipe
Surfactant	Isopropanol	Used to increase the viscosity of the fracture fluid

The pressure created by the fluids injected into the tight gas formation opens the fractures further. The proppant is forced into these cracks and allows them to remain open after the

pressure of the fluid has been reduced to increase the flow of oil or natural gas to the well bore. This process is shown in Figure 2.4.

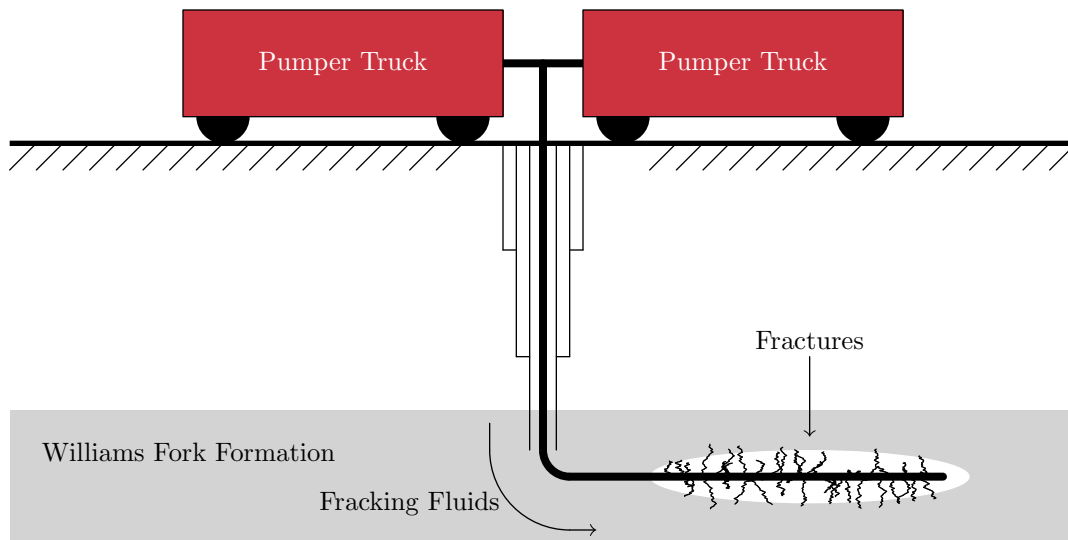


FIGURE 2.4. Schematic of a hydraulic fracturing operation in Garfield County. The lateral portion of the well is perforated using small explosives. Pumper trucks then force fluids into the well to fracture the formation.

The lateral portion of the well is fracked in several stages. This reduces the pressures required to fracture the formation (the pressure required to frack the entire lateral portion of the well at once would be much higher)[39]. The fracturing stages begin at the far end of the borehole and move sequentially uphole until the entire lateral section has been fractured, as each section of the well is fractured, it is capped with a specialized plug awaiting the next phase of the operation[38].

The pressure at which the fracturing fluid must be injected is greater than 69 000 kPa and therefore a large energy source is required to achieve these pressures[34]. Many of the oil and gas sites in Garfield County were in remote locations with little access to power grids. Specially designed diesel and diesel/natural gas hybrid generators are transported to the well

pad to provide the required power therefore there are emissions from these generators during the hydraulic fracturing process. In Garfield County, hydraulic fracturing occurs over two to six days per well.

2.3. FLOWBACK

Once the shale formation has been adequately fractured, the injected fluids are allowed to flow back to the surface for collection[40]. Since portions of the well have been fracked separately and sealed, the seals must be broken by re-drilling into the well. This process of breaking the seals is known as “popping”. Once each seal has been popped, the fluids are allowed to return to the surface. The injected sand props each crack open and allows the natural gas to escape and be collected at the surface during the production phase of the well.

The fluids that return to the surface are hot and have increased concentration of dissolved salts, and organic compounds [40, 41], which could volatilize when returning to the surface. Figure 2.5 shows a schematic of a flowback operation.

The flowback process can take 2 hours – 2 days to complete per well in Garfield County, Colorado. During this flowback period, natural gas begins to flow to the surface and is collected and separated from the flowback fluids with a vapor recovery unit shown in Figure 2.6. This phase introduces potential fugitive emission sources such as valves, flanges, gauges, pipe connectors, compressors and pumps.

The fracturing fluid that returns to the surface is stored in large tanks or lined pits in Colorado. The compounds used in the fracturing fluid will partition into the gas phase and have the potential to escape. Flowback tanks are periodically opened to perform routine maintenance checks. For example, workers must gauge the level of fluid within the tanks. During this process, the tanks are open to the atmosphere allowing volatile species

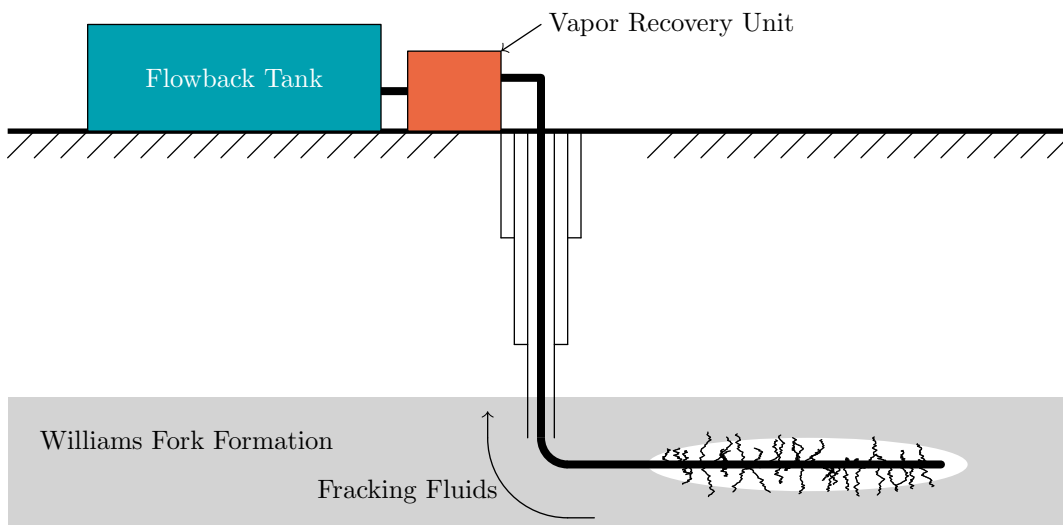


FIGURE 2.5. Schematic of a flowback operation in Garfield County. The pressure is reduced and the fluid flows back to the surface. The vapor recovery unit (Figure 2.6) will separate the fluids and send the gas to production facilities.

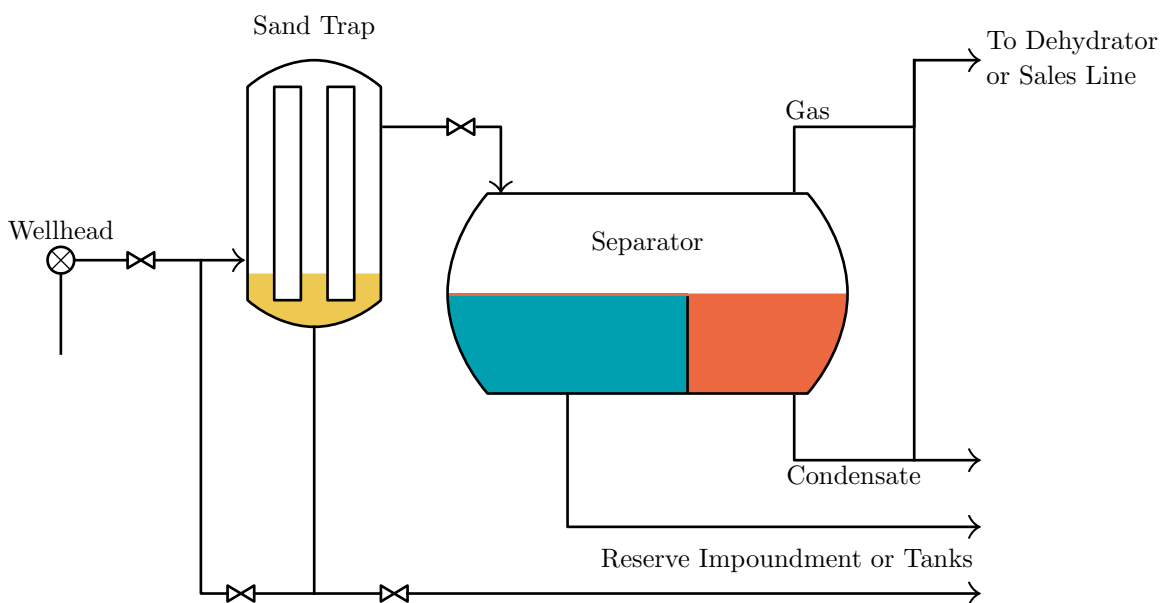


FIGURE 2.6. Schematic of a vapor recovery unit. Adapted from the EPA [42].

to escape[20]. These tanks also have pressure release valves that are tripped if the pressure within the tank becomes too high.

2.4. PRODUCTION

Once natural gas is able to flow from the shale/tight gas formation to the surface, it is transported to separate facilities to remove water from the mixture. The gas is then transported to a production facility where it enters a production line. Producing wells can remain operational for decades and can be a long-term source of hydrocarbons into the atmosphere[34, 43]. There are potential emissions from every piece of equipment on the well pad during the production phase. Examples include emissions from: dehydrators, heaters, separator units, compressor units and fugitive emissions from leaks of flanges, valves, gauges, pipe connectors and pumps[44–46]

2.5. COMBINATION SITES

While performing experiments in Garfield County, some sites had multiple operations occurring simultaneously. During “simops” it is possible for a single well pad to have fracturing, flowback and drilling being performed. This was noted during experiments and these results were separated from sites with a single operation type.

CHAPTER 3

METHODS

3.1. TRACER RATIO METHOD

Our field study was designed to release a tracer gas on the well pad in order to use the tracer ratio method (TRM) for emissions quantification. The TRM estimates emission rates of unknown compounds using information of a tracer gas release and the concentrations of the tracer and the gases downwind. The use of this method can be found in many studies. Wells et al. (2015) used data from a test release of two gases to quantify the errors in the TRM[47]. Galle et al. (2001) and Mønster et al. (2014) used this method to estimate methane fluxes from landfills [48, 49], Guenther et al. (1996) for isoprene fluxes from a forested site[50], Kaharabata et al. (2000) for a feedlot [51], Kantamaneni et al. (1996) for PM₁₀ emissions from roadways[52], Lamb et al. (1995) for natural gas facilities[53], Lassey et al. (1997) for grazing livestock[54], Möllmann-Coers et al. (2002) for the entire city of Augsburg[55], Rumburg et al. (2008) for cow housing[56], and Scholtens et al. (2004) for livestock buildings and manure stores[57]. We used acetylene (also known as ethyne, C₂H₂) as our tracer gas during the field experiments. Acetylene was chosen because of its relatively long lifetime in the atmosphere of two weeks[58], its ease of detection at high time resolution and low concentration, and its absence as a major emission of oil and gas operations. The TRM is described mathematically using the following formula:

$$(3.1) \quad Q_{\text{VOC}} = Q_{\text{C}_2\text{H}_2} \cdot \frac{X_{\text{VOC}}}{X_{\text{C}_2\text{H}_2}}$$

where Q_{VOC} is the estimated emission rate of the desired species, $Q_{\text{C}_2\text{H}_2}$ is the known release rate of a tracer gas (acetylene), X_{VOC} and $X_{\text{C}_2\text{H}_2}$ are the concentrations of the tracer gas and the desired VOC, respectively. The concentrations can also be integrated over space and/or time depending on the type of analysis being performed. We used both the instantaneous and time integrated concentrations during data analysis. The basic assumptions of this method are as follows:

- The emission rate of the tracer is accurately known.
- The concentrations measured downwind are accurate.
- The two gaseous species disperse in a similar manner.
- The tracer is co-located with the unknown emission source.
- Neither the tracer nor the target VOC are altered by deposition or chemical reaction between the release and detection points.

The appeal of the TRM is that no knowledge of the local meteorology is required to estimate the emission rate of an unknown gas. Furthermore, TRM quantification is possible based on even a single ratio measured in space or time; a full plume does not need to be observed. The biases of this method have been estimated by the following publications given in Table 3.1.

TABLE 3.1. Tracer ratio method biases reported by various publications.

Publication	Bias [%]
Wells et al. (2015) [47]	+17
Mønster et al. (2014) [49]	< ±5
Scholtens et al. (2004) [57]	-25 to +43
Galle et al. (2001) [48]	±15 to ±30
Kaharabata et al. (2000) [51]	±30
Lamb et al. (1995) [53]	±15

Because this study had industry partners, our fieldwork team was permitted to emit the tracer gas on the well pad as close to the activity of interest as possible. This unique opportunity allowed us to accurately measure emission rates of VOCs using this well characterized method.

3.2. FIELD MEASUREMENTS

Our team studied oil and gas sites in Garfield County, Colorado in 2013-2015. The goal of quantifying emission rates of VOCs required the use of many specialized pieces of equipment. The experimental setup is described in this section. Figure 3.1 shows a schematic of a typical oil and gas site that is referenced throughout this Chapter.

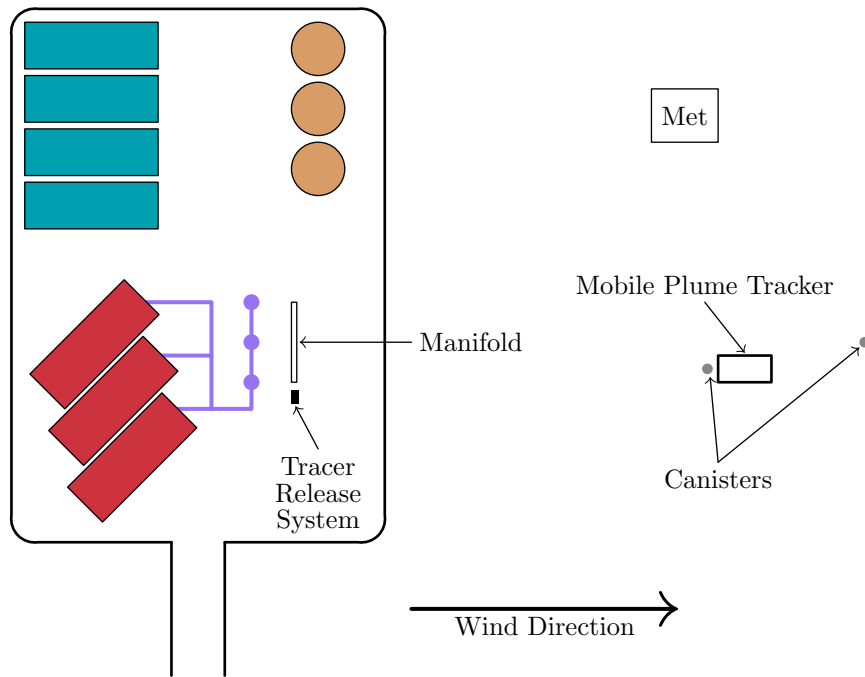


FIGURE 3.1. Overview of fieldwork setup. The tracer release system (Figure 3.2) and the manifold (Figure 3.3) are set up on the well pad. Downwind a meteorological station (Met), the mobile plume tracker (Figure 3.4), the canister triggering systems are in position to take measurements.

3.2.1. TRACER RELEASE SYSTEM. The TRM required us to release a tracer gas co-located with the emission source of VOCs. We designed the following system to accurately control the release rate of a tracer gas (acetylene) used in calculating the emissions rates of other species. Figure 3.2 below shows a schematic of the tracer release system.

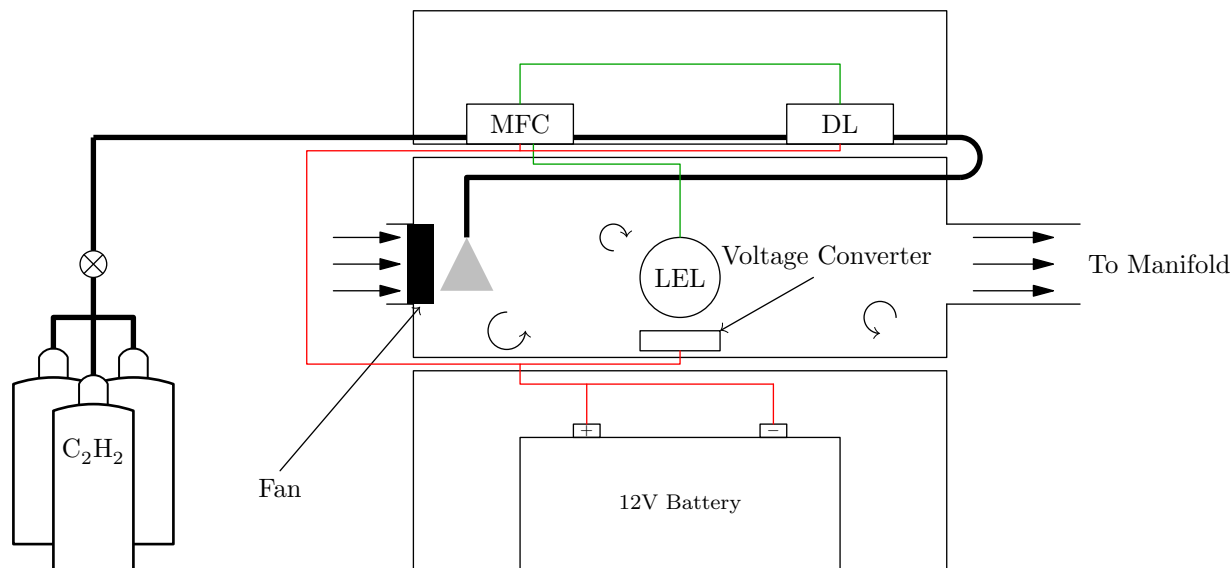


FIGURE 3.2. Diagram of the tracer release system adapted from Wells et al. (2015)[47]. Acetylene tanks are connected to a Mass Flow Controller (MFC) and sent into a mixing box with a Lower Explosive Limit (LEL) detector. The acetylene is then sent to a manifold (Figure 3.3). Data is collected using a Data Logger (DL) and powered by a 12 V battery.

This schematic was adapted from Wells et al. (2015)[47] and is summarized as follows. Acetylene cylinders are not hollow, they are packed with porous rock that is saturated with acetone[59]. In our our tracer release system, we connected three acetylene tanks to a regulator so that the release system was equally distributed. This configuration was chosen because acetone tanks have a maximum recommended flow rate and three tanks are needed to stay below this limit. The regulator controlled the pressure of acetylene as it entered Bev-A-Line IV non-reactive plastic tubing. The acetylene gas flowed to an Alicat M-Series Mass

Flow Controller (Alicat Scientific, Inc., Tuscon AZ, USA), which allowed the appropriate mass flux of gas to pass through and into a mixing chamber below. The acetylene gas was then diluted with ambient air to keep the concentration below the Lower Explosive Limit (LEL). This system was referred to as the Tracer Release System. The diluted tracer gas was then transported via accordion hose to a 3 m long perforated manifold for release. Typically release flow rates of at least 10 L min^{-1} were required to ensure that mixing ratios were at least an order of magnitude above background concentrations. The manifold is shown in Figure 3.3.

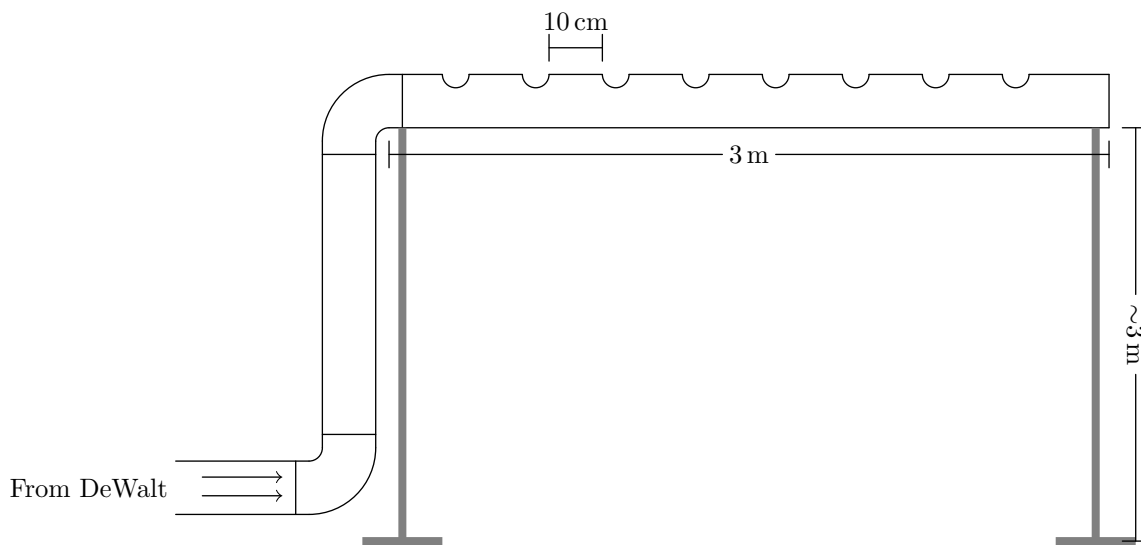


FIGURE 3.3. Diagram of manifold used to disperse acetylene into the atmosphere.

An accurate flow rate was important for analysis using the tracer ratio method. We used a Campbell Scientific CR850 Data Logger (DL) (Campbell Scientific, Inc., Logan UT, USA) to record the temperature, pressure and acetylene mass flow rate as a function of time with a temporal frequency of 1 Hz.

3.2.2. METEOROLOGICAL SYSTEM. We continuously measured atmospheric variables during field measurements for use in dispersion modeling. High-temporal resolution 3D wind vectors, temperature, relative humidity, and pressure were collected at two heights simultaneously (3 m and 10 m). I used these data to characterize the stability of the atmosphere using methods described in Section 3.5. A summary of the meteorological instruments that were used and the data collected is given in Table 3.2.

TABLE 3.2. Measurement capabilities of the meteorological station.

Instrument Type	Model	Maker	Measurements
Sonic Anemometer	WindMaster	Gill	3D wind vectors, temperature, water vapor concentration
All-In-One Weather Station	All-In-One	Climatronics	2D wind vectors, temperature, pressure, relative humidity
Data Logger	CR100	Campbell Scientific	Data acquisition and storage

3.2.3. MOBILE PLUME TRACKER. Downwind of the tracer release system, a mobile plume tracker was deployed to measure the concentration of acetylene (the tracer gas) and methane (a known emission from oil and gas sites [45, 60, 15]). This mobile plume tracker consists of a Picarro A0931 mobile measurement kit (Picarro, Inc., Santa Clara CA, USA) that measured the mixing ratio of the two aforementioned gases as well as water vapor using cavity ring-down spectroscopy (CRDS). This measurement system was secured within a Chevrolet Tahoe hybrid sport utility vehicle. An inlet was located 3 m above the front of the truck and was connected to 4.62 m of teflon tubing that fed ambient air into the Picarro system at 5 L min^{-1} . Adjacent to the Picarro inlet was a Global Positioning System (GPS) and an All-In-One meteorological sensor. Table 3.3 summarizes the measurement capabilities of this system.

TABLE 3.3. Measurement capabilities of the mobile plume tracker.

Instrument Type	Model	Maker	Measurements
Mobile CRDS	A0931	Picarro	Mixing ratios of methane, acetylene, and water vapor
GPS	A21	Hemisphere	Latitude and longitude
Sonimometer	Part 102779-A1-C1-D0	Climatronix	2D wind vectors

The mobile plume tracking system was used to obtain information about the spatial and temporal variability of the two gases to determine the emission rate of methane from various oil and gas sites. Figure 3.4 shows a diagram of the mobile plume tracking system.

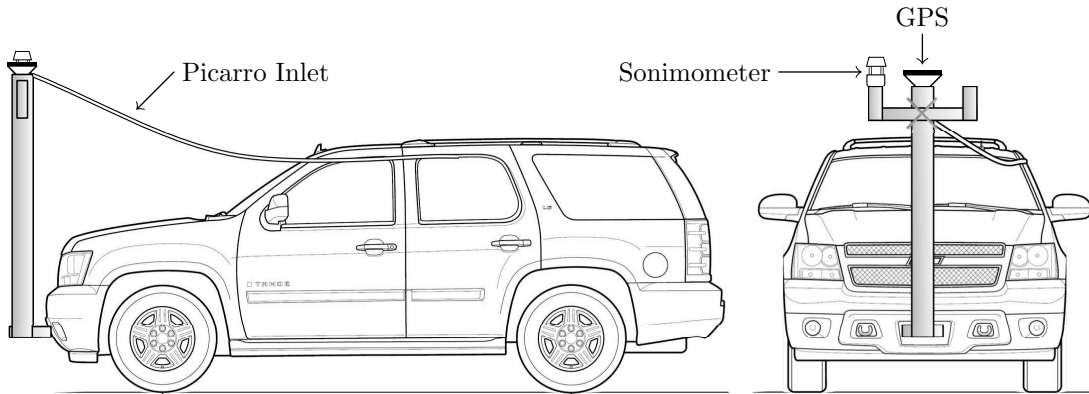


FIGURE 3.4. Schematic of the mobile plume tracker used during field-work. A mast is attached to the front of the vehicle for the placement of the Picarro inlet, GPS and sonimometer. Tahoe blueprint taken from <https://getoutlines.com/blueprints/7121/2009-chevrolet-tahoe-suv-blueprints> under Creative Commons License.

Cavity ring-down spectroscopy is a measurement technique that relies on the absorption of light by gases. Every gas has its own unique absorption spectrum that can be exploited to determine its concentration. The Picarro A0931 instrument used a variable wavelength laser that was tuned to specific absorption frequencies of each gas. In the case of this field study, the Picarro instrument used multiple wavelengths of light that are purposely chosen to be located at absorbing regions of the acetylene, methane and water vapor spectra. During operation, pulses of light are sent into a cavity containing ambient air and three highly

reflective mirrors. The laser-light bounces between the mirrors and once the light pulses reach resonance, the laser is abruptly deactivated and the light will continue to reflect off the three mirrors with an exponentially decaying intensity. In a perfect vacuum, the light will exponentially decay because the mirrors are not perfectly reflective. A three mirror system is used within the cavity to improve the signal-to-noise ratio compared to a traditional two mirror system[61]. When the Picarro contains the air sample, the intensity of light decreases with a shorter e-folding time because the gases will also absorb a certain fraction of this light. Using a photodiode, the intensity of light is measured as a function of time and can be described by Equation 3.2:

$$(3.2) \quad I(t) = I_0 \exp \left[-\frac{t}{\tau(\lambda)} \right]$$

where t is time, I_0 is the initial intensity, λ is the wavelength of light, and τ is given by Equation 3.3:

$$(3.3) \quad \tau(\lambda) = \frac{1}{c \ln R(\lambda) + c\alpha(\lambda)}$$

where c is the speed of light in vacuum, R is the reflectivity of the mirrors, and α is the absorption coefficient of the gas at a particular wavelength. Figure 3.5 shows a schematic of the intensity of light as measured by the photodiode.

The light intensity builds up to a threshold value and then the laser is shut off. The decaying light intensity is measured and a value of τ is fit to the ring-down section of the curve. This analysis is performed automatically by the Picarro for various wavelengths of light. Because the relationship between α and λ is known, the mixing ratio concentration of the gas can be determined[62].

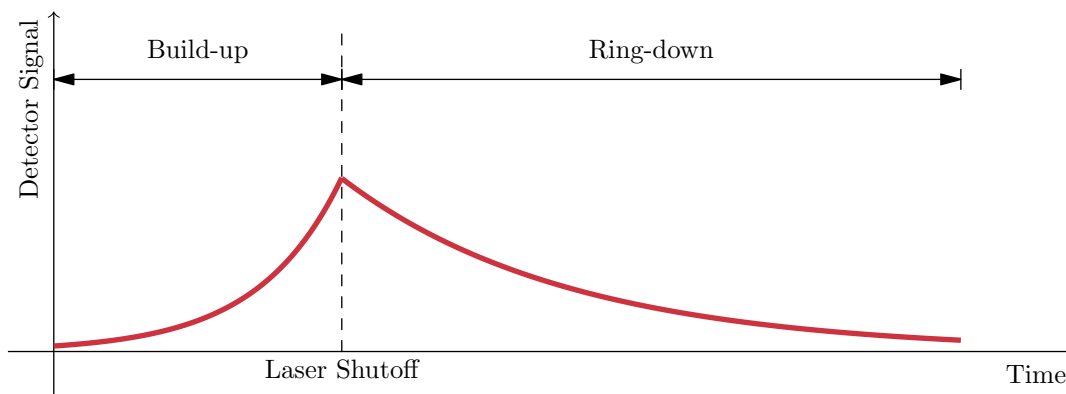


FIGURE 3.5. Schematic of light intensity within Picarro cavity. The light intensity builds up to resonance and is switched off and allowed to decay. After performing this measurement over many different wavelengths, the mixing ratio of the gas can be estimated.

3.2.4. CANISTER TRIGGERING SYSTEM. Along with online measurements of methane and acetylene, we took canister samples of air downwind from the oil and gas sites. Evacuated 1.4 L VOC sampling canisters were triggered to open and close remotely to collect ambient air samples. Typically, three canisters were deployed instantaneously: two positioned adjacent to the mobile plume tracking system inlet at 1.83 m and 4.88 m above the ground referred to as “tahoe down” and “tahoe up” respectively. We positioned another canister either further downwind or upwind of the mobile plume tracker based on the terrain and general layout of the oil and gas site on a tripod 2 m above the ground.

Each triggering system used an Arduino UNO microcontroller controlled valve that is opened for a total of 180 seconds to allow ambient air to be trapped for later analysis. A pressure sensor was used to collect information about the pressure within the evacuated canister to determine the volume of sampled air. A GPS and a temperature sensor were also placed within the fiberglass enclosure. A detailed list of the components is found in Table 3.4.

TABLE 3.4. List of canister triggering system components.

Component Type	Model	Maker
Microcontroller	UNO	Arduino
GPS	PMB-688	Polstar
Temperature Sensor	LM35	Texas Instruments
Wireless Modem	XBee-PRO 900HP	Digi
Pressure Sensor	OEM 0-15 PSIA	Honeywell
Solenoid Valve	S311PF15V2AD5L	GC

A custom LabVIEW interface remotely triggers the canisters to open simultaneously using a portable netbook computer.

3.3. VOC ANALYSIS BY GAS CHROMATOGRAPHY

The ambient air samples collected within the canisters were analyzed for 58 VOCs that are summarized in Tables B.1 through B.3 located in the Appendix B. Gas Chromatography (GC) coupled with mass spectrometry (MS), flame ionization detection (FID), or electron capture detection (ECD) is a common technique for identifying and quantifying a wide range of VOCs[46]. Samples are first pre-concentrated using a low temperature trap and then injected into the GC. An inert carrier gas moves the sample through a column, housed in an oven to permit the column temperature to be controlled. The stationary phase of the column is chosen to interact with compounds of interest in an injected sample. Compounds of differing volatility and polarity will interact to varying extents with a particular column type. The greater the interaction, the more slowly a particular compound moves through the column. A ramp of increasingly column temperature is employed to sequentially elute compounds of decreasing volatility. The amount of time that a compound stays in the column is known as the retention time. Eluting compounds are sent to an FID, MS, or ECD detector. The MS fragments and ionizes the compounds using electron impact ionization.

Using a scanning electromagnetic field, the fragments are accelerated to the detector. As voltage is scanned, ions of changing mass accelerate sufficiently to reach the detector. Each eluted and ionized compound will have a mass/charge spectrum made up of characteristic ion fragments that are used to identify the compound. The concentration of the compound is determined by the measured ion current at the detector, following a standard calibration. FID also can be used to detect eluting compounds. In this setup eluting organic compounds are combusted in a hydrogen flame. Resulting ions are proportional to the organic content of the column eluent. In GC-FID, compound identification is based simply on retention time; with GC-MS, the MS spectra provide additional information concerning compound structure. Both techniques allow quantification of emitted compounds.

For this study, the canisters were analyzed using a multidetector GC system[63–66]. Two GC systems detected non-methane hydrocarbon and halocarbon compounds. Three other GC systems measure VOC and oxygenated VOC (OVOC) compounds. Canister samples were cryogenically preconcentrated prior to analysis to allow for pptv-level detection limits.

3.4. EMISSION RATIOS

The ratio of NM-VOCs emission rates to methane was a quantity of interest in this study. This information can be used to provide estimates of NM-VOC emission rates if only data concerning methane are available in future studies. Equation 3.4 defines emission ratio in the context of this thesis:

$$(3.4) \quad \text{Emission Ratio} = \frac{Q_{\text{NMVOC}}}{Q_{\text{CH}_4}}$$

where Q_{NMVOC} is the emission rate of the NM-VOC in question and Q_{CH_4} is the emission rate of methane. Emission ratio data only apply to specific drilling and completion operations in Garfield County.

3.5. AERMOD

This section describes the atmospheric dispersion model that was used in this thesis. Every dispersion model has its own strengths and weaknesses depending on the pollutant emission scenario. The AMS and EPA Regulatory Model (AERMOD) was developed through a partnership between the Environmental Protection Agency (EPA) and the American Meteorological Society (AMS) in February 1991[67]. AERMOD is used frequently for new source apportionment[68]. It has the ability to incorporate complex terrain, and have multiple sources and receptors. This model was built to determine downwind concentration fields within 50 km of the source[69]. AERMOD disperses plumes using hourly averaged meteorology therefore it does not have the capability of explicitly resolving turbulence – instead it relies on parameterizations. It assumes the plume to be Gaussian within the Stable Boundary Layer (SBL), and in the convective boundary layer (CBL), the plume is treated as Gaussian in the horizontal and bimodal in the vertical as shown by Willis and Deardorff (1981)[70] and Briggs (1993)[71].

AERMOD was used in two major capacities in this study:

- (1) Replicating the time/location of each field measurement in Garfield County using a combination of field meteorological measurements and reanalysis data. Through this analysis, we evaluate AERMOD against ambient measurements.
- (2) Simulating each field measurement over a range of meteorological conditions relying entirely on reanalysis meteorological fields. Through this analysis, we can estimate

concentration probability profiles of various VOCs at different distances from the source.

Table 3.5 gives the meteorological variables that are required to run AERMOD. This table summarizes the source(s) of these data depending on the application.

3.5.1. REPLICATING FIELD MEASUREMENTS. Meteorological inputs are required to run AERMOD. A meteorological preprocessor (AERMET) was originally designed to incorporate surface observations and twice daily sounding data taken by the National Weather Service[72]. These input data are no longer easily accessible in the required format. Furthermore, the field measurement locations are approximately 80 km from the nearest sounding location. I took a different approach to provide AERMOD with meteorological information. The National Center for Environmental Prediction (NCEP) North American Regional Reanalysis (NARR) provides high spatial and temporal resolution meteorological fields over

TABLE 3.5. List of atmospheric variables required to run AERMOD. The source of these variables is given based on the application.

Variable	Site-Specific Simulation	Several Meteorological Conditions
Temperature at 2 m	Met-Station	NARR
Pressure at 2 m		
Sensible Heat Flux		
Surface Wind Vector		
Friction Velocity		
Convective Velocity Scale		
Monin-Obukhov Length		
Planetary Boundary Layer	NARR	
Bowen Ratio		
Vertical Potential Temperature Gradient above PBL		
Albedo		
Vertical Temperature Profile		
Vertical Wind Vector Profile		
Surface Roughness	GEOS-5	

North America[73]. Using the NCEP Eta model[74] and the Regional Data Assimilation System (RDAS), this dataset provides 8-times daily data at approximately 32 km resolution with data available at 29 pressure levels. I linearly interpolated these data spatially for each fieldwork location as well as temporally to 1 hour resolution (AERMOD requires that meteorological data is given every hour of simulation time). I used data from the NARR database to obtain values for vertical profiles of atmospheric variables as well as values of albedo, planetary boundary layer height, and other values listed in Table 3.5. AERMOD also requires a quantity known as the Bowen ratio, which I calculated using Equation 3.5:

$$(3.5) \quad B = \frac{Q_h}{Q_e}$$

where Q_h is the sensible heat flux and Q_e is the latent heat flux. I obtained both of these quantities from the NARR database.

I estimated the remaining meteorological parameters using *in situ* measurements. The meteorological station provided data that were used to give values of surface temperature, wind speed, and dispersion related parameters. Friction velocity, u_* , is a velocity scale that represents the contribution of vertical shear stress to turbulence. It is given by the following relationship:

$$(3.6) \quad u_* = \sqrt{\frac{\tau_s}{\rho}} = \left[\overline{u'w'^2} + \overline{v'w'^2} \right]^{\frac{1}{4}}$$

where τ_s is the shear stress in a layer of fluid and ρ is the density. Shear stress arises from very calm winds just above the surface ($u \sim 0$) and a vertical gradient of wind speed. Within the mixed layer of the atmosphere, the friction velocity is given by the square sum of the

mean velocity[75]. I calculated this value for each hour of simulated meteorology, using 20 Hz data from the 10 m sonic anemometer.

Monin-Obukhov Length, L , is another quantity required by AERMOD and is given by Equation 3.7:

$$(3.7) \quad L = -\frac{\rho c_p T}{\kappa g} \frac{u_*^3}{Q_h}$$

where κ is the von Kármán constant (~ 0.4), g is the acceleration due to gravity, T is the temperature, ρ is the density of air, c_p is the specific heat capacity of air, Q_h is the sensible heat flux, and u_* is the friction velocity. Essentially, Monin-Obukhov Length is the ratio of the turbulent kinetic energy to buoyant kinetic energy. When $L < 0$, there is a positive heat flux into the atmosphere ($Q_h > 0$) and it is considered unstable. Conversely when $L > 0$, the atmosphere is stable. When $Q_h = 0$, $L = \infty$ and the atmosphere is said to be neutral. The magnitude of L indicates whether turbulent kinetic energy or buoyant energy is dominating the turbulence.

The convective velocity scale is required by AERMOD and is given by:

$$(3.8) \quad w_* = \left(\frac{g}{T_v} z_i \overline{w'\theta'} \right)^{\frac{1}{3}}$$

where T_v is the virtual temperature, z_i is the average depth of the mixed layer and the overbar term is the kinematic vertical turbulent flux of virtual potential temperature near the surface. The convective velocity scale, also known as the Deardorff Velocity, gives a velocity scale to describe convection-driven turbulence in the mixed layer. I calculated this variable directly using information from the reanalysis database or from field measurements.

The sensible heat flux can be calculated using Equation 3.9.

$$(3.9) \quad Q_h = \overline{w'T'}$$

where w' is the fluctuation of vertical wind speed and T' is the fluctuation of temperature. We measured these two quantities at a frequency of 20 Hz using the 10 m sonic anemometer.

The variances of horizontal and vertical wind are other parameters required for the Gaussian modeling of the plumes. Our sonic anemometer provided 3D wind vectors that I used to calculate these quantities for each hour of meteorology.

Surface roughness length, z_0 , is a representation of the roughness of the surface. A larger z_0 implies more atmospheric interaction with the surface. This variable was not available as part of the NARR database. Instead, I took this variable from GEOS-5 meteorology[76].

3.5.2. DISPERSION MODELING UNDER VARIOUS METEOROLOGICAL CONDITIONS. When performing simulations for typical meteorological conditions, field site data were not available. This meant I used NARR to calculate *all* meteorological parameters that AERMOD required to run. The NARR database does provide information regarding surface temperature and wind vectors. Some quantities are not directly provided by NARR and had to be estimated using other methods.

Monin-Obukhov length and friction velocity were estimated using the algorithm in AERMET [77]. Because these two quantities are intimately related to each other, I calculated them iteratively using Equation 3.10.

$$(3.10) \quad u_* = \frac{\kappa u_{\text{ref}}}{\ln(z_{\text{ref}}/z_0) - \Psi_m\{z_{\text{ref}}/L\} + \Psi_m\{z_0/L\}}$$

where κ is the von Kármán constant, u_{ref} is the wind speed at a reference height of z_{ref} , and z_0 is the roughness length. The stability terms are given by the following equations:

$$(3.11a) \quad \Psi_m\{z_{\text{ref}}/L\} = 2 \ln\left(\frac{1+\mu}{2}\right) + \ln\left(\frac{1+\mu^2}{2}\right) - 2 \arctan \mu + \frac{\pi}{2}$$

$$(3.11b) \quad \Psi_m\{z_0/L\} = 2 \ln\left(\frac{1+\mu_0}{2}\right) + \ln\left(\frac{1+\mu_0^2}{2}\right) - 2 \arctan \mu_0 + \frac{\pi}{2}$$

where $\mu = (1 - 16z_{\text{ref}}/L)^{\frac{1}{4}}$ and $\mu_0 = (1 - 16z_0/L)^{\frac{1}{4}}$. Then using friction velocity, I calculated Monin-Obukhov length using Equation 3.7. I repeated this process iteratively until successive values did not change by more than 0.001%.

AERMOD requires values for the standard deviation of both the horizontal wind direction (σ_θ) and the vertical wind component (σ_w). These parameters are not available as part of the NARR reanalysis database and instead I estimated them by determining a stability class for each hour using downwelling solar radiation, wind speed and total cloud cover[78]. I characterized the stability class using tables created by Pasquill, Gifford, & Turner. Because AERMOD was run over one Julian year to examine the concentration fields over a wide range of meteorological conditions and the PG&T tables only give ranges for values of dispersion parameters, I used a random number generator to obtain a representative value of σ_θ and σ_w for each hour of meteorology.

3.5.3. COMPLEX TERRAIN. I used AERMAP to incorporate the complex terrain of Garfield County into the model. This tool read in Digital Elevation Model (DEM) files that were taken from the United States Geological Survey (Data Credit: National Elevation Dataset <http://ned.usgs.gov>). From these data, AERMAP calculated elevation for each

latitude and longitude required. Representing this in the model is important to accurately predict concentrations downwind.

When running AERMOD with terrain included, the model will calculate the concentration field as a weighted average of the horizontal plume (no terrain) and the terrain following plume:

$$(3.12) \quad C(x, y, z) = fC_f(x, y, z) + (1 - f)C_f(x, y, z_e)$$

where f is the weighting factor calculated by determining the buoyancy of the plume and the atmospheric stability conditions. Under very stable conditions, f goes to unity and the plume is described entirely by the horizontal plume. Under very unstable conditions f goes to $1/2$ and the plume is described by an equal proportion of the horizontal and terrain following plumes[79].

This thesis will examine the ability of AERMOD to predict concentrations for individual wells under meteorological conditions measured at the field site and over various other conditions. The field sites that I replicated are over small spatial scales (under 2 km). AERMOD is typically used for larger time scales which could introduce error when modeling so close to the source.

CHAPTER 4

DATA PROCESSING

4.1. PICARRO DATA

The Picarro CRDS measures the mixing ratios of methane and acetylene at a frequency of 3 Hz. I used this high temporal resolution data to calculate a point-by-point distribution of methane emission rates during the field measurements. In order to accurately calculate the emission rate, I subtracted the background mixing ratios of methane and acetylene from the time series. The background concentrations of acetylene in Garfield county were relatively low (10 – 100 pptv) compared to the signal (typically > 50 ppbv). The only major source of acetylene in the atmosphere is the combustion of gasoline [75]. The background concentration of acetylene did not change significantly with time and I used the average of the lowest 5% of values for each day of measurement. Some other instruments located downwind were powered by mobile generators that emitted acetylene. We noted whenever the Picarro detected acetylene from these mobile generators and these data points were not included in the analysis or in the background calculation.

The background mixing ratio of methane is approximately 1900 ppbv in the Northern Hemisphere[80]. Sources of methane relevant to Garfield County, in addition to oil and gas production, include: cattle, biomass burning, and the decomposition of solid waste[81]. Many oil and gas wells are close together so there was also potential influence from methane emission at other locations. To address the variability in the methane background, an interpolated background was used. By using a portable VOC meter, we released the tracer gas close to the VOC emission source on the well pad. When the Picarro detected acetylene concentrations were at background (i.e. out-of-plume), I considered the methane concentrations

also out-of-plume. Throughout the measurement period, methane background concentrations were changing as a function of time. I quantified the new background methane mixing ratio during each of these out-of-plume time periods. During the in-plume time periods I assumed the methane background changed linearly with time. The benefits of using this background correction method can be found in Wells et al. (2015)[47].

To combat the natural temporal variability of the acetylene concentrations, I performed Butterworth low-pass smoothing on the data using a cutoff frequency of 0.005 s^{-1} . Figure 4.1 shows a time series of acetylene with and without a Butterworth low-pass filter applied.

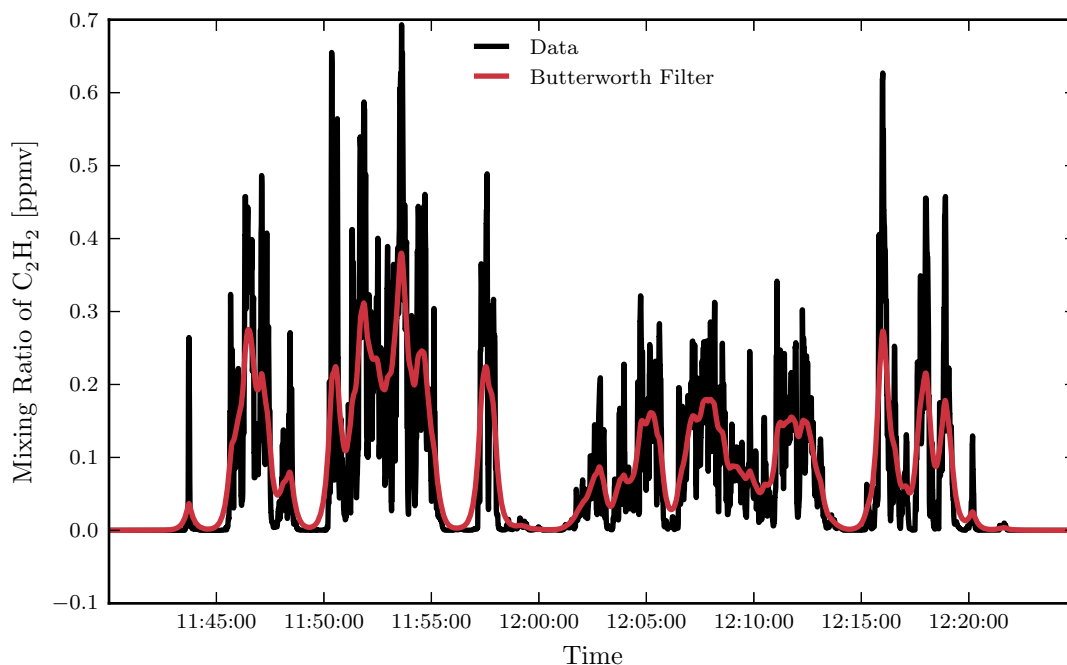


FIGURE 4.1. An example of an acetylene time series with smoothing. A low-pass Butterworth filter was used with a cutoff value of 0.005 s^{-1} . This allowed the algorithm to locate acetylene plumes rather than single mixing ratio spikes.

The low-pass filter allowed the algorithm to more accurately identify an entire acetylene plume rather than a single spike of concentration. In Figure 4.1, there are many times past 12:00 where the algorithm might assume that acetylene was out-of-plume and assign

methane to also be out-of-plume during that period. The Picarro could still be measuring methane and it would assign an unrealistically high methane background concentration for that period. The results from this algorithm were checked visually to ensure that background corrections were reasonable. The smoothed data were only used for determining background time periods and not used to calculate emission rates.

Figure 4.2 shows an interpolated background correction made to methane measurements.

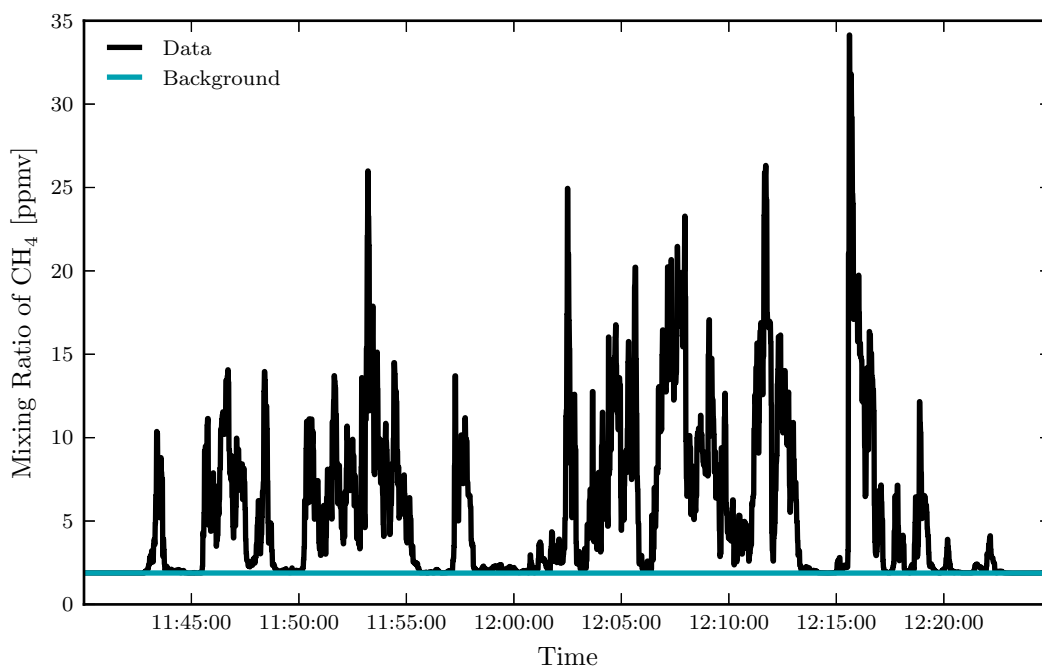


FIGURE 4.2. Methane concentration as a function of time with the estimated background using the interpolated background algorithm.

Once the data had been background corrected, I performed the TRM on a point-by-point basis. This produced *distributions* of emission rates for each operation type. Not all Picarro data collected during the experiment period were used. I only performed the TRM when the following criteria were met:

- (1) Mobile plume tracker was stationary.
- (2) Tracer release system was set to be releasing more than 1 L min^{-1} of acetylene.
- (3) Acetylene was above the cutoff value of 0.8 ppbv.
- (4) Correlation coefficient, r , of methane and acetylene concentrations was above 0.5.

This assured that the calculated emission rates of methane were directly from the oil and gas pad. Details of points (3) and (4) are described below.

Regarding point (3), Figure 4.3 shows the measured acetylene concentration distribution for day 1 at site F1. This distribution appears to be bimodal. In fact, when this plot was made for the rest of the sites, most exhibited this bimodal characteristic. We considered the mode centered around the lower concentrations as the acetylene concentration when the mobile plume tracker was out-of-plume. The mode centered around the higher mixing ratios represented the concentrations when the plume tracker was in-plume. Along with a background correction, we chose an acetylene cutoff value that represented all of the sites: 0.8 ppbv. When performing the TRM using this cutoff value, the emission rate distributions of methane were *conservative*, i.e. a lower estimate of the emission rate distributions because methane and VOC emissions rates were generally calculated to be higher at lower acetylene concentrations due to dividing by a small number. When the low mixing ratios were removed from the analysis, the large methane emission rate outliers were removed.

Regarding point (4), this cutoff correlation coefficient between acetylene and methane helped ensure that when we were in the acetylene plume, we were also in the plume from the pad. The correlation coefficient was calculated for each data point using the data one minute before up to one minute after. Only data that were above the $r = 0.5$ correlation coefficient cutoff were used to calculate emission rates. Other correlation coefficients were

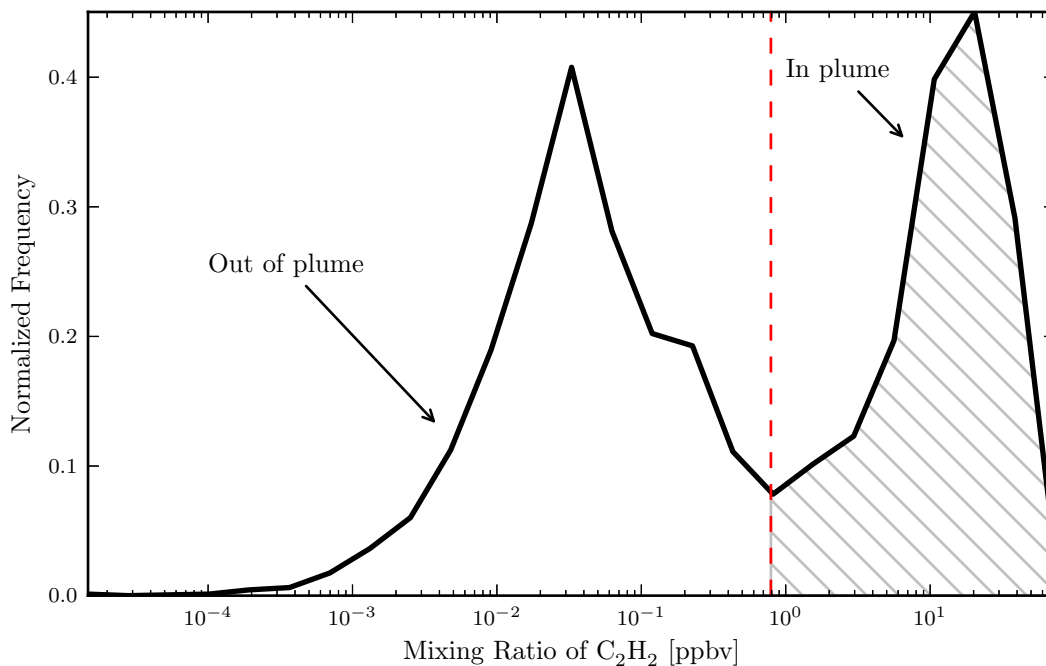


FIGURE 4.3. Acetylene mixing ratio PDF for day 1 at Site F1. The mixing ratio distribution is bimodal with a separation at 0.8 ppbv. This was used as the acetylene cutoff value for all field data.

tested. With a relatively high cut off value of 0.8, the estimated emission rate distributions did not change their shape. This analysis is found in Appendix D.

4.2. CANISTER DATA

We analyzed the canisters that collect ambient air samples for three minutes for acetylene as well as a suite of VOCs. I performed the TRM on these data. The background correction involved subtracting the mixing ratios measured from at least one canister deployed upwind for 3 minutes during each experiment period. Acetylene was being released at the time of background collection and the mobile plume tracker was used to ensure that no above background acetylene was observed during collection. We assumed this upwind canister was representative of the background concentration of all the NM-VOCs for each day of field measurements.

CHAPTER 5

DATA ANALYSIS RESULTS

5.1. METHANE CONCENTRATIONS

We measured methane mixing ratios using the Picarro CRDS analyzer at 18 sites (field measurement sites summarized in Table A.1). These time series provide insight into the typical methane mixing ratios surrounding oil and gas drilling and completion operations. Figure 5.1 shows the background corrected distribution of methane mixing ratios for sites measured in Garfield County. The methane mixing ratio distributions for drilling, fracturing, and flowback include data from all sites where that particular operation type was occurring. There were two sites with simultaneous operations that could not be attributed to any single operation type.

The x -axis is plotted using a logarithmic scale because the observed mixing ratios span six orders of magnitude. The data used in this plot were selected based on the criteria outlined in Section 4.1. Downwind measurements during flowback operations tended to have the highest mixing ratios of methane. The variation of methane concentrations is attributed to many possible causes, including measurements being taken at different distances, wells with different operators or sub-contractors, different meteorological conditions, and different emission rates. These results should not be used quantitatively, rather they give an estimate of the range methane concentrations located within ~ 500 m from oil and gas operations in Garfield County.

Leifer et al. (2013) collected measurements of methane concentrations associated with natural gas production. The most relevant measurements for this study were methane mixing ratios taken at Kern River and Elk Hills in California. Air samples near these oil fields were

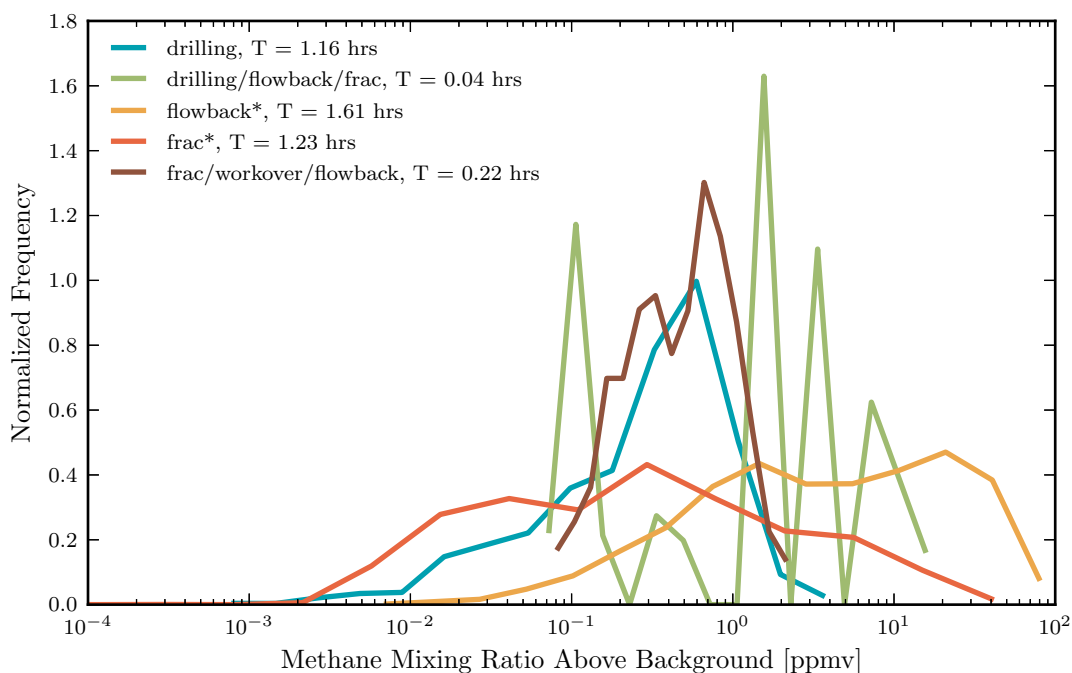


FIGURE 5.1. Mixing ratio of methane (above background) for each operation type. T is the total measurement time for each distribution. Any operation types with an asterisk consist of multiple sub-operation types.

measured to have (7.13 ± 5.64) ppmv and (2.97 ± 0.93) ppmv of methane respectively[82]. Another study performed in Washington, DC measured methane mixing ratios attributed to natural gas pipelines that run through the city. A median mixing ratio of 3.1 ppmv, and a maximum mixing ratio of 88.6 ppmv was measured across 1500 road miles of the city [83]. These measurements are comparable to the mixing ratios determined in Garfield County.

5.2. SELECTED VOC CONCENTRATIONS

The mixing ratios of 58 VOCs from canisters taken at field sites in Garfield County were determined by GC by my colleagues. For the purposes of this thesis, only the measurements of benzene, toluene, and ethane are discussed in this section. Benzene and toluene are of special interest due to their roles as air toxics; ethane is a high abundance compound in natural gas. Figure 5.2 shows the non-background corrected mixing ratio distributions of

these three compounds separated by well completion operation type. I chose box and whisker plots because the canister distributions had significantly fewer data points compared to the methane concentration distributions.

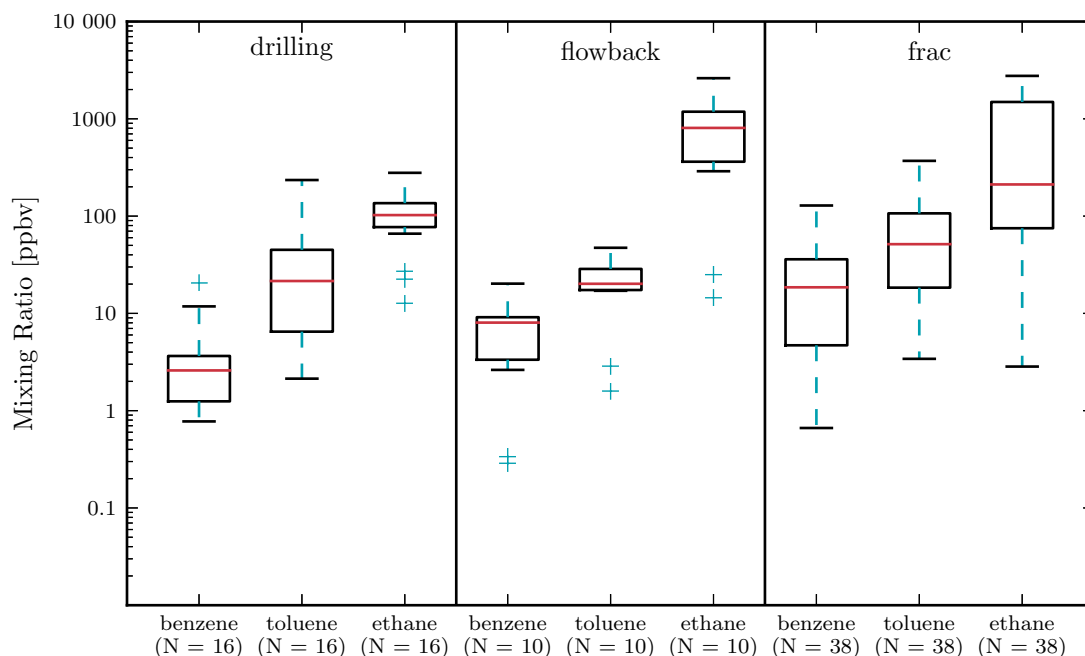


FIGURE 5.2. Mixing ratio distribution for benzene, toluene, and ethane. N is the number of canister samples in each distribution. These distributions were **not** background corrected.

The red line gives the median, the box spans the interquartile range and the whiskers represent the maxima (minima). Any maxima (minima) that were above (below) 1.5 times the interquartile range are plotted using a cross. The y -axis of the plot uses a log-scale due to the mixing ratios spanning several orders of magnitude. I created the mixing ratio distributions presented above using canister samples taken at various distances away from the well pad. These data are only meant to give a qualitative pattern of VOC mixing ratios observed downwind of different operation types. Benzene and toluene are part of the BTEX compound family which might derive from combustion operations (e.g., generators, truck

traffic) or be released from the hydrocarbon deposit. Ethane is the second most abundant component of natural gas (after methane) and may act a tracer for emissions from the tight gas formation. I found the highest median value of benzene mixing ratios during fracking operations.

The measured concentrations of benzene are similar to those found in other studies. The concentrations reported by Esswein et al. (2014) applied strictly to well pad workers. For full-shift breathing zone samplers, the benzene mixing ratios varied from 7 to 590 ppbv for workers in the Piceance Basin. These mixing ratios are slightly higher than those shown in Figure 5.2, perhaps due to our canisters sampling further away from the well pad (concentrations are generally assumed to decrease exponentially with distance). Esswein et al. (2014) found that benzene concentrations are highest for times during flowback, i.e. employees performing tasks on flowback tanks saw the highest concentrations of benzene compared to other tasks[20]. Swarthout et al. (2013) reported benzene concentrations that ranged from 39 to 865 pptv measured at the Boulder Atmospheric Observatory (BAO). This is on the lower end of the distributions shown in Figure 5.2. BAO is much further from regions of high well density in Weld County where majority of wells are in production phase, but is also influenced by BTEX emissions from other Front Range urban and highway emissions[21]. McKenzie et al. (2012) also measured benzene mixing ratios downwind of well completions in Garfield County. Their study found a median mixing ratio of 1 ppbv with values spanning from 0.34 to 26 ppbv[19]. These mixing ratios fall within the distributions shown in Figure 5.2. This thesis goes an important step further by calculating emission rates of benzene and other VOCs in Section 5.4.

Toluene was another BTEX compound measured in the canisters using the GC system. The median values of toluene are very similar across the three different operation types with some distributions being narrower than others. McKenzie et al. (2012) measured toluene concentrations near well completion activities in Garfield County and found a median mixing ratio of 2.5 ppbv with values that ranged from 0.8 to 100 ppbv[19]. These mixing ratios are on the same order of magnitude as the values shown in Figure 5.2. Swarthout et al. (2013) reported mixing ratios of toluene that ranged from 10 to 1620 pptv near operations in the Denver Basin[21]. Warneke et al. (2014) measured toluene mixing ratios in Utah around 10 - 100 ppbv near new well operations. All studies also found that toluene mixing ratios were relatively higher than benzene concentrations[23]. The values presented in Figure 5.2 are usually much higher than previous studies of oil and gas operations, but comparisons of concentrations are difficult to interpret due to differences in dilution between studies.

Ethane mixing ratios were much higher during flowback measurement periods than during drilling or hydraulic fracturing measurements. This could indicate that a larger portion of the natural gas leaking during flowback compared to the other operations, but that hypothesis can be better evaluated using emissions results.

Ethane mixing ratios were measured in the Denver Basin by Swarthout et al. (2013). A median value of 13.6 ppbv was measured during the field campaign and attributed to oil and gas operations in this basin[21]. The values of ethane in Figure 5.2 are much higher than this value, possibly reflecting source proximity. Gilman et al. (2013) also measured ethane concentrations in the Denver Basin area and found a median value of 22 ppbv of ethane over a two week measurement period in 2011[22]. This value is similar to the observations from Swarthout et al. (2013). Concentrations are highly dependent on local meteorological

conditions and distances away from the source. The comparison of our results to other studies is meant only to put our results into perspective. The estimated emission rates presented in Section 5.4 will remove any dependence on atmospheric stability, terrain, distances, etc.

Performing the tracer ratio method means the mixing ratio data must be background corrected. Figure 5.3 shows the background corrected mixing ratios of benzene, toluene, and ethane.

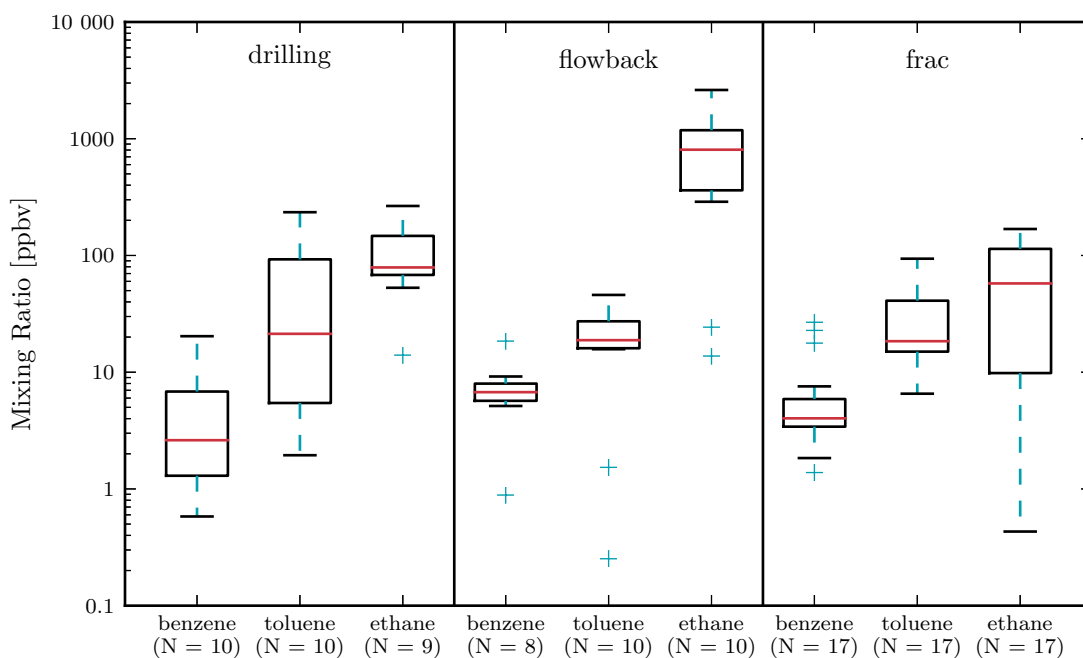


FIGURE 5.3. Mixing ratio distribution for benzene, toluene, and ethane. N is the number of canisters samples in each distribution. These distributions **were** background corrected.

5.3. EMISSIONS ESTIMATE: METHANE

I used the high temporal resolution data of methane and acetylene to create a point-by-point distribution of methane emission rates from all sites. Using the methods described in Chapters 3 and 4, the emission rate distributions for methane are shown in Figure 5.4:

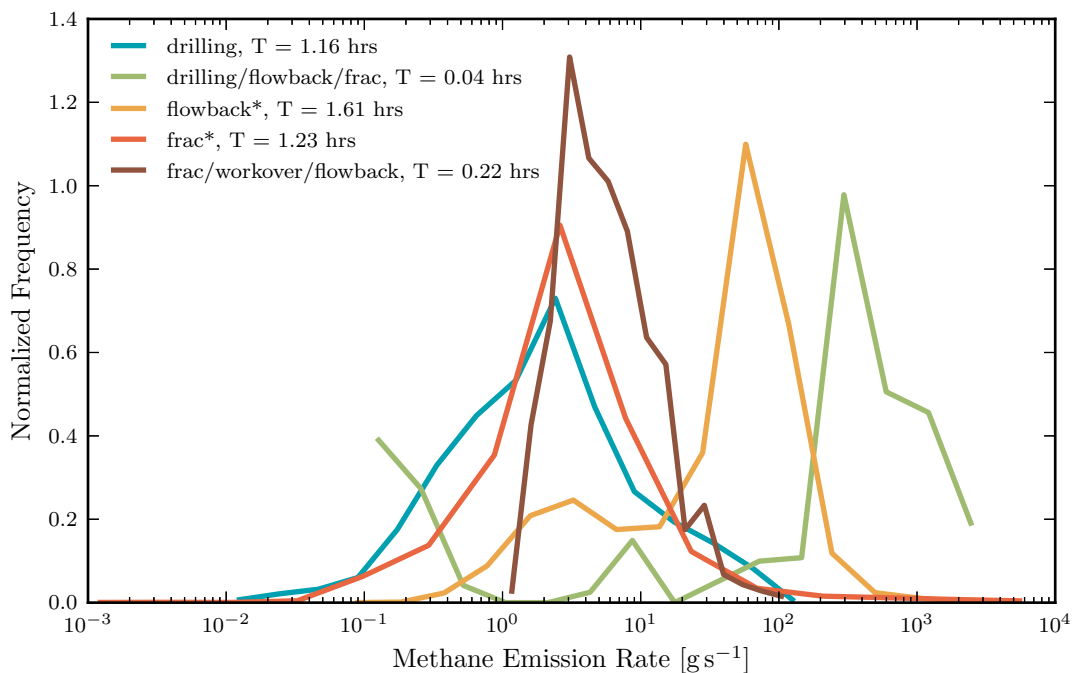


FIGURE 5.4. Methane emission rate distribution by operation type. T is the total measurement time for each distribution. Any operation types with an asterisk consist of multiple sub-operation types.

The x -axis is the estimated emission rate on a log-scale and the y -axis gives the Probability Distribution Function (PDF) calculated in log-space. Each emission rate distribution corresponds to well drilling or completion operations that were studied in Garfield County. The locations that had simultaneous operations are shown in this plot as separate curves (i.e. drilling/flowback/frac and frac/workover/flowback). T indicates the total measurement time for each distribution. Each data point contains data measured over $1/3$ of a second. Table 5.1 quantifies the results in Figure 5.4:

Emission rates that span many orders of magnitude were not out of the ordinary. In general, Figure 5.4 shows that all operation types had emission rates that span at least two orders of magnitude. This plot captured variability associated with site location, operator, and subcontractor in Garfield County.

TABLE 5.1. Emission rate distributions of methane calculated using the tracer ratio method. These data were separated into their respective operation types: drilling, fracking, flowback, and two combination sites. Sites is the number of sites measured, T is the total measurement time for each distribution, Med is the median, and SD is the standard deviation taken in log-space.

Operation Type	Sites	T [hrs]	Mean [g s ⁻¹]	Med [g s ⁻¹]	25 th %ile [g s ⁻¹]	75 th %ile [g s ⁻¹]	SD
drilling	5	1.2	6.2	1.9	0.71	4.8	0.67
drilling/flowback/frac	1	0.036	490	260	11	560	1.4
flowback	3	1.6	64	53	13	83	0.67
frac	8	1.2	29	2.8	1.4	5.5	0.63
frac/workover/flowback	1	0.22	8.1	5.1	3.2	9.2	0.34

5.3.1. FLOWBACK. The yellow line in Figure 5.4 represents the emission rate distribution for all flowback operations. The flowback process allows fracturing fluids to return to the surface. As the hydraulic pressure on the shale formation decreases, natural gas can escape the tight gas formation and travel to the surface with the fracturing fluids. Once at the surface, the natural gas may be emitted into the atmosphere increasing the methane mixing ratios surrounding the well. Green completion operations are designed to reduce such emissions. The flowback emissions distribution appears to exhibit bi-modal behavior and was fit using two log-normal curves centered around 3.6 g s⁻¹ and 68 g s⁻¹ (Figure H.1). This bimodal behavior might be due to:

- (1) The tracer gas and the methane source not being exactly co-located.
- (2) Methane emission rates changing dramatically during a single flowback operation.
- (3) Different flowback operations having very different methane emission rates between sites.

The variability due to the tracer not being exactly co-located with the methane source on the well pad is difficult to isolate and its effects are therefore not quantifiable in this analysis; however, our correlation-coefficient-filtering method (Chapter 3) will have removed

many of these cases. Figure 5.5 shows the flowback emission rate distribution after it has been separated into operations that only had flowback and an operation that had a combination of flowback/popping. These distributions both exhibit this bimodal behavior.

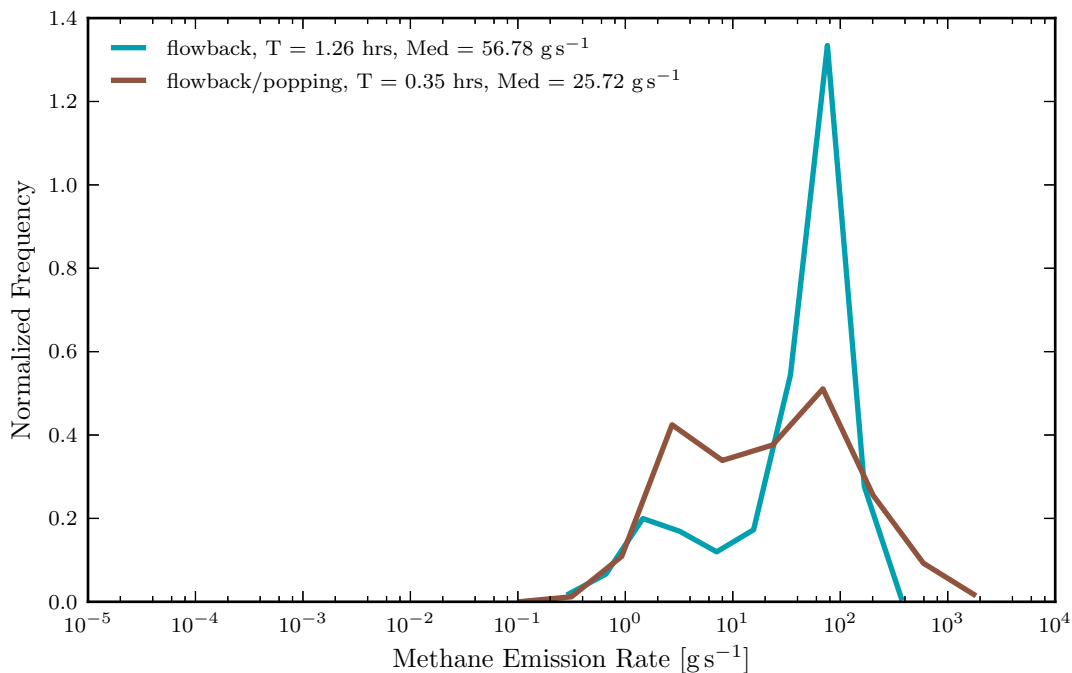


FIGURE 5.5. Methane emission rate distributions for flowback (only) and flowback/popping. Popping involves drilling through sealed fracked regions to allow flowback of the entire lateral region. The median value of each curve is given in the legend.

Figure 5.6 shows the flowback distribution broken down into separate measurement days. Site I3 has the bi-modal feature that was seen in the total flowback distribution. Sites B3, F1, I4 have only one mode. Site I4 is an example of a flowback operation with relatively low methane emissions. The emission rates from sites B3 and F1 are one and two orders of magnitude larger than site I4, respectively. Measurements at sites I3 and I4 had the same well pad, and subcontractor and yet the emission distributions were quite different. Some instances the flowback is a small source of methane into the atmosphere, other instances

it can be a non-trivial source. Site I3 emissions span four orders of magnitude which also confirms large emission rate variability during an individual site measurement.

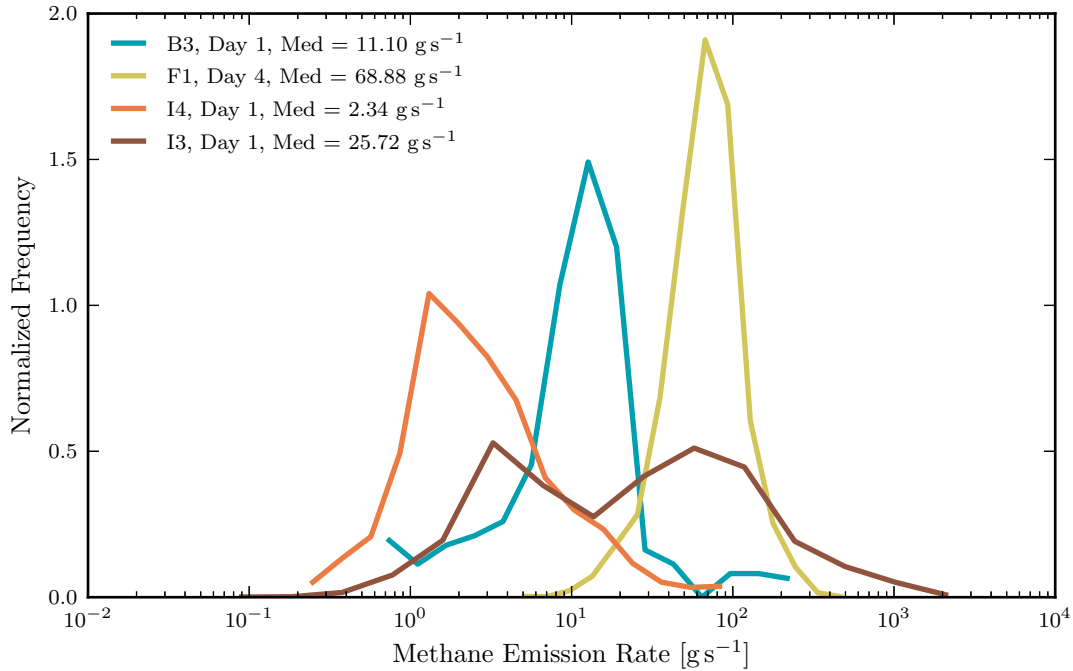


FIGURE 5.6. Methane emission rate distribution separated by each day of fieldwork when flowback was occurring. The median value of each curve is given in the legend.

Allen et al. (2013) measured emission rates of methane during flowback periods of several wells across the US and found an average emission rate per well of 8.4 g s^{-1} [13]. The estimate of Allen et al. (2013) is comparable to the mean calculated for Garfield County given in Table 5.1. Howarth et al. (2011) also measured methane emission rates for flowback operations in many oil and gas basins including the Piceance Basin. This study estimated methane leaked at a rate of 6.03 g s^{-1} during flowback[45]. This estimate is much closer to the values measured in Garfield County, but it is still close to an order of magnitude smaller than the median emission rate. The emissions from site I4 are more similar to the emissions that

Howarth et al. (2011) measured during their field campaign, with median emissions rates of 2.3 and 6.03 g s^{-1} respectively.

5.3.2. DRILLING. Figure 5.4 shows a log-normal emission rate distribution of methane during well drilling experiments. The PDF has a median value of 1.9 g s^{-1} and spans approximately four orders of magnitude. Drilling is not expected to be a large source of methane because the emissions are expected to be primarily from the shale removed by the drill bit, although occasionally the drill penetrates pockets of gas that yield larger emissions. It is also possible that emissions from other equipment on site could have been contributing to the methane concentrations surrounding the well (such as diesel/natural gas powered hybrid generators). Figure 5.7 shows the drilling distribution broken down by field experiment site and day.

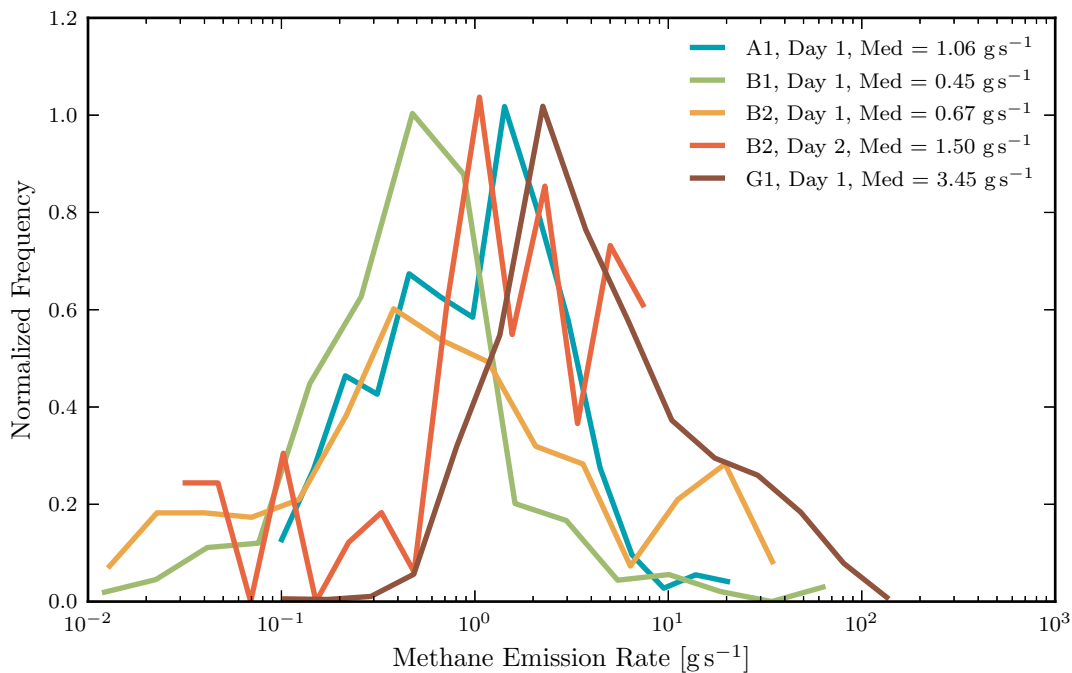


FIGURE 5.7. Methane emission rate distribution separated by each day of fieldwork when drilling was occurring. The median value of each curve is given in the legend.

Most methane emission rate PDFs from drilling sites in Garfield County were centered near 1 g s^{-1} . Drilling had the most consistent emission rates across all different operations tested, suggesting that a single log-normal distribution with a median of $\sim 1 \text{ g s}^{-1}$ could be used to represent drilling methane fluxes for wells in Garfield County.

5.3.3. HYDRAULIC FRACTURING. Seven sites were included in the hydraulic fracturing PDF in Figure 5.4. Hydraulic fracturing has a broad distribution of methane emission rates – similar to the emission rate distribution of drilling. Even with fluids begin forced into the well, methane was able to escape from the reservoir. This distribution suggests that the emission rates during the fracturing phase of well completion could be predicted using a log-normal distribution. The distribution has a median value of 2.8 g s^{-1} and includes several different types of fracturing techniques. These individual techniques are plotted in Figure 5.8.

Three sites did not fall directly into the strictly hydraulic fracturing category. One site was perforating and fracturing two wells simultaneously. This is shown as the yellow line in Figure 5.8. This distribution is centered one order of magnitude lower than the pure fracturing sites. Remote fracturing involves the fracturing of several wells using a centralized pumping location. Pipes with pressurized fracturing fluids run along the surface to other well pads up to three miles away to fracture those wells. In this way, the oil and gas subcontractor can fracture multiple wells that are separated by large distances in a short period of time, reducing emissions associated with truck traffic and fracturing pumps in the area. Measurements were taken at a central fracking location, near pumping trucks that were performing a remote fracturing operation. The estimated emission rates of methane from this type of fracturing operation are also about an order of magnitude lower than

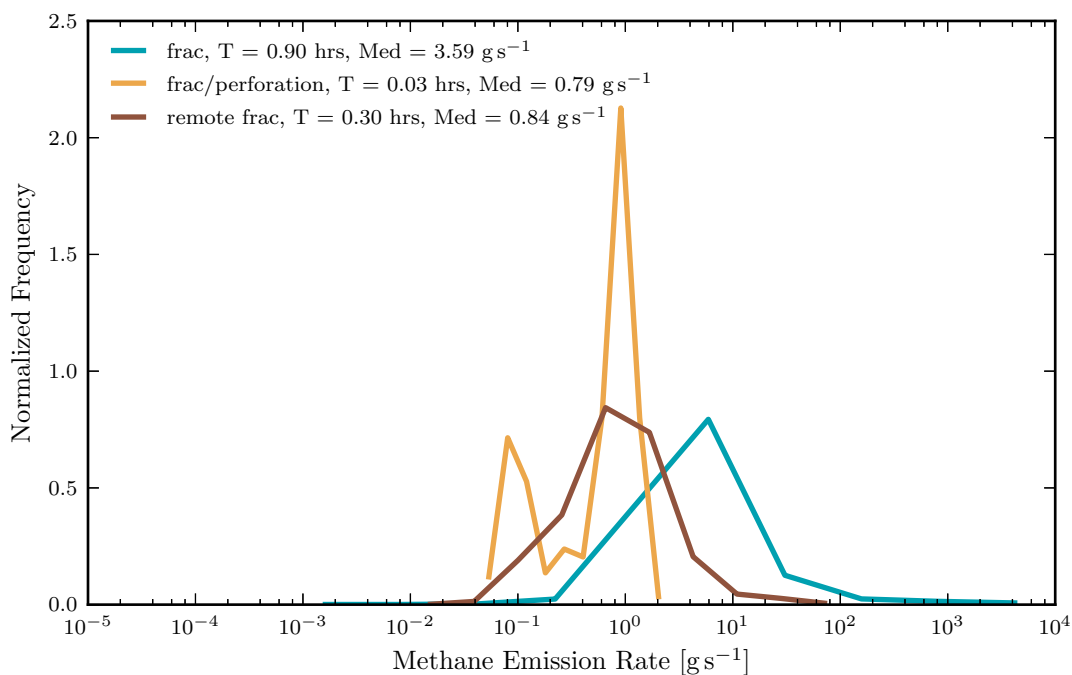


FIGURE 5.8. Methane emission rate distributions for hydraulic fracturing (only), fracking/perforation, remote fracking, and gel fracking. Perforation refers to the detonation of small explosives to initiate fractures in the well. Remote fracking is the fracturing of multiple spatially separated wells from a centralized location. Gel fracking uses a gel substance instead of water to reduce waste. The median value of each curve is given in the legend.

normal fracturing operations. This suggested that a large fraction of methane emissions during hydraulic fracturing operations can be attributed to methane leaking from the shale formations at the wellhead itself and not from equipment associated with fracking or fracking liquid storage containers. Finally, a site was visited where a gel solution was used to fracture the shale. Gels were being used to eliminate the need for large volumes of water to frack tight gas formations. I did not report any data from the site with gel fracking solution as the acetylene cutoff and the acetylene and methane correlation coefficient requirements were not met.

The hydraulic fracturing distribution can be broken down further and separated by site code and field experiment day as shown in Figure 5.9.

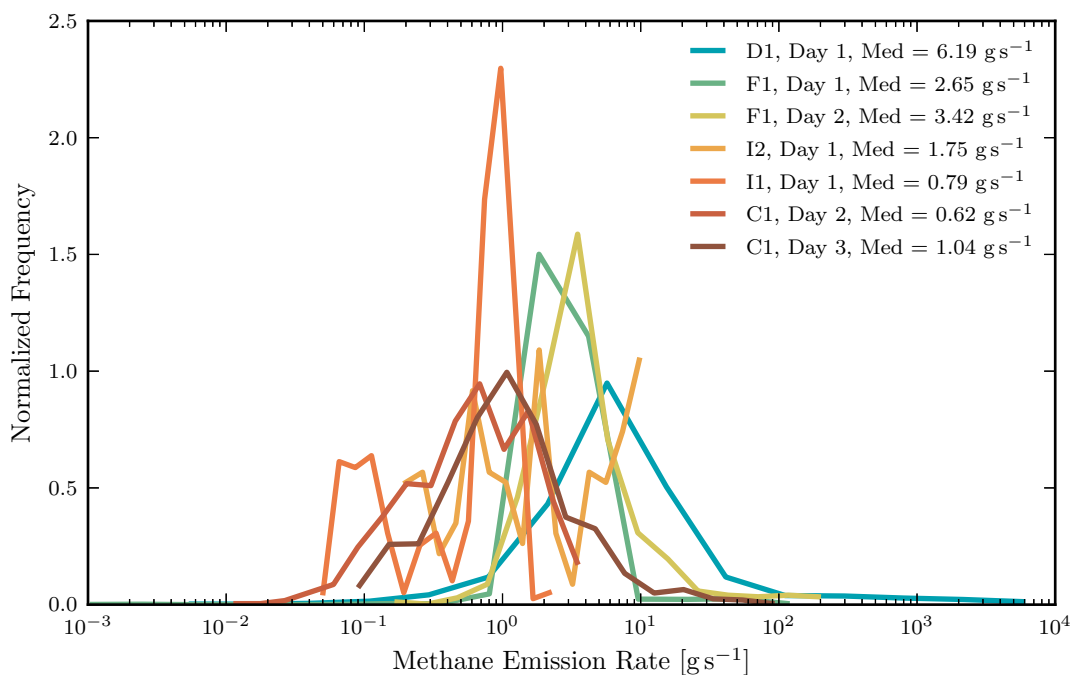


FIGURE 5.9. Methane emission rate distribution separated by each day of fieldwork when hydraulic fracturing was occurring. The median value of each curve is given in the legend.

There were several different sites (and multiple measurement days at certain sites) where hydraulic fracturing took place. Sites I1, I2, and C1 have PDFs medians below 2 gs^{-1} whereas sites A2 and F1 have PDFs with median values around 6 and 3 gs^{-1} respectively. Hydraulic fracturing emission rate distributions are similar to those of drilling, possibly due to similar emission sources (combustion) between the operation types. Both have diesel generator emissions along with methane escaping the oil and gas reservoir.

5.3.4. FRACKING/WORKOVER/FLOWBACK. Day 3 at site F1 provided the opportunity to observe emissions during three simultaneous operations. Drilling, flowback, and workover were being performed on three separate wells located on the same well pad. Workover is a process where a producing well is revisited to replace malfunctioning equipment or for re-stimulation. With three separate operations occurring simultaneously, it is surprising that

the emission rate distribution's standard deviation (in log-space) is the smallest compared to other operation types. This site was an example of a relatively constant methane emission rate, in contrast to the other simops site.

5.3.5. DRILLING/FLOWBACK/FRACKING. Site G2 had the three main operation types occurring simultaneously: drilling, fracking, and flowback. The PDF of combined methane emission rates is shown in Figure 5.4 by the green line. The distribution has a median value around 9 g s^{-1} . There are three major peaks: one near 0.1 g s^{-1} , another near 10 g s^{-1} and the largest peak above 100 g s^{-1} . It is possible that the three different operation types sampled on this day correspond to three distinct peaks. This PDF has the fewest points in Figure 5.4, which could also contribute to such a sporadic distribution.

5.3.6. COMPARISON TO OTHER STUDIES. Other studies have examined the emission rate of methane from various processes associated with the production and transport of natural gas. Although these estimates do not correspond exactly to the operation types examined in this thesis, they still provide useful context for the methane emission rates depicted in Figure 5.4. Mitchell et al. (2015) measured the methane emission from processing and gathering facilities. These operations had emission rates that ranged from 0.83 to 166.7 g s^{-1} and 0.19 to 194.4 g s^{-1} respectively [12] which fall within the range of values shown in Figure 5.4, indicating that emission rates measured at processing plants and facilities had comparable emissions to a single well during completion. Mitchell et al. (2015) also found that emission rates span over several orders of magnitude.

In 2012, methane fluxes were characterized for the entire Denver Basin by Pétron et al. (2012) [15]. After normalized by the number of wells in the basin ($\sim 20\,000$), this study found an emission rate of $(0.20 \pm 0.09) \text{ g s}^{-1} \text{ well}^{-1}$ attributed to oil and gas operations. The

emission rates estimated in Garfield county were several orders of magnitude larger than the values for the Denver Basin. The per-well value of methane emissions from Pétron et al. (2012) represents an average methane emission rate during the lifetime of a well (drilling + well completion + production). Karion et al. (2013) also examined total methane fluxes over a basin. For this aircraft study the total emissions from (mostly producing) oil and gas wells were measured for Uintah County, Utah. When these emissions were normalized by the number of wells ($\sim 15\,000$), the average methane emission rate was found to be $(1.0 \pm 0.3) \text{ g s}^{-1} \text{ well}^{-1}$ [84]. This average emission rate is larger than that found in the Denver basin but is still smaller than the mean emission of all the PDFs in Figure 5.4, again suggesting that emissions rates during the drilling and completion operations studies here generally exceed those of the time-averaged well-lifetime emissions.

Brantley et al. (2014) used a mobile plume tracker to estimate the methane fluxes emitted from production pads at three different basins. Emission rates from the Barnett, Denver, and Pinedale basins were 0.33 (0.23, 0.48), 0.14 (0.11, 0.19), and 0.59 (0.47, 0.74) g s^{-1} respectively where the terms in the parentheses are the 95% confidence intervals[85]. Like the aforementioned studies, all methane emission rates remained at or below 1 g s^{-1} . Although the duration of the completion operations is much shorter than many of the operations mentioned above (several weeks versus several decades), the cumulative emissions are non-trivial (Chapter 5.6).

Figure 5.10 summarizes the emission rates calculated for this study and compares them to other relevant studies:

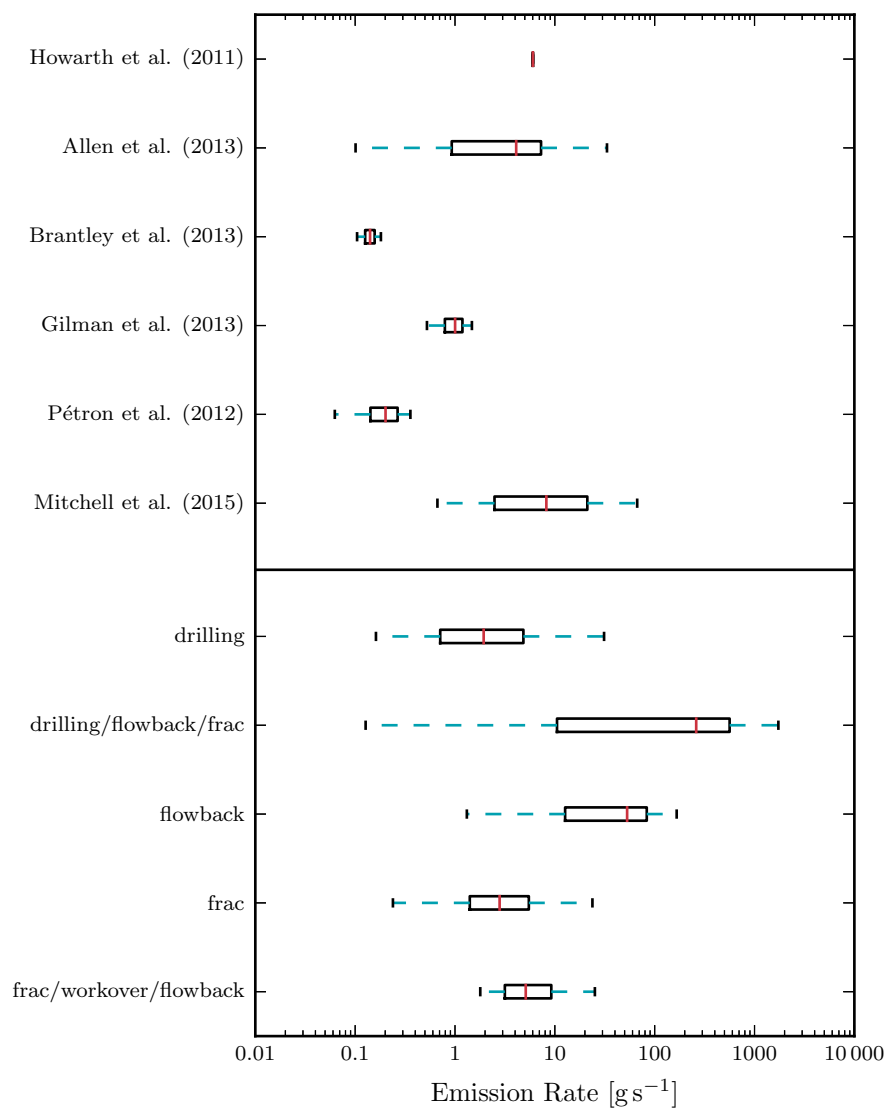


FIGURE 5.10. Comparison of methane emission rates calculated for this study compared to other studies.

5.3.7. METHANE EMISSIONS DURING CANISTER DEPLOYMENT. Each canister collected ambient air samples for a total of 3 minutes during field measurements. Figure 5.11 shows the methane emission rate distributions using data only when the canisters were collecting air samples. This provides insight to gauge if the times when canisters were collecting

were significantly different to all the times included in the distributions in Figure 5.4. The legend shows that the number of points for each operation drops significantly. Some of the operation types have significantly different distributions than Figure 5.4. The high values of the drilling/flowback/fracking distribution are no longer as prevalent. Conversely, the fracking/workover/flowback distribution shifted more towards higher methane emission rates.

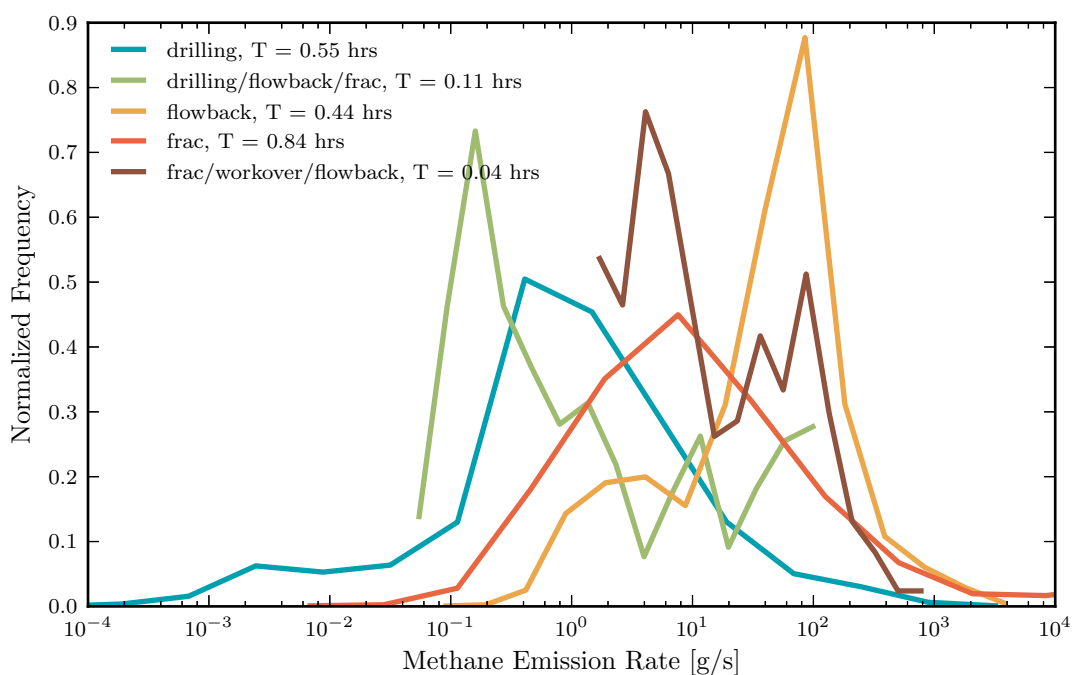


FIGURE 5.11. Methane emission rate distributions during canister sampling times.

Table 5.2 quantifies the details of the emission rate distributions only using time periods during canister collection. When performing emission ratio calculations (Chapter 5.5), the emission rates of various VOCs were normalized by methane emission rates calculated when the canisters were sampling ambient air. The distributions shown in Figure 5.11, not Figure 5.4, will determine the emission factor distributions for the VOCs.

A direct comparison of emission rate distribution metrics can be found in Table G.1.

TABLE 5.2. Emission rate distributions of methane calculated using the tracer ratio method only during times when the canisters were sampling. These data were separated into their respective operation types: drilling, fracking, flowback, and two combination sites. N is the number of canister samples, Med is the median, and SD is the standard deviation (taken in log-space).

Operation Type	Sites	T [hrs]	Mean [g s ⁻¹]	Med [g s ⁻¹]	25 th %ile [g s ⁻¹]	75 th %ile [g s ⁻¹]	SD
drilling	5	0.55	14	0.94	0.33	3.3	1.0
drilling/flowback/frac	1	0.11	13	0.59	0.17	8.7	1.0
flowback	3	0.44	100	52	14	98	0.73
frac	8	0.84	2900	8.2	2.3	37	1.1
frac/workover/flowback	1	0.041	43	9.0	3.8	56	0.66

5.4. EMISSIONS ESTIMATES: VOCs

We used the GC system to determine the mixing ratios for a suite of different compounds. Using the background-subtracted concentrations of acetylene and all the VOCs, we estimated the emission rates of each VOC. Like Section 5.2, the focus of this section will be benzene, toluene, and ethane. The remaining VOCs can be found in Appendix C.

Figure 5.12 shows the emission rate distributions for the three compounds separated by operation type. There were only enough data available to show the emission rate distributions for drilling, hydraulic fracturing, and flowback.

Figure 5.12 shows that benzene has the lowest emission rate in general (compared to toluene and ethane). Hydraulic fracturing fluid has been shown to contain benzene[86] which returns to the surface during the flowback phase. The volatilization of this compound could have contributed to the total benzene emission rate. Hydraulic fracturing had emission rates up to 1 g s⁻¹. During this well completion phase, many large diesel engines were operated at maximum capacity to pump fracturing fluids into the well at high pressure. Benzene is a known additive to petroleum products and has been shown to be emitted during combustion[87]. Drilling requires the generation of power through diesel powered generators

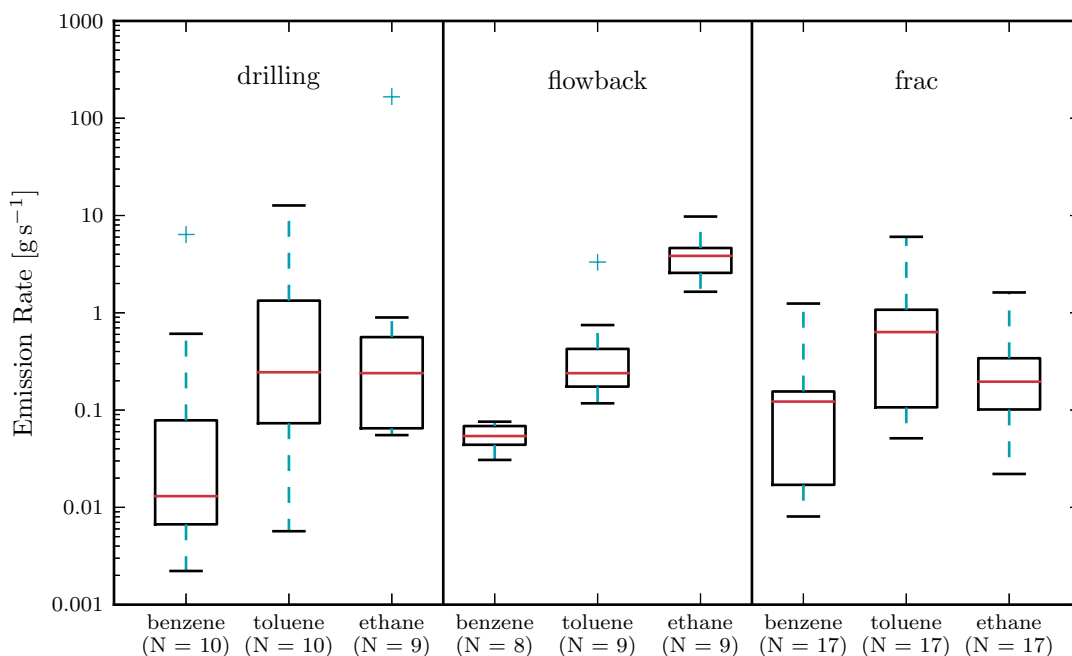


FIGURE 5.12. Emission rate distributions for benzene, toluene, and ethane. These were calculated for each different operation type. N is the number of canister samples.

that emit benzene into the atmosphere. This operation had some of the highest emission rates possibly due to the emissions from the generators. Finally, tight gas formations contain low concentrations of benzene that can be released into the atmosphere[88]. The benzene emission-rate distributions span many orders of magnitude, perhaps due to the variability of engine power and associated exhaust emission rates from the diesel engines. Flowback was found to have a relatively narrow emission rate distribution meaning that the emission rates were more constant during this operation phase. Table 5.3 quantifies the emission rate distributions of benzene.

Pétron et al. (2012) calculated the total flux of benzene from the Denver basin using aircraft measurements. The basin-wide emission rate was normalized by the number of wells ($\sim 20\,000$) in the basin, which gave an estimate of the average emission rate of benzene per well.

TABLE 5.3. Emission rates of benzene calculated using the tracer ratio method. These data were separated into their respective operation types: drilling, fracking, and flowback. N is the number of canister samples, Med is the median, and SD is the standard deviation taken in log-space.

Operation Type	N	Mean [g s ⁻¹]	Med [g s ⁻¹]	25 th %ile [g s ⁻¹]	75 th %ile [g s ⁻¹]	SD
drilling	10	0.72	0.014	0.0067	0.078	1.0
flowback	8	0.055	0.054	0.044	0.069	0.14
frac	17	0.23	0.12	0.017	0.16	0.63

Benzene was measured to be emitting at an average rate of $(2.0 \pm 0.9) \times 10^{-3} \text{ g s}^{-1} \text{ well}^{-1}$ [15]. This rate is at least an order of magnitude lower than the median values calculated from all the canisters available. Swarthout et al. (2013) also estimated the flux of benzene from the Denver basin. This study estimated a benzene flux of $(9 \pm 3) \times 10^{-4} \text{ g s}^{-1} \text{ well}^{-1}$ [21]. The benzene emission rates measured during drilling and well completion were about $3\times$ higher, on average, than from the aforementioned production sites.

Like benzene, toluene is also a tracer for combustion therefore it is not surprising that the highest emission rates were measured during the drilling and hydraulic fracturing phases of the well. Toluene was also found to be an additive to the hydraulic fracturing fluid[86] which could have also contributed to the mixing ratios during fracturing and flowback. Finally, toluene has been shown to be contained within natural gas deposits[89]. Toluene emission rates were about an order of magnitude higher than benzene emission rates for all operation types. The width of the toluene emission rate distribution was also consistent with the benzene distribution width across the three different operation types, which indicates that benzene and toluene were emitted from the same source. The combustion of diesel fuel is most likely the largest source of these BTEX compounds. No other studies have reported the toluene emission rate from oil and gas operations. Table 5.4 quantifies the emission rate distributions shown in Figure 5.12:

TABLE 5.4. Emission rates of toluene calculated using the tracer ratio method. These data were separated into their respective operation types: drilling, fracking, and flowback. N is the number of canister samples, Med is the median, and SD is the standard deviation taken in log-space.

Operation Type	N	Mean [g s ⁻¹]	Med [g s ⁻¹]	25 th %ile [g s ⁻¹]	75 th %ile [g s ⁻¹]	SD
drilling	10	2.4	0.25	0.073	1.3	1.0
flowback	9	0.63	0.24	0.17	0.43	0.42
frac	17	1.2	0.63	0.11	1.1	0.62

Figure 5.13 shows the emission rates of benzene and toluene plotted against each other.

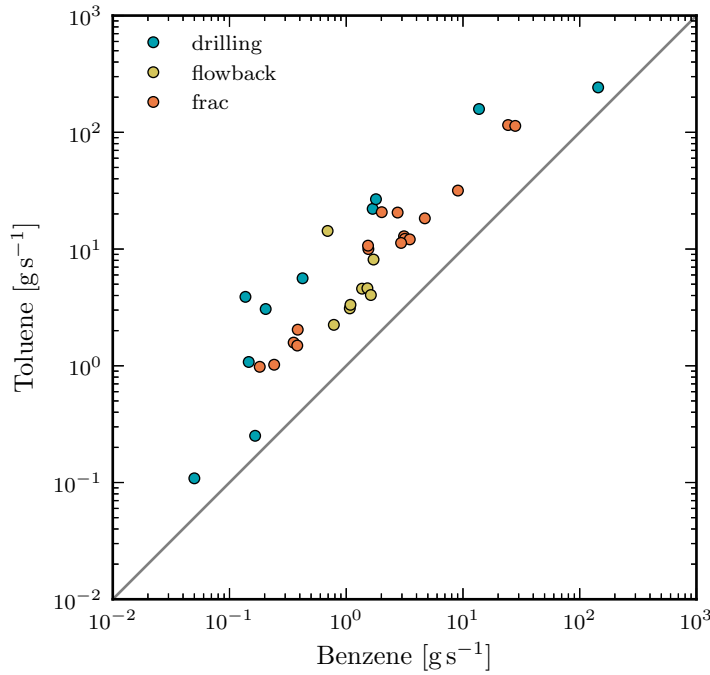


FIGURE 5.13. Emission rates of benzene and toluene plotted against each other. These data have an r^2 of 0.84 (log-space), a log-mean bias of 0.72, and a slope of 8.3.

The data have an r^2 of 0.84 (log-space), a log-mean bias of 0.72, and a slope of 8.3. The two compounds correlate with each other across all three operation types.

Ethane is considered a tracer for natural gas. The ethane emission rates were of similar magnitude to toluene during drilling and hydraulic fracturing. During flowback, however,

the emission rate of ethane was an order of magnitude larger than toluene. This suggests that natural gas from the Williams Fork formation was emitted at much higher rates during flowback than during the other two operation types. Ethane emission rates were non-trivial for drilling and hydraulic fracturing; therefore, natural gas was a smaller, yet still significant, source of hydrocarbons into the atmosphere during these operations. Table 5.5 quantifies the emission rate distributions for ethane:

TABLE 5.5. Emission rates of ethane calculated using the tracer ratio method. These data were separated into their respective operation types: drilling, fracking, and flowback. N is the number of canister samples, Med is the median, and SD is the standard deviation taken in log-space.

Operation Type	N	Mean [g s ⁻¹]	Med [g s ⁻¹]	25 th %ile [g s ⁻¹]	75 th %ile [g s ⁻¹]	SD
drilling	9	19	0.24	0.065	0.56	1.0
flowback	9	4.2	3.8	2.6	4.6	0.21
frac	17	0.35	0.20	0.10	0.34	0.48

Swarthout et al. (2013) estimated that $(0.05 \pm 0.01) \text{ g s}^{-1}$ of ethane was emitted per well in the Denver Basin[21]. I normalized the emission rate reported in the study by the number of wells in that region in 2013 ($\sim 20\,000$). This value is much lower than any ethane emission rates estimated in this study indicating that well drilling and completion operations emit natural gas into the atmosphere at a much higher rate than production sites.

5.5. EMISSION RATIOS

Calculating emission rates for VOCs provided the opportunity to calculate emission ratios of NM-VOCs with respect to methane. This information can be used to infer the emission rates of NM-VOCs when only information about methane emissions is available. I performed this calculation using the average methane emission rate (from the Picarro) over the three

minutes that each canister was deployed. The emission factor distributions for benzene, toluene and ethane are shown in Figure 5.14.

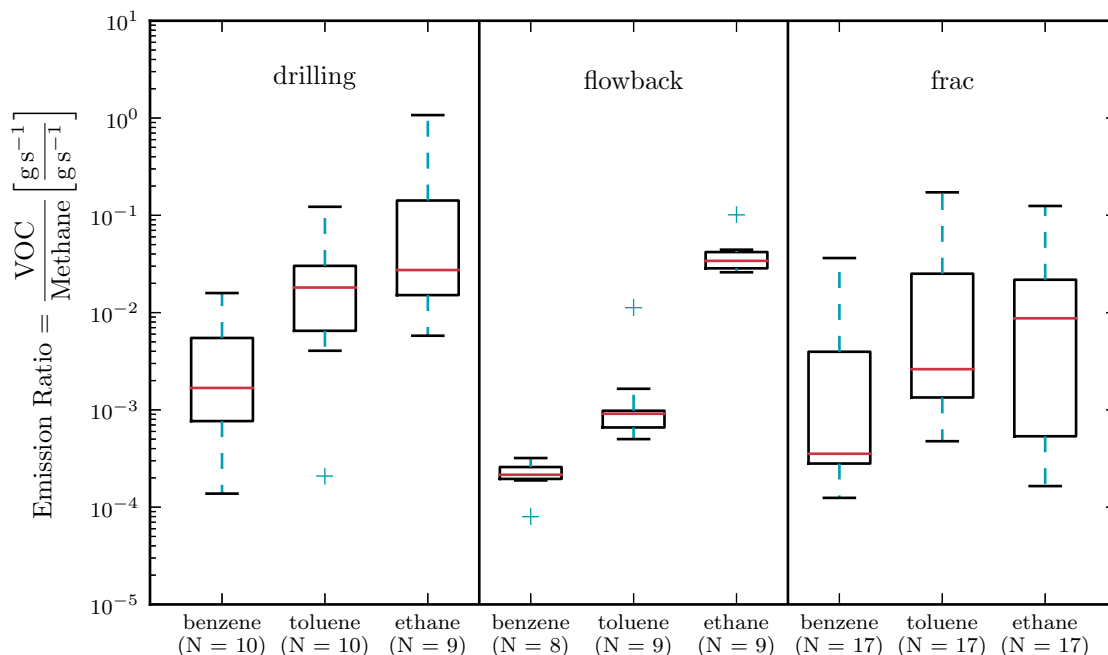


FIGURE 5.14. Emission ratio distributions for benzene, toluene, and ethane. N is the number of canister samples.

Ethane was found to have emission rates that were higher than benzene and toluene during flowback (Figure 5.12); therefore, it is no surprise that ethane also has flowback emission *ratios* higher than benzene and toluene. This indicates that a larger amount of natural gas was emitted during the flowback phase. Emission ratio distributions during flowback are very narrow in comparison to drilling and hydraulic fracturing which means flowback operations measured during the field study had more constant emission rates of VOCs. Drilling and hydraulic fracturing have ethane emission ratios that are comparable to toluene (a tracer for combustion). During drilling operations, the ethane emission ratio distribution is slightly higher than benzene and toluene. There were natural gas emissions during drilling but not as much as during flowback. Hydraulic fracturing had some of the

lowest ethane emission ratios suggesting this operation type does not emit as much natural gas into the atmosphere compared to the other operation types. Table 5.6 quantifies the ethane emission ratios for ethane:

TABLE 5.6. Emission ratios of ethane. These data were separated into their respective operation types: drilling, fracking, and flowback. N is the number of canister samples, Med is the median, and SD is the standard deviation taken in log-space.

Operation Type	<i>N</i>	Mean	Med	25 th %ile	75 th %ile	SD
drilling	9	0.19	0.027	0.015	0.14	0.70
flowback	9	0.042	0.034	0.029	0.042	0.17
frac	17	0.021	0.0087	0.000 54	0.022	0.89

The ethane emission ratios changing over different operation phases could be partly due to the composition of natural gas changing between site locations. Harris et al. (2013) found that the wetness of natural gas in the Piceance Basin can change by about 15% when sampled at four different locations in Garfield County[88]. Sources of methane and ethane at the well pads that were not directly from the Williams Fork formation could have also changed the ethane emission ratio.

The emission ratios of toluene are consistently greater than those of benzene by about an order of magnitude. The emission ratios of benzene and toluene are quantified in Tables 5.7 and 5.8 respectively.

TABLE 5.7. Emission ratios of benzene. These data were separated into their respective operation types: drilling, fracking, and flowback. N is the number of canister samples, Med is the median, and SD is the standard deviation taken in log-space.

Operation Type	<i>N</i>	Mean	Med	25 th %ile	75 th %ile	SD
drilling	10	0.0040	0.0017	0.000 77	0.0055	0.61
flowback	8	0.000 22	0.000 22	0.000 20	0.000 26	0.18
frac	17	0.0041	0.000 35	0.000 28	0.0040	0.74

TABLE 5.8. Emission ratio of toluene. These data were separated into their respective operation types: drilling, fracking, and flowback. N is the number of canister samples, Med is the median, and SD is the standard deviation taken in log-space.

Operation Type	N	Mean	Med	25 th %ile	75 th %ile	SD
drilling	10	0.033	0.018	0.0065	0.030	0.75
flowback	9	0.0020	0.000 91	0.000 66	0.000 98	0.38
frac	17	0.019	0.0026	0.0013	0.025	0.74

In general, 1000 g of methane is emitted for every 1 g of benzene during drilling and hydraulic fracturing and during flowback 10 000 g of methane is emitted for every 1 g of benzene. Of note is the significant drop of benzene and toluene emission ratios during flowback. Diesel generators are not as prevalent during the flowback stage as during drilling or hydraulic fracturing providing further evidence that benzene and toluene are emitted primarily as combustion products from diesel generators.

5.6. ANALYSIS OF INTEGRATED EMISSIONS OVER PROCESS LIFETIME

The emission rates calculated in this study for drilling and completion operations were generally found to be much higher than the rates measured in other basins for production sites. The duration of drilling and completion operations, on the other hand, is much shorter than the lifetime of a producing well. The cumulative emissions of methane for each completion operation normalized by the cumulative 30-year average emissions found in Pétron et. al (2012) are shown in Figure 5.15. The typical duration of each operation was estimated using field measurement information and communication with the oil and gas industry partners. I randomly sampled the emission rate distributions and typical time scales to create the probability distribution functions.

Using the total (drilling + fracking + flowback) distribution in Figure 5.15, cumulative emissions from drilling and completion can contribute from 0.1 to 10% (with a peak around 4%) of the total methane emissions during a well's 30 year lifetime.

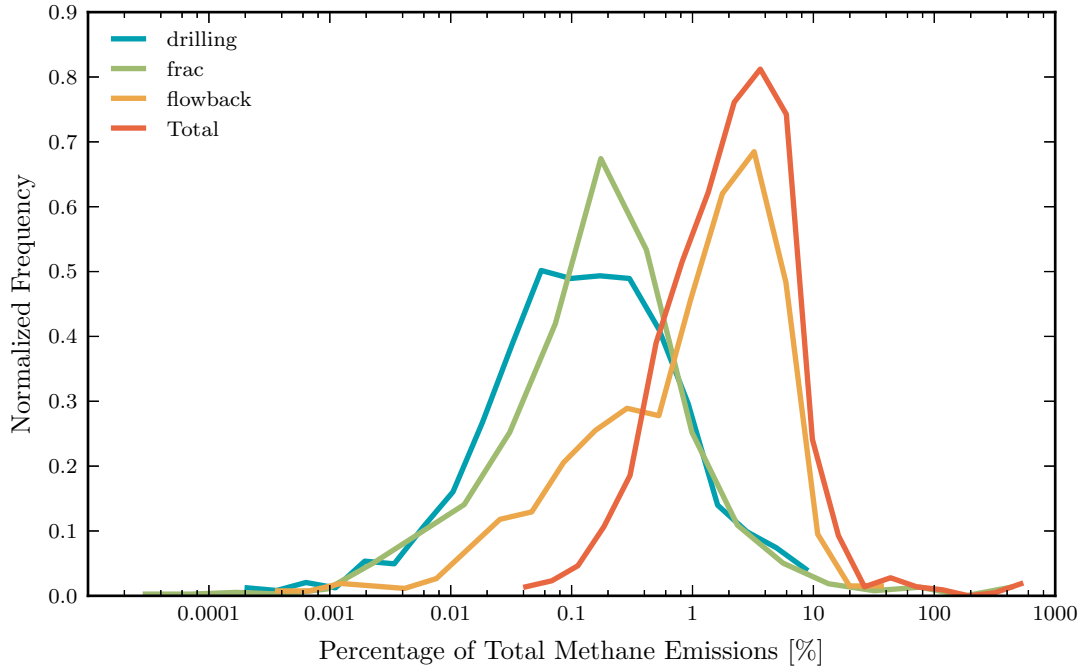


FIGURE 5.15. Percentage of total methane emissions during drilling, fracking, and flowback compared to the total emissions estimated using values from Pétron et al. (2012).

Methane emissions during well completion are typically considered to be insignificant compared to production. This result emphasizes that well completion emits a non-trivial amount of methane that should be considered when creating emission inventories for the oil and gas industry.

CHAPTER 6

DISPERSION MODELING RESULTS

6.1. REPLICATION OF FIELD MEASUREMENTS

We used AERMOD to model the downwind concentrations for specific field sites that were measured during the field campaign (< 500 m). Information from the meteorological station regarding the atmospheric boundary layer properties was used in AERMOD to perform this modeling experiment (explained in Section 3.5). We replicated the dispersion of the tracer, acetylene, in the model because it was the only gas where both the release rate and location were accurately known. The GC system was able to determine the concentration of acetylene within the canisters, therefore model receptors were placed exactly where the measurement canisters were placed (vertically and horizontally). We compared the background-corrected (using the background canister) concentration of acetylene for each canister to the hourly averaged concentration predicted by AERMOD in Figure 6.1 where each different color represents a different site.

I adjusted the predicted mixing ratios of AERMOD using the following equation:

$$(6.1) \quad C_2 = C_1 \left(\frac{\Delta t_1}{\Delta t_2} \right)^q$$

where q was suggested to be 0.17 by Nonhebel[90]. This accounts for the differences in Gaussian plume shapes because of the difference in sampling times between the model and the canisters (1 hour vs. 3 minutes). In general, AERMOD was able to predict concentrations with a low bias but with a large amount of scatter. The model and measurements had a correlation coefficient of 0.0007, a log-mean bias of -0.007 , and a slope of 0.91. Some

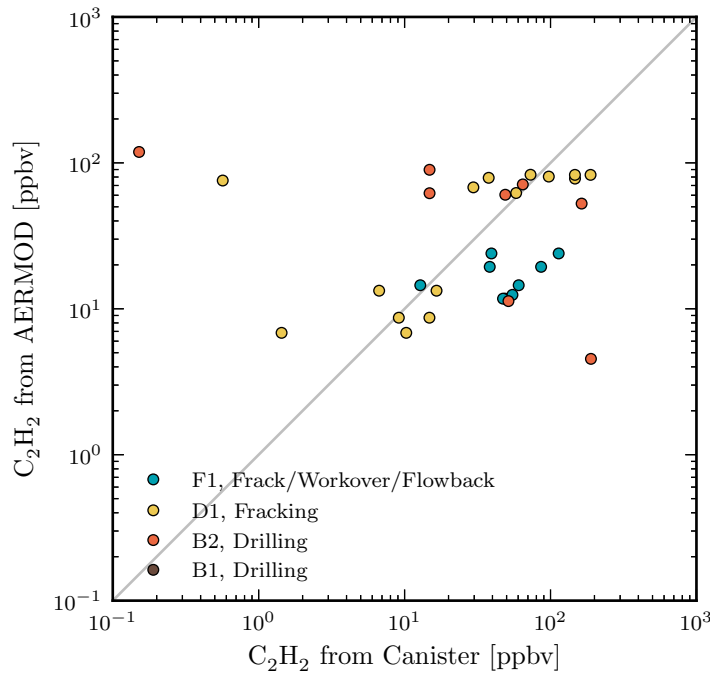


FIGURE 6.1. Comparison of canister acetylene mixing ratio measurements to AERMOD estimates. These data have a correlation coefficient of $R^2 = 0.0007$, a log-mean bias of -0.007 , and a slope of 0.91 .

points are situated close to the one-to-one line and there were times when AERMOD was able to capture the general trend of emissions. The higher outliers may have been caused by AERMOD underpredicting the atmospheric instability and not allowing the acetylene plume to be adequately diluted. Low outliers may be due to the plume not being advected to the same location as it was during fieldwork and the AERMOD predicted concentration therefore is lower. AERMOD could also be over-predicting the atmospheric instability causing the plume to be more dilute.

Considering the canisters were open for three minutes and AERMOD was only capable of resolving concentration fields at one hour intervals, the general agreement gave credibility to performing dispersion modeling over different meteorological conditions experienced in

Garfield County. With no strong bias, AERMOD can be used to determine concentration fields on longer time scales where instantaneous concentrations are not as important.

6.2. DISPERSION MODELING UNDER VARIOUS METEOROLOGICAL CONDITIONS

With the accuracy of the model examined, we modeled the concentration fields surrounding the well pads for different operation types under a series of different meteorological conditions. The NARR dataset for 2014 was used as inputs for surface and vertical profile parameters. The year 2014 was chosen because it was the most recent, complete Julian year of meteorological data in NARR.

Figure 6.2 shows the seasonal-mean concentration fields of benzene surrounding site D1 for a series of meteorological conditions, a hydraulic fracturing site. The mean value from the hydraulic fracturing emission rate distribution was chosen as the emission rate of benzene for this simulation. The oil and gas well pad is located at $(x, y) = (1000 \text{ m}, 1000 \text{ m})$ and this model was run with a horizontal resolution of 25 m. The white circles denote various distances away from the well pad (350, 500, 1000, and 2000 ft). The colors represent the average mixing ratio of benzene surrounding the site after modeling the meteorology of 2014. The colorbar used a log-scale due to the mixing ratios spanning three orders of magnitude over the 4 km^2 domain.

The seasonal-mean concentration fields are somewhat evenly distributed radially surrounding the well pad. There was some preference for the wind direction to be coming from the southwest using the NARR meteorology. This location is situated within a valley so the winds were funnelled from south to north. This explains the higher concentrations of methane in the NNW. Field work was valuable because the actual concentrations of VOCs downwind were measured. While it was impossible to measure the concentrations gases downwind for

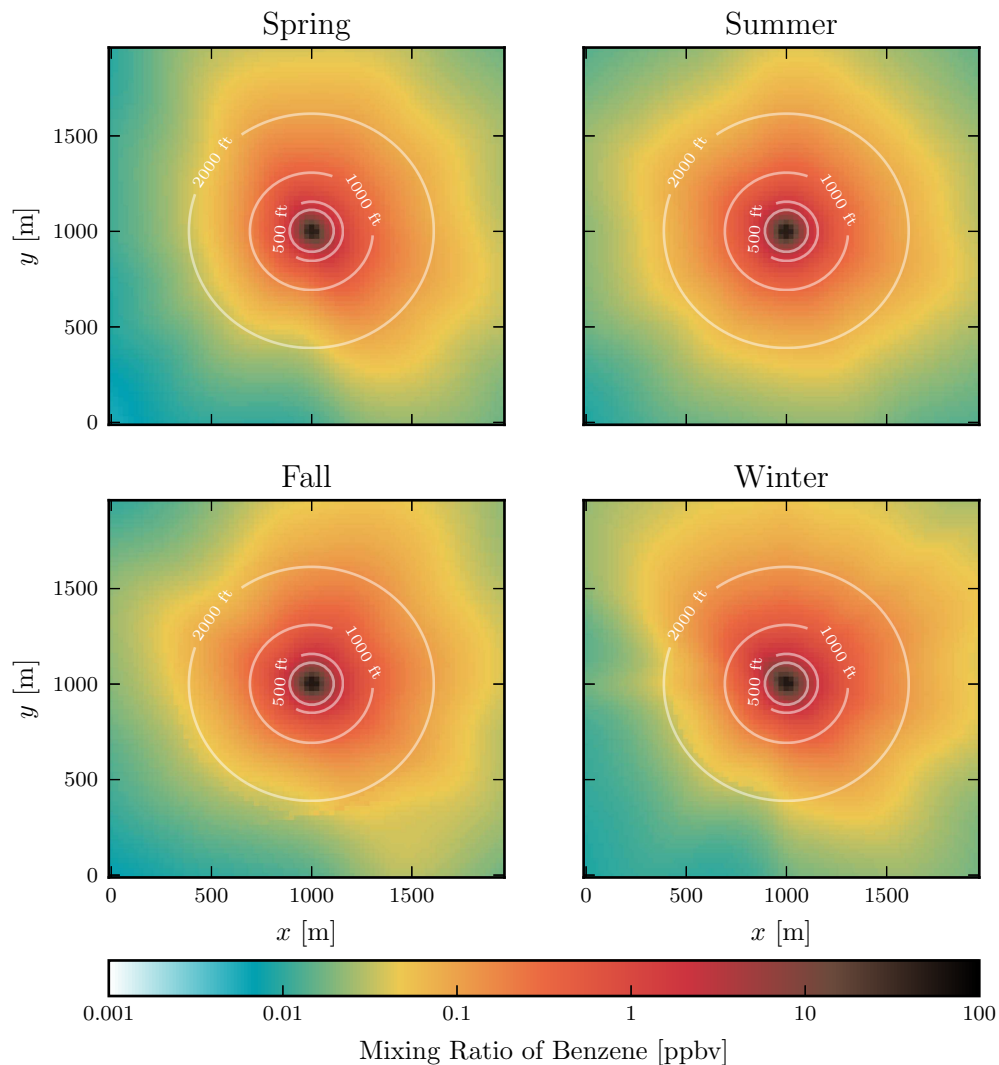


FIGURE 6.2. Mixing ratio field of benzene predicted by AERMOD for site D1 using the mean hydraulic fracturing emission rate for 4 seasons. The four concentric circles indicate various distances away from the well pad (in feet).

all meteorological conditions, dispersion modeling allowed us to estimate concentration fields using emission rates calculated with data collected in the field. An important assumption was that the emission rate did not change over all of the meteorological conditions. For a given location, operation type, and emission rate, this modeling study provided downwind concentrations for the variety of meteorological conditions that Garfield County encounters

on an annual basis This analysis provides the concentration probabilities at a given distances for the meteorological condistions experienced in Garfield County.

For the annual simulations with AERMOD, 36 receptors were placed at distances of 350, 500, 1000, and 2000 ft away from the well pad. Figure 6.3 shows a PDF of the mixing ratios of benzene at different distances away from the well pad for each hour of 2014. These distributions are log-normal and slightly skewed to lower values. The arithmetic means for each distribution is plotted using dashed lines. This represents the annual mean mixing ratio at each distance away from the well. The mean mixing ratios of benzene in Figure 6.3 are below 1 ppbv at distances greater than 350 ft; however, instantaneous concentrations can be much higher than 1 ppbv at distances greater than 350 ft depending on the meteorology.

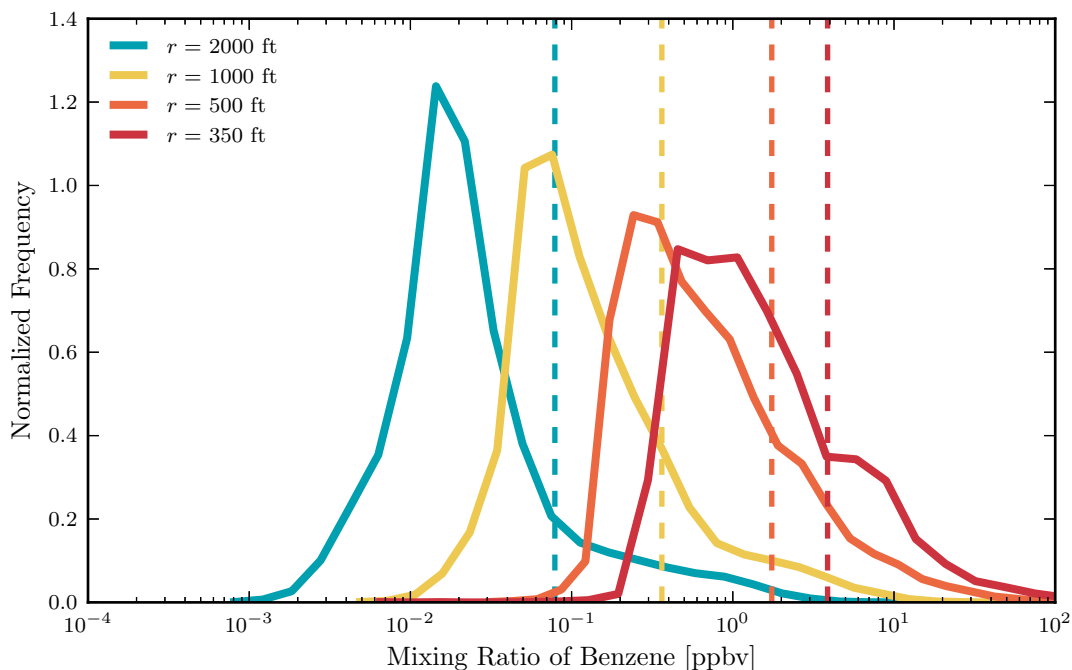


FIGURE 6.3. Predicted benzene mixing ratio distributions for various distances away from the well pad using AERMOD. The distribution is made up of the hourly-averages mixing ratios over the year 2014. The mean benzene emission rate from hydraulic fracturing distributions was used.

On average there are higher concentrations at 350 ft due to the plume not having as much time to mix with the ambient air. Figure 6.3 shows that using only one emission rate, the mixing ratios can vary over two orders of magnitude for a single distance from the well pad. Exact mixing ratios surrounding oil and gas wells are extremely difficult to predict due to changing meteorological conditions. The most informative method is to give a distribution of values rather than a single value.

6.3. MODELING OF ALL SITES

In the previous Section, the analysis has only been performed for site D1. Figure 6.4 was made by simulating and combining all the oil and gas sites measured during the field campaign and creating a cumulative distribution function (CDF). Since the meteorological station was not present for the entire year of 2014, the NARR database was used exclusively to calculate the surface and vertical- profile meteorological information. The steps taken to calculate the surface meteorological variables are outlined in Section 3.5. This plot gives general information about the concentration field of a particular gas in Garfield County if the emission rate is known.

These CDFs in Figure 6.4 can help estimate upper limits on concentration given a distance from the source and an emission rate. For example, 2000 ft away from a source emitting 1 g s^{-1} of methane, 99% of the concentrations are expected to be below $\sim 11 \mu\text{g m}^{-3}$. If the observed variability of emission rates is also included in this analysis, it is nearly impossible to definitively determine an exact concentration surrounding an oil and gas site for a specific time/place downwind.

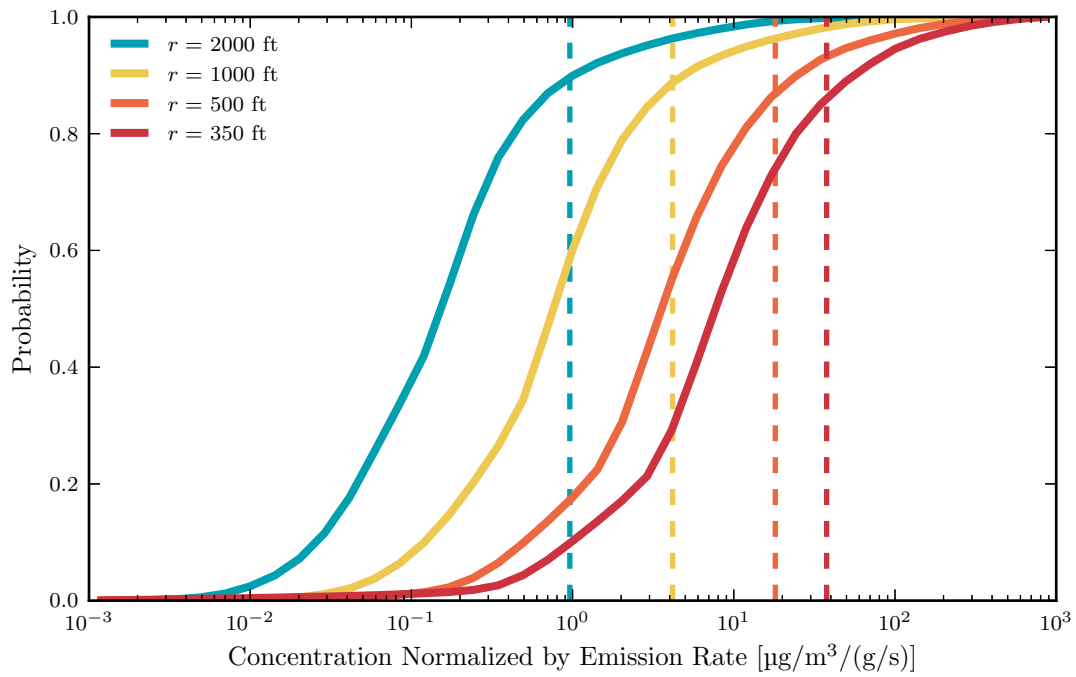


FIGURE 6.4. Concentration CDFs normalized by emission rate. The distribution is made up of all the hourly-average concentrations from each fieldwork site over the year 2014.

CHAPTER 7

CONCLUSIONS

Measurements of methane and VOCs were taken at 18 oil and gas sites in Garfield County, Colorado. Overall, the methane and benzene emission rates were found to be substantially higher than other studies that measured emission rates from production sites. Toluene emission rates were consistently higher than benzene emission rates – there were no studies to compare our values of emission rates of toluene. Drilling and fracking emissions appear to be strongly influenced by combustion emissions from pad equipment while flowback emissions are more strongly dominated by release of natural gas from the mineral deposit. The drilling and well completion sites were found to emit much more methane and VOCs than production sites but over a shorter amount of time. The cumulative methane emissions during well drilling and completions could account from 0.1 to 10% of what is emitted during a 30 year production phase. Drilling and well completion was found to be an important source of methane emissions into the atmosphere that should be accounted for in oil and gas emission inventories.

Some completion operation types were found to be more predictable than others. Drilling, for example, had a fairly consistent lognormal methane emission rate distribution centered around 1 g s^{-1} . Whereas fracking had emission rates that varied over six orders of magnitude and thus varied in time and/or location.

The emissions reported in this thesis were measured at 18 sites with a total measurement time of 4.25 hours. This small sample size indicates there could be a large amount of uncertainty in the results. Given the small number of studies examining the emissions from

drilling and well completion operations, this field study is beginning to fill the information gap of these operation types.

AERMOD is an atmospheric chemical dispersion model. The model was challenged to accurately predict individual short term concentration fields due to the model's one hour timestep, but the resulting concentration predictions had relatively low bias on average. We used this model to predict the concentration field surrounding oil and gas wells over one year of meteorology. The predicted average concentrations at various distances away from the well pad spanned at least two orders of magnitude when using a constant emission rate. If we included the variance in emission rates, the predicted concentration fields could span nearly five or six orders of magnitude.

Predicting concentration fields surrounding a particular well site in Garfield County is challenging. The emission-rate distributions show that some days have low emission rates of methane and HAPs whereas others can have extremely high emission rates. This study has made major strides by quantifying the emission rates from various drilling and completion operations.

CHAPTER 8

FUTURE WORK

There is much to be explored with the valuable data that was collected in Garfield County, Colorado. The dataset that was used in this thesis is incomplete, and we expect the number of cases to increase from what is used here by 33%. Therefore, the analysis of the complete dataset may provide more complete results.

The EPA has developed a method known as the OTM33A method, which calculates species emissions rates without the use of a passive tracer (unlike the TRM used in this thesis). OTM33A assumes a Gaussian point source plume and uses concentration and meteorological measurements to estimate the emission rate. Since the mobile plume tracker collects methane concentration information at a high temporal frequency, this method could easily be applied to the field data. This would allow comparison between the tracer ratio method and the OTM33A method to contribute further to the findings of Wells et al. (2015), which compared TRM and OTM33A for controlled-release experiments and found the TRM to be a more accurate method.

We found AERMOD to perform poorly when comparing to measured acetylene concentrations. The use of a more advanced fluid-dynamics model (e.g. one that more-explicitly calculates turbulent diffusion and flow around topography) could improve estimates of methane and NM-VOC concentrations downwind. OpenFOAM is a model that is well suited for this purpose as it can include terrain and use many different atmospheric turbulence schemes. Although more computational power is required, this model could yield more realistic results.

Finally, field measurement techniques could be improved. Sampling further downwind for longer time-scales might yield more accurate results because the tracer and VOC plumes will be more homogeneous and well mixed.

BIBLIOGRAPHY

- [1] M. A. Toman and B. Jemelkova, “Energy and economic development: an assessment of the state of knowledge,” *Energy Journal*, vol. 24, no. 4, pp. 93–112, 2003.
- [2] U.S. Energy Information Administration, “Annual energy outlook 2015 with projections to 2040,” tech. rep., April 2015.
- [3] U.S. Energy Information Administration, “Annual energy outlook 2013 with projections to 2040,” tech. rep., April 2013.
- [4] A. P. Hamblin, “The ‘shale gas’ concept in canada: a preliminary inventory of possibilities,” tech. rep., Geological Survey of Canada, September 1 2006.
- [5] Field, Soltis, and Murphy, “Air quality concerns of unconventional oil and natural gas production,” *Environmental Science: Processes & Impacts*, vol. 16, no. 5, 2014.
- [6] M. K. Hubbert and D. G. Willis, “Mechanics of hydraulic fracturing,” *Mem.-Am.Assoc.Pet.Geol.:(United States)*, vol. 18, 1972.
- [7] Colorado Oil and Gas Conservation Commission, (COGCC), “Colorado weekly & monthly oil & gas statistics,” January 15 6.
- [8] J. G. Weber, “The effects of a natural gas boom on employment and income in colorado, texas, and wyoming,” *Energy Economics*, vol. 34, no. 5, pp. 1580–1588, 2012.
- [9] G. Myhre, D. Shindell, F. M. Bréon, W. Collins, J. Fuglestedt, J. Huang, D. Koch, J. F. Lamarque, D. Lee, B. Mendoza, T. Nakajima, A. Robock, G. Stephens, T. Takemura, and H. Zhang, *Anthropogenic and Natural Radiative Forcing*, pp. 659–740. Climate Change 2013: The Physical Science Basis. Contribution of Working Group I to the Fifth Assessment Report of the Intergovernmental Panel on Climate Change,

- Cambridge, United Kingdom and New York, NY, USA: Cambridge University Press, 2013.
- [10] Alvarez, Pacala, Winebrake, Chameides, and Hamburg, “Greater focus needed on methane leakage from natural gas infrastructure,” *Proceedings of the National Academy of Sciences*, vol. 109, no. 17, pp. 6435–6440, 2012.
- [11] K. Larsen, M. Delgado, and P. Marsters, “Untapped potential: Reducing global methane emissions from oil and natural gas systems,” tech. rep., Environmental Defense Fund, April 2015.
- [12] Mitchell, Tkacik, Roscioli, Herndon, Yacovitch, Martinez, Vaughn, Williams, Sullivan, Floerchinger, Omara, Subramanian, Zimmerle, Marchese, and Robinson, “Measurements of methane emissions from natural gas gathering facilities and processing plants: Measurement results,” *Environmental Science & Technology*, vol. 49, no. 5, pp. 3219–3227, 2015.
- [13] Allen, Torres, Thomas, Sullivan, Harrison, Hendler, Herndon, Kolb, Fraser, Hill, Lamb, Miskimins, Sawyer, and Seinfeld, “Measurements of methane emissions at natural gas production sites in the united states,” *Proceedings of the National Academy of Sciences*, vol. 110, no. 44, pp. 17768–17773, 2013.
- [14] U.S. Environmental Protection Agency, “Inventory of u.s. greenhouse gas emissions and sinks: 1990 – 2011,” tech. rep., April 12 2013. EPA 430-R-13-001.
- [15] G. Pétron, G. Frost, B. R. Miller, A. I. Hirsch, S. A. Montzka, A. Karion, M. Trainer, C. Sweeney, A. E. Andrews, L. Miller, J. Kofler, A. Bar-Ilan, E. J. Dlugokencky, L. Patrick, C. T. Moore, T. B. Ryerson, C. Siso, W. Kolodzey, P. M. Lang, T. Conway, P. Novelli, K. Masarie, B. Hall, D. Guenther, D. Kitzis, J. Miller, D. Welsh, D. Wolfe,

- W. Neff, and P. Tans, “Hydrocarbon emissions characterization in the colorado front range: A pilot study,” *Journal of Geophysical Research: Atmospheres*, vol. 117, no. D4, 2012.
- [16] N. G. Phillips, R. Ackley, E. R. Crosson, A. Down, L. R. Hutyra, M. Brondfield, J. D. Karr, K. Zhao, and R. B. Jackson, “Mapping urban pipeline leaks: Methane leaks across boston,” *Environmental Pollution*, vol. 173, p. 4, February 2013.
- [17] D. A. Savitz and K. W. Andrews, “Review of epidemiologic evidence on benzene and lymphatic and hematopoietic cancers,” *American Journal of Industrial Medicine*, vol. 31, no. 3, pp. 287–295, 1997.
- [18] A. L. Bolden, C. F. Kwiatkowski, and T. Colborn, “New look at BTEX: Are ambient levels a problem?,” *Environmental Science & Technology*, 2015. doi: 10.1021/es505316f.
- [19] L. M. McKenzie, R. Z. Witter, L. S. Newman, and J. L. Adgate, “Human health risk assessment of air emissions from development of unconventional natural gas resources,” *Science of The Total Environment*, vol. 424, p. 87, 2012.
- [20] E. J. Esswein, J. Snawder, B. King, M. Breitenstein, M. Alexander-Scott, and M. Kiefer, “Evaluation of some potential chemical exposure risks during flowback operations in unconventional oil and gas extraction: Preliminary results,” *Journal of Occupational and Environmental Hygiene*, vol. 11, no. 10, p. D184, 2014. doi: 10.1080/15459624.2014.933960.
- [21] R. F. Swarthout, R. S. Russo, Y. Zhou, A. H. Hart, and B. C. Sive, “Volatile organic compound distributions during the nachtt campaign at the boulder atmospheric observatory: Influence of urban and natural gas sources,” *Journal of Geophysical Research: Atmospheres*, vol. 118, no. 18, p. 637, 2013.

- [22] Gilman, Lerner, Kuster, and de Gouw, “Source signature of volatile organic compounds from oil and natural gas operations in northeastern colorado,” *Environmental Science & Technology*, 2013.
- [23] Warneke, Geiger, Edwards, Dube, Pétron, Kofler, Zahn, Brown, Graus, Gilman, Lerner, Peischl, Ryerson, de Gouw, and Roberts, “Volatile organic compound emissions from the oil and natural gas industry in the uintah basin, utah: oil and gas well pad emissions compared to ambient air composition,” *Atmospheric Chemistry and Physics*, vol. 14, no. 20, p. 10988, 2014.
- [24] U.S. Environmental Protection Agency, “National ambient air quality standards for ozone; final rule,” *Federal Register*, vol. 73, no. 60, p. 38856, 2008.
- [25] U.S. Environmental Protection Agency, “U.S. EPA. air quality criteria for ozone and related photochemical oxidants,” tech. rep., 2006. EPA/600/R-05/004aF-cF.
- [26] R. C. Schnell, S. J. Oltmans, R. R. Neely, M. S. Endres, J. V. Molenaar, and A. B. White, “Rapid photochemical production of ozone at high concentrations in a rural site during winter,” *Nature Geoscience*, vol. 2, no. 2, pp. 120–122, 2009. 10.1038/ngeo415.
- [27] Field, Soltis, McCarthy, Murphy, and Montague, “Influence of oil and gas field operations on spatial and temporal distributions of atmospheric non-methane hydrocarbons and their effect on ozone formation in winter,” *Atmospheric Chemistry and Physics*, vol. 15, no. 6, pp. 3527–3542, 2015.
- [28] Edwards, Young, Aikin, deGouw, Dubé, Geiger, Gilman, Helmig, Holloway, Kercher, Lerner, Martin, McLaren, Parrish, Peischl, Roberts, Ryerson, Thornton, Warneke, Williams, and Brown, “Ozone photochemistry in an oil and natural gas extraction

- region during winter: simulations of a snow-free season in the Uintah basin, Utah,” *Atmospheric Chemistry and Physics*, vol. 13, no. 17, pp. 8955–8971, 2013.
- [29] Colorado Department of Public Health and Environment, (CDPHE), “Denver metropolitan area and north front range 8-hour ozone state implementation plan,” tech. rep., 2008.
- [30] Committee on Management and Effects of Coalbed Methane Development and Produced Water in the Western United States and Committee on Earth Resources and Board on Earth Sciences and Resources and Water Science and Technology Board and Division on Earth and Life Studies and National Research Council, *Management and Effects of Coalbed Methane Produced Water in the Western United States*. The National Academies Press.
- [31] V. A. Kuuskraa and J. Ammer, “Tight gas sands development—how to dramatically improve recovery efficiency,” *GasTIPS*, vol. 10, no. 1, pp. 15–20, 2004.
- [32] E. D. Alcock, H. H. Aronson, and C. F. Knutson, “Massive fracturing of tight gas-bearing sandstone reserves in the Piceance Creek basin, Colorado,” *Rocky Mountain Association of Geologists*, pp. 199–203, 1974.
- [33] Colorado Oil and Gas Conservation Commission, (COGCC), “Cogis permits.”
- [34] D. Dennison, “Drilling of a natural gas well and natural gas production in the Piceance basin.”
- [35] Colorado Oil and Gas Conservation Commission, (COGCC), “Casing cement nomenclature: Various configurations.”
- [36] Meyer & Associates Inc, *Meyer Fracturing Simulators User’s Guide*. ninth edition ed., 2011.

- [37] D. J. Lampe and J. F. Stolz, “Current perspectives on unconventional shale gas extraction in the appalachian basin,” *Journal of Environmental Science and Health, Part A*, vol. 50, no. 5, pp. 434–446, 2015. doi: 10.1080/10934529.2015.992653.
- [38] Ground Water Protection Council and ALL Consulting, “Modern shale gas development in the united states: A primer,” tech. rep., U.S. Department of Energy, April 2009.
- [39] W. K. Overbrey Jr., A. B. Yost, and D. A. Wilkins, “Inducing multiple hydraulic fractures from a horizontal wellbore,” *Society of Petroleum Engineers*, 1988.
- [40] L. O. Haluszczak, A. W. Rose, and L. R. Kump, “Geochemical evaluation of flowback brine from marcellus gas wells in pennsylvania, usa,” *Applied Geochemistry*, vol. 28, p. 61, January 2013.
- [41] Y. Lester, I. Ferrer, E. M. Thurman, K. A. Sitterley, J. A. Korak, G. Aiken, and K. G. Linden, “Characterization of hydraulic fracturing flowback water in colorado: Implications for water treatment,” *Science of The Total Environment*, vol. 512–513, no. 0, pp. 637–644, 2015.
- [42] U.S. Environmental Protection Agency, “Reduced emissions completions for hydraulically fractured natural gas wells,” tech. rep., 2011.
- [43] C. Clark, A. Burnham, C. Harto, and R. Horner, “Hydraulic fracturing and shale gas production: Technology, impacts and regulations.,” tech. rep., U.S. Department of Energy, April 2013.
- [44] Allen, Pacsi, Sullivan, Zavala-Araiza, Harrison, Keen, Fraser, D. Hill, Sawyer, and Seinfeld, “Methane emissions from process equipment at natural gas production sites

- in the united states: Pneumatic controllers,” *Environmental Science & Technology*, vol. 49, no. 1, pp. 633–640, 2015.
- [45] Howarth, Santoro, and Ingraffea, “Methane and the greenhouse-gas footprint of natural gas from shale formations,” *Climatic Change*, vol. 106, no. 4, pp. 679–690, 2011.
- [46] Zavala-Araiza, Allen, Harrison, George, and Jersey, “Allocating methane emissions to natural gas and oil production from shale formations,” *ACS Sustainable Chemistry & Engineering*, vol. 3, no. 3, pp. 492–498, 2015.
- [47] B. Wells, “The validation of emission rate estimation methods,” Master’s thesis, Colorado State University, 2015.
- [48] B. Galle, J. Samuelsson, B. H. Svensson, and G. Börjesson, “Measurements of methane emissions from landfills using a time correlation tracer method based on ftir absorption spectroscopy,” *Environmental Science & Technology*, vol. 35, no. 1, pp. 21–25, 2001. doi: 10.1021/es0011008.
- [49] J. G. Mønster, J. Samuelsson, P. Kjeldsen, C. W. Rella, and C. Scheutz, “Quantifying methane emission from fugitive sources by combining tracer release and downwind measurements – a sensitivity analysis based on multiple field surveys,” *Waste Management*, vol. 34, no. 8, pp. 1416–1428, 2014.
- [50] A. Guenther, W. Baugh, K. Davis, G. Hampton, P. Harley, L. Klinger, L. Vierling, P. Zimmerman, E. Allwine, S. Dilts, B. Lamb, H. Westberg, D. Baldocchi, C. Geron, and T. Pierce, “Isoprene fluxes measured by enclosure, relaxed eddy accumulation, surface layer gradient, mixed layer gradient, and mixed layer mass balance techniques,” *Journal of Geophysical Research*, vol. 101, no. D13, pp. 18555–18567, 1996.

- [51] S. K. Kaharabata, P. H. Schuepp, and R. L. Desjardins, “Estimating methane emissions from dairy cattle housed in a barn and feedlot using an atmospheric tracer,” *Environmental Science & Technology*, vol. 34, no. 15, pp. 3296–3302, 2000. doi: 10.1021/es990578c.
- [52] R. Kantamaneni, G. Adams, L. Bamesberger, E. Allwine, H. Westberg, B. Lamb, and C. Claiborn, “The measurement of roadway pm10 emission rates using atmospheric tracer ratio techniques,” *Atmospheric Environment*, vol. 30, no. 24, pp. 4209–4223, 1996.
- [53] Lamb, McManus, Shorter, Kolb, Mosher, Harriss, Allwine, Blaha, Howard, Guenther, Lott, Siverson, Westberg, and Zimmerman, “Development of atmospheric tracer methods to measure methane emissions from natural gas facilities and urban areas,” *Environmental Science & Technology*, vol. 29, no. 6, pp. 1468–1479, 1995.
- [54] K. R. Lassey, M. J. Ulyatt, R. J. Martin, C. F. Walker, and I. D. Shelton, “Methane emissions measured directly from grazing livestock in new zealand,” *Atmospheric Environment*, vol. 31, no. 18, pp. 2905–2914, 1997.
- [55] M. Möllmann-Coers, D. Klemp, K. Mannschreck, and F. Slemr, “Determination of anthropogenic emissions in the augsburg area by the source–tracer–ratio method,” *Atmospheric Environment*, vol. 36, Supplement 1, p. 107, 2002.
- [56] B. Rumburg, G. H. Mount, J. Filipy, B. Lamb, H. Westberg, D. Yonge, R. Kincaid, and K. Johnson, “Measurement and modeling of atmospheric flux of ammonia from dairy milking cow housing,” *Agricultural Air Quality: State of the Science (AAQ-2006)*, vol. 42, no. 14, pp. 3364–3379, 2008.

- [57] R. Scholtens, C. J. Dore, B. M. R. Jones, D. S. Lee, and V. R. Phillips, “Measuring ammonia emission rates from livestock buildings and manure stores—part 1: development and validation of external tracer ratio, internal tracer ratio and passive flux sampling methods,” *Atmospheric Environment*, vol. 38, no. 19, pp. 3003–3015, 2004.
- [58] Y. Xiao, D. J. Jacob, and S. Turquety, “Atmospheric acetylene and its relationship with co as an indicator of air mass age,” *Journal of Geophysical Research*, vol. 112, no. D12, p. D12305, 2007.
- [59] E. Almqvist, *History of Industrial Gases*. Springer US, 2003.
- [60] Brandt, Heath, Kort, O’Sullivan, Petron, Jordaan, Tans, Wilcox, Gopstein, Arent, Wofsy, Brown, Bradley, Stucky, Eardley, and Harriss, “Methane leaks from north american natural gas systems,” *Science*, vol. 343, no. 6172, pp. 733–735, 2014.
- [61] Picarro, “Cavity ring-down spectroscopy (crds).”
- [62] M. D. Wheeler, S. M. Newman, A. J. Orr-Ewing, and M. N. R. Ashfold, “Cavity ring-down spectroscopy,” *J. Chem. Soc., Faraday Trans.*, vol. 94, no. 3, pp. 337–351, 1998.
- [63] B. C. Sive, Y. Zhou, D. Troop, Y. Wang, W. C. Little, O. W. Wingenter, R. S. Russo, R. K. Varner, and R. Talbot, “Development of a cryogen-free concentration system for measurements of volatile organic compounds,” *Analytical Chemistry*, vol. 77, no. 21, p. 6998, 2005. doi: 10.1021/ac0506231.
- [64] Y. Zhou, H. Mao, R. S. Russo, D. R. Blake, O. W. Wingenter, K. B. Haase, J. Ambrose, R. K. Varner, R. Talbot, and B. C. Sive, “Bromoform and dibromomethane measurements in the seacoast region of new hampshire, 2002–2004,” *Journal of Geophysical Research*, vol. 113, no. D8, p. D08305, 2008.

- [65] R. S. Russo, Y. Zhou, K. B. Haase, O. W. Wingenter, E. K. Frinak, H. Mao, R. W. Talbot, and B. C. Sive, “Temporal variability, sources, and sinks of c1-c5 alkyl nitrates in coastal new england,” *Atmospheric Chemistry and Physics*, vol. 10, no. 4, p. 1883, 2010.
- [66] R. F. Swarthout, *Volatile organic compound emissions from unconventional natural gas production: Source signatures and air quality impacts*. PhD thesis, University of New Hampshire, 2014. Copyright - Copyright ProQuest, UMI Dissertations Publishing 2014.
- [67] A. Cimorelli, S. Perry, A. Venkatram, J. Weil, R. Paine, R. Wilson, R. Lee, W. Peters, R. Brode, and J. Paumier, “Aermod: Description of model formation,” tech. rep., U.S. Environmental Protection Agency, September 2004.
- [68] W. B. Faulkner, B. W. Shaw, and T. Grosch, “Sensitivity of two dispersion models (aermod and iscst3) to input parameters for a rural ground-level area source,” *Journal of the Air & Waste Management Association*, vol. 58, no. 10, pp. 1288–1296, 2008. doi: 10.3155/1047-3289.58.10.1288.
- [69] A. S. Rood, “Performance evaluation of aermod, calpuff, and legacy air dispersion models using the winter validation tracer study dataset,” *Atmospheric Environment*, vol. 89, no. 0, pp. 707–720, 2014.
- [70] G. E. Willis and J. W. Deardorff, “A laboratory study of dispersion from a source in the middle of the convectively mixed layer,” *Atmospheric Environment*, vol. 15, no. 2, pp. 109–117, 1981.

- [71] G. A. Briggs, “Plume dispersion in the convective boundary layer. part ii: Analyses of condors field experiment data,” *Journal of Applied Meteorology*, vol. 32, no. 8, pp. 1388–1425, 1993. doi: 10.1175/1520-0450(1993)032;1388:PDITCB;2.0.CO;2.
- [72] Office of Air Quality Planning and Standards Emissions, Monitoring, and Analysis Division, “User’s guide for the aermom meteorological preprocessor (aermet),” tech. rep., U.S. Environmental Protection Agency, November 2004.
- [73] F. Mesinger, G. DiMego, E. Kalnay, K. Mitchell, P. C. Shafran, W. Ebisuzaki, D. Jović, J. Woollen, E. Rogers, E. H. Berbery, M. B. Ek, Y. Fan, R. Grumbine, W. Higgins, H. Li, Y. Lin, G. Manikin, D. Parrish, and W. Shi, “North american regional reanalysis,” *Bulletin of the American Meteorological Society*, vol. 87, no. 3, pp. 343–360, 2006. doi: 10.1175/BAMS-87-3-343.
- [74] F. Mesinger, S. Chou, J. Gomes, D. Jovic, P. Bastos, J. Bustamante, L. Lazic, A. Lyra, S. Morelli, I. Ristic, and K. Veljovic, “An upgraded version of the eta model,” *Meteorology and Atmospheric Physics*, vol. 116, no. 3-4, p. 79, 2012.
- [75] R. A. Whitby and E. R. Altwicker, “Acetylene in the atmosphere: Sources, representative ambient concentrations and ratios to other hydrocarbons,” *Atmospheric Environment*, vol. 12, no. 6–7, p. 1296, 1978.
- [76] N. Air and S. Administration, “Global modeling and assimilation office (gmao).”
- [77] A. J. Cimorelli, S. G. Perry, A. Venkatram, J. C. Weil, R. Paine, R. B. Wilson, R. F. Lee, W. D. Peters, and R. W. Brode, “Aermod: A dispersion model for industrial source applications. part i: General model formulation and boundary layer characterization,” *Journal of Applied Meteorology*, vol. 44, no. 5, pp. 682–693, 2005. doi: 10.1175/JAM2227.1.

- [78] D. B. Turner, “Workbook of atmospheric dispersion estimates,” tech. rep., U.S. Environmental Protection Agency, 1970.
- [79] A. Venkatram, R. Brode, A. Cimorelli, R. Lee, R. Paine, S. Perry, W. Peters, J. Weil, and R. Wilson, “A complex terrain dispersion model for regulatory applications,” *Atmospheric Environment*, vol. 35, no. 24, pp. 4211–4221, 2001.
- [80] T. J. Blasing, “Recent greenhouse gas concentrations,” February 2014.
- [81] J. C. Sheppard, H. Westberg, J. F. Hopper, K. Ganesan, and P. Zimmerman, “Inventory of global methane sources and their production rates,” *Journal of Geophysical Research*, vol. 87, no. C2, pp. 1305–1312, 1982.
- [82] I. Leifer, D. Culling, O. Schneising, P. Farrell, M. Buchwitz, and J. P. Burrows, “Transcontinental methane measurements: Part 2. mobile surface investigation of fossil fuel industrial fugitive emissions,” *Atmospheric Environment*, vol. 74, no. 0, p. 441, 2013.
- [83] Jackson, Down, Phillips, Ackley, Cook, Plata, and Zhao, “Natural gas pipeline leaks across washington, dc,” *Environmental Science & Technology*, vol. 48, no. 3, pp. 2051–2058, 2014.
- [84] A. Karion, C. Sweeney, G. Pétron, G. Frost, R. M. Hardesty, J. Koffler, B. R. Miller, T. Newberger, S. Wolter, R. Banta, A. Brewer, E. Dlugokencky, P. Lang, S. A. Montzka, R. Schnell, P. Tans, M. Trainer, R. Zamora, and S. Conley, “Methane emissions estimate from airborne measurements over a western united states natural gas field,” *Geophysical Research Letters*, vol. 40, no. 16, pp. 4393–4397, 2013.

- [85] Brantley, Thoma, Squier, Guven, and Lyon, “Assessment of methane emissions from oil and gas production pads using mobile measurements,” *Environmental Science & Technology*, vol. 48, no. 24, pp. 14508–14515, 2014.
- [86] Office of Ground Water and Drinking Water, “Evaluation of impacts to underground sources of drinking water by hydraulic fracturing of coalbed methane reservoirs study,” tech. rep., U.S. Environmental Protection Agency, June 2004. EPA 816-R-04-003.
- [87] A. for Toxic Substances and A. Disease Registry, “Toxicological profile for benzene,” tech. rep., The Center for Disease Control, 2007.
- [88] N. Harris, T. Ko, R. P. Philp, M. D. Lewan, C. J. Ballentine, Z. Zhou, and D. L. Hall, “Geochemistry of natural gases from tight-gas-sand fields in the rocky mountains,” tech. rep., U.S. Department of Energy, December 20 2013.
- [89] I. International Agency for Research on Cancer, “Monographs on the evaluation of the carcinogenic risk of chemicals to humans: Toluene,” tech. rep., World Health Organization, 1989.
- [90] G. Nonhebel, “Recommendations on heights for new industrial chimneys,” *J. Inst. Fuel*, vol. 33, p. 479, 1960.
- [91] T. Carreon and R. L. Herrick, *Patty’s Toxicology*. New York, NY: John Wiley & Sons, Inc., 6th edition ed., 2013. ethane.
- [92] C. Thompson, J. Hueber, and D. Helmig, “Data from: Influence of oil and gas emissions on ambient atmospheric non-methane hydrocarbons in residential areas of northeastern colorado,” *Elementa: Science of the Anthropocene* 2, 2014.
- [93] E. M. Fujita, J. G. Watson, J. C. Chow, and Z. Lu, “Validation of the chemical mass balance receptor model applied to hydrocarbon source apportionment in the

- southern california air quality study,” *Environmental Science & Technology*, vol. 28, no. 9, pp. 1633–1649, 1994. doi: 10.1021/es00058a016.
- [94] U.S. National Library of Medicine, “HSDB: Isobutane.” CASRN: 75-28-5.
- [95] R. R. Arnts and S. A. Meeks, “Biogenic hydrocarbon contribution to the ambient air of selected areas,” *Atmospheric Environment*, vol. 15, no. 9, pp. 1643–1651, 1981.
- [96] U. Östermark and G. Petersson, “Assessment of hydrocarbons in vapours of conventional and alkylate-based petrol,” *Chemosphere*, vol. 25, no. 6, pp. 763–768, 1992.
- [97] C. V. Hampton, W. R. Pierson, T. M. Harvey, W. S. Updegrave, and R. S. Marano, “Hydrocarbon gases emitted from vehicles on the road. 1. a qualitative gas chromatography/mass spectrometry survey,” *Environmental Science & Technology*, vol. 16, no. 5, pp. 287–298, 1982. doi: 10.1021/es00099a011.
- [98] A. P. Institute, “Transport and fate of non-btex petroleum chemicals in soils and groundwater,” tech. rep., 1994.
- [99] T. E. Graedel, *Chemical Compounds in the Atmosphere*. New York, NY: Academic Press, 1978.
- [100] R. Snyder, *Volume 1: Hydrocarbons*, p. 237. Ethel Browning’s Toxicity and Metabolism of Industrial Solvents, Amsterdam, New York, Oxford: Elsevier, 1987.
- [101] J. J. Schauer, M. J. Kleeman, G. R. Cass, and B. R. T. Simoneit, “Measurement of emissions from air pollution sources. 5. c1c32 organic compounds from gasoline-powered motor vehicles,” *Environmental Science & Technology*, vol. 36, no. 6, pp. 1169–1180, 2002. doi: 10.1021/es0108077.

- [102] J. G. Watson, J. C. Chow, and E. M. Fujita, "Review of volatile organic compound source apportionment by chemical mass balance," *Atmospheric Environment*, vol. 35, no. 9, pp. 1567–1584, 2001.
- [103] M. Sanchez, S. Karnae, and K. John, "Source characterization of volatile organic compounds affecting the air quality in a coastal urban area of south texas," *International Journal of Environmental Research and Public Health*, vol. 5, no. 3, pp. 130–138, 2008.
- [104] J. E. Sigsby, S. Tejada, W. Ray, J. M. Lang, and J. W. Duncan, "Volatile organic compound emissions from 46 in-use passenger cars," *Environmental Science & Technology*, vol. 21, no. 5, pp. 466–475, 1987. doi: 10.1021/es00159a007.
- [105] R. B. Zweidinger, R. K. Stevens, C. W. Lewis, and H. Westburg, "Identification of volatile hydrocarbons as mobile source tracers for fine-particulate organics," *Environmental Science & Technology*, vol. 24, no. 4, pp. 538–542, 1990. doi: 10.1021/es00074a012.
- [106] C. Anselme, K. N'guyen, A. Bruchet, and J. Mallevalle, "Characterization of low molecular weight products desorbed from polyethylene tubings," *Organic Micropollutants in Drinking Water and Health*, vol. 47, no. 0, pp. 371–384, 1985.
- [107] International Agency for Research on Cancer, (IARC), "Monographs on the evaluation of the carcinogenic risk of chemicals to humans: Ethylene," tech. rep., World Health Organization, 1994.
- [108] K. Verschueren, *Handbook of Environmental Data on Organic Chemicals*. New York, NY: Van Nostrand Reinhold Co., 3rd edition ed., 1996.

- [109] J. D. Fuentes, D. Wang, H. H. Neumann, T. J. Gillespie, G. D. Hartog, and T. F. Dann, “Ambient biogenic hydrocarbons and isoprene emissions from a mixed deciduous forest,” *Journal of Atmospheric Chemistry*, vol. 25, no. 1, p. 95, 1996.
- [110] R. A. Field, M. E. Goldstone, J. N. Lester, and R. Perry, “The sources and behaviour of tropospheric anthropogenic volatile hydrocarbons,” *Atmospheric Environment*, vol. 26, no. 16, pp. 2983–2996, 1992.
- [111] P. Gabele, “Exhaust emissions from four-stroke lawn mower engines,” *Journal of the Air & Waste Management Association*, vol. 47, no. 9, pp. 945–952, 1997. doi: 10.1080/10473289.1997.10463951.
- [112] D. Schuetzle, W. O. Siegl, T. E. Jensen, M. A. Dearth, E. W. Kaiser, R. Gorse, W. Kreucher, and E. Kulik, “The relationship between gasoline composition and vehicle hydrocarbon emissions: a review of current studies and future research needs.,” *Environmental Health Perspectives*, vol. 102, no. Suppl 4, pp. 3–12, 1994.
- [113] R. L. Williams, F. Lipari, and R. A. Potter, “Formaldehyde, methanol and hydrocarbon emissions from methanol-fueled cars,” *Journal of the Air & Waste Management Association*, vol. 40, no. 5, pp. 747–756, 1990. doi: 10.1080/10473289.1990.10466720.
- [114] M. J. O’Neil, ed., *The Merck Index - An Encyclopedia of Chemicals, Drugs, and Biologicals*. Whitehouse Station, NJ: Merck and Co., Inc., 1996.
- [115] U.S. Environmental Protection Agency, “Summary health assessment document for propylene,” tech. rep., July 1988. EPA Contract No 68-02-4030.
- [116] R. S. Martin, I. Villanueva, J. Zhang, and C. J. Popp, “Nonmethane hydrocarbon, monocarboxylic acid, and low molecular weight aldehyde and ketone emissions from

- vegetation in central new mexico,” *Environmental Science & Technology*, vol. 33, no. 13, pp. 2186–2192, 1999. doi: 10.1021/es980468q.
- [117] M. Cloke, *Encyclopedia of chemical technology (4th edition)*, vol. 62. John Wiley & Sons, Inc., 1995.
- [118] H. Westberg, K. Sexton, and D. Flyckt, “Hydrocarbon production and photochemical ozone formation in forest burn plumes,” *Journal of the Air Pollution Control Association*, vol. 31, no. 6, pp. 661–664, 1981. doi: 10.1080/00022470.1981.10465259.
- [119] P. Nunes and P. B. Jr., “Effects of the water-soluble fraction of cook inlet crude oil on the marine alga, *dunalliella tertiolecta*,” *Bulletin of Environmental Contamination and Toxicology*, vol. 21, no. 1, p. 732, 1979.
- [120] International Agency for Research on Cancer, (IARC), “Monographs on the evaluation of carcinogenic risks to humans,” Tech. Rep. 47, World Health Organization, 1989.
- [121] Agency for Toxic Substances & Disease Registry (ATSDR), “Toxicological profile for automotive gasoline,” tech. rep., The Center for Disease Control, June 1995.
- [122] N. V. Mody, A. A. de la Cruz, D. H. Miles, and P. A. Hedin, “The essential oil of *distichlis spicata*,” *Phytochemistry*, vol. 14, no. 2, pp. 599–601, 1975.
- [123] S. Y. Hwang and S. S. Chen, *Cumene*. Kirk-Othmer Encyclopedia of Chemical Technology, John Wiley & Sons, Inc., 2000.
- [124] C. V. Hampton, W. R. Pierson, T. M. Harvey, and D. Schuetzle, “Hydrocarbon gases emitted from vehicles on the road. 2. determination of emission rates from diesel and spark-ignition vehicles,” *Environmental Science & Technology*, vol. 17, no. 12, pp. 699–708, 1983. doi: 10.1021/es00118a003.

- [125] R. A. Harley, M. P. Hannigan, and G. R. Cass, “Respeciation of organic gas emissions and the detection of excess unburned gasoline in the atmosphere,” *Environmental Science & Technology*, vol. 26, no. 12, pp. 2395–2408, 1992. doi: 10.1021/es00036a010.
- [126] F. Jüttner, “Emission of aromatic hydrocarbons and aldehydes into the water by a four-stroke outboard motor: Quantitative measurements,” *Chemosphere*, vol. 29, no. 2, pp. 191–200, 1994.
- [127] E. Gomez, C. A. Ledbetter, and P. L. Hartsell, “Volatile compounds in apricot, plum, and their interspecific hybrids,” *Journal of Agricultural and Food Chemistry*, vol. 41, no. 10, pp. 1669–1676, 1993. doi: 10.1021/jf00034a029.
- [128] E. Tsani-Bazaca, A. McIntyre, J. Lester, and R. Perry, “Ambient concentrations and correlations of hydrocarbons and halocarbons in the vicinity of an airport,” *Chemosphere*, vol. 11, no. 1, pp. 11–23, 1982.

APPENDIX A

FIELDWORK SITES

TABLE A.1. List of all fieldwork sites with corresponding operation(s).

Site	Day	Operation Type	Time of Year
A1	1	Drilling	July
A2	1	Fracking	December
B1	1	Drilling	October
B2	1	Drilling	May
	2		
B3	1	Fracking	June
C1	1	Remote Fracking	May
D1	1	Fracking	May
F1	1	Fracking	August
	2	Fracking/Workover/Flowback	
	3	Flowback	
G1	1	Drilling	November
G2	1	Drilling/Flowback/Fracking	December
H1	1	Gel Fracking	January
I1	1	Fracking/Perforation	February
I2	1	Fracking	February
I3	1	Flowback/Popping	March
I4	1	Flowback	March

APPENDIX B

INFORMATION ABOUT VOCs

Tables B.1 through B.3 give information about the VOCs measured by the GC system and their relevant sources.

TABLE B.1. List of alkane compounds measured by the GC system. The generic chemical formula and the possible sources for each compound are listed.

Compound	Formula	Relevant Source(s)
ethane	C_2H_6	Constituent of crude oil and natural gas [91],
propane	C_3H_8	Oil and natural gas [92]
i-butane	C_4H_{10}	Petroleum and natural gas [93], blending agent for fuels [94]
n-butane		Petroleum and natural gas [95], vehicular exhaust [96]
cyclopentane	C_5H_{10}	Product of combustion engines [97]
i-pentane	C_5H_{12}	Oil and gas production [22]
n-pentane		Combustion [22]
cyclohexane	C_6H_{12}	Gasoline combustion [98], natural occurrence in crude oil [99]
n-hexane	C_6H_{14}	Crude oil refining [95]
methylcyclohexane	C_7H_{14}	cracked petroleums [100]
n-heptane	C_7H_{16}	gasoline combustion [101]
2,4-dimethylpentane		gasoline combustion, biomass burning [99]
2,3-dimethylpentane		gasoline combustion, natural gas [99]
2-methylhexane		gasoline combustion [102]
3-methylhexane		refinery operations, vehicular exhaust, fugitive gasoline emissions, natural gas sources [103]
2,2,4-trimethylpentane		Automotive emissions [104], wood combustion [105], and polyethylene pipes that distribute drinking water [106]
2,3,4-trimethylpentane	C_8H_{18}	automotive emissions [99]
n-octane		automotive emissions [97]
2-methylheptane		combustion, gasoline vapor, natural gas, paint [99]
3-methylheptane		combustion, gasoline vapor, tobacco smoke, paint [99]
n-nonane	C_9H_{20}	Constituent of crude oil and natural gas, combustion [91]
n-decane	$C_{10}H_{22}$	Constituent of crude oil and natural gas [91], combustion of gasoline [97]

TABLE B.2. List of alkane and alkene compounds measured by the GC system. The generic chemical formula and the major sources for each compound are listed.

Compound	Formula	Relevant Source(s)
ethene	C_2H_4	Emitted by fruits, flowers, leaves, roots and tubers [107]
t-2-butene	C_4H_8	Diesel exhaust, evaporate from gas tanks [108]
1-butene		Desiduous forests [109], exhaust from gasoline [110] and diesel [111]
i-butene		exhaust of automobiles [112, 113]
c-2-butene		gasoline [108], coal gas [114]
propene	C_3H_6	biomass burning, natural gas [99], automobile combustion [115]
isoprene	C_5H_8	biogenic emitted by trees [116]
t-2-pentene	C_5H_{10}	crude oil and gasoline [117]
1-pentene		biomass burning [118], combustion of gasoline and diesel [99]
cis-2-pentene		crude oil and gasoline [117]

TABLE B.3. List of aromatic compounds measured by the GC system. The generic chemical formula and the possible sources for each compound are listed.

Compound	Formula	Relevant Sources	
benzene	C_6H_6	consituent of crude oil, combustion product [99],	
toluene	C_7H_8	natural gas deposits [89], combustion product [99]	
styrene	C_8H_8	emission from Styracaceae plant [91], spark-ignition engines [97]	
ethylbenzene	C_8H_{10}	biomass burning [99], component of crude oil [119], combustion [91]	
m+p-xylene		natural gas [120]	
o-xylene		natural gas [120], component of gasoline [121]	
isopropylbenzene	C_9H_{12}	marsh grasses [122], gasoline consituent [123]	
n-propylbenzene		natural constituent of petroleum [108], exhaust from gasoline and diesel engines [124]	
2-ethyltoluene		automobile exhaust, biomass burning, gasoline vapor, paint [99]	
3-ethyltoluene		automobile exhaust, biomass burning, gasoline vapor, paint [99]	
4-ethyltoluene		automobile exhaust, biomass burning, gasoline vapor, paint [99]	
1,3,5-trimethylbenzene		component of gasoline [125], combustion of gasoline [126]	
1,2,4-trimethylbenzene		component of gasoline [125], combustion of gasoline [126]	
1,2,3-trimethylbenzene		volatile component of plums [127]	
1,3-diethylbenzene		$C_{10}H_{14}$	component of gasoline [108], combustion of gasoline [128]
1,4-diethylbenzene			component of gasoline [108], combustion of gasoline [128]

APPENDIX C

ALL VOC EMISSION RATES

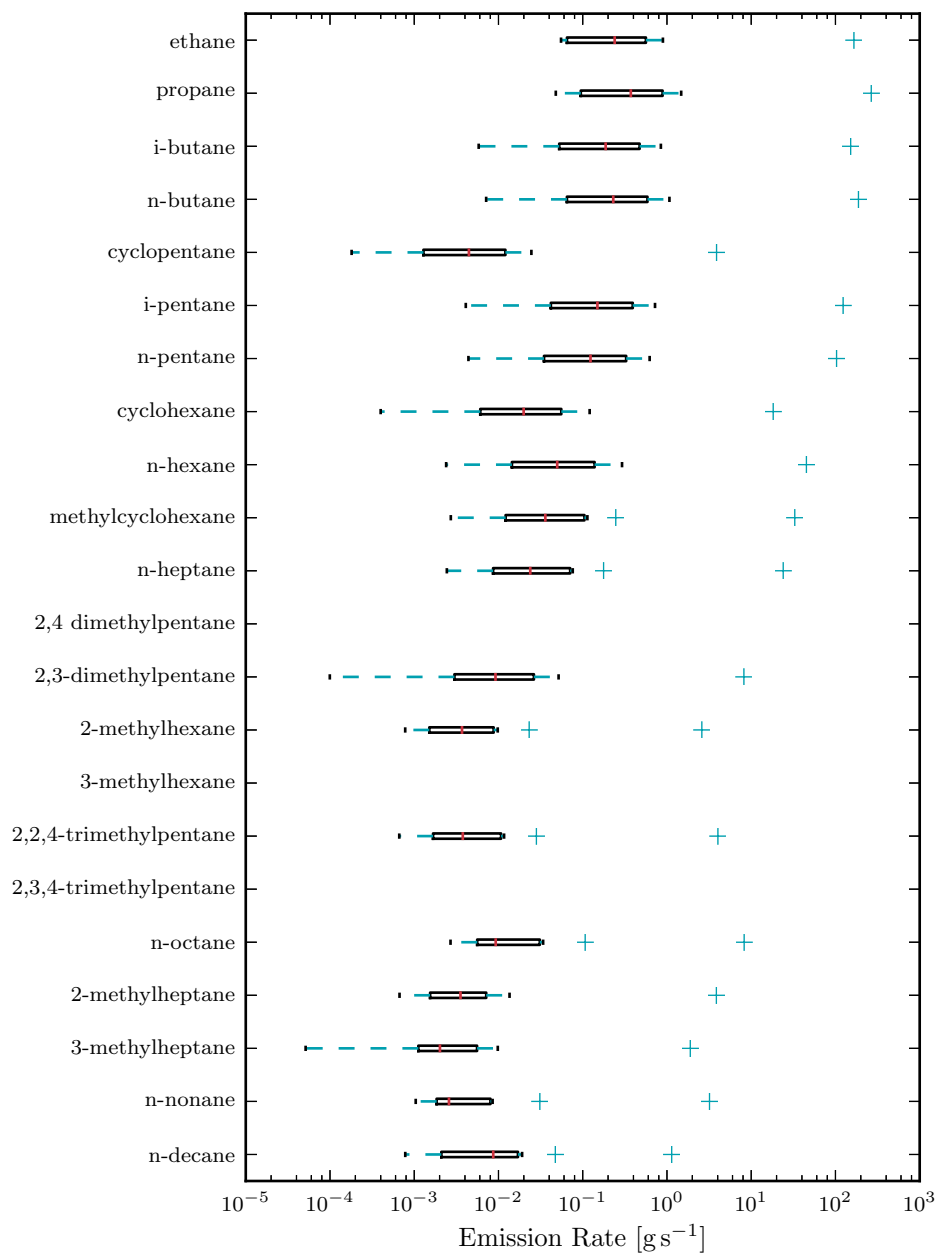


FIGURE C.1. Canister alkane emission rate distributions for drilling operations.

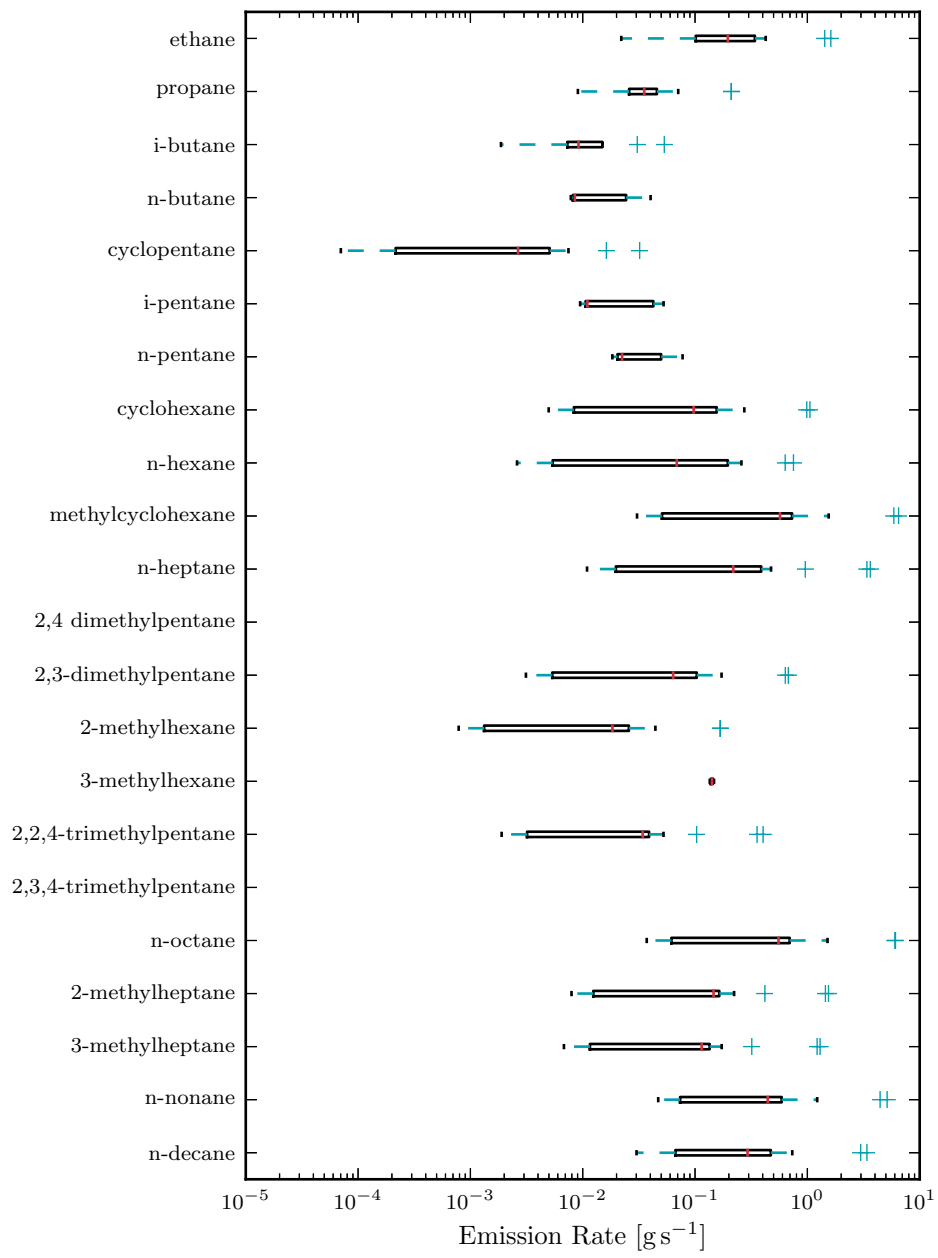


FIGURE C.2. Canister alkane emission rate distributions for hydraulic fracturing operations.

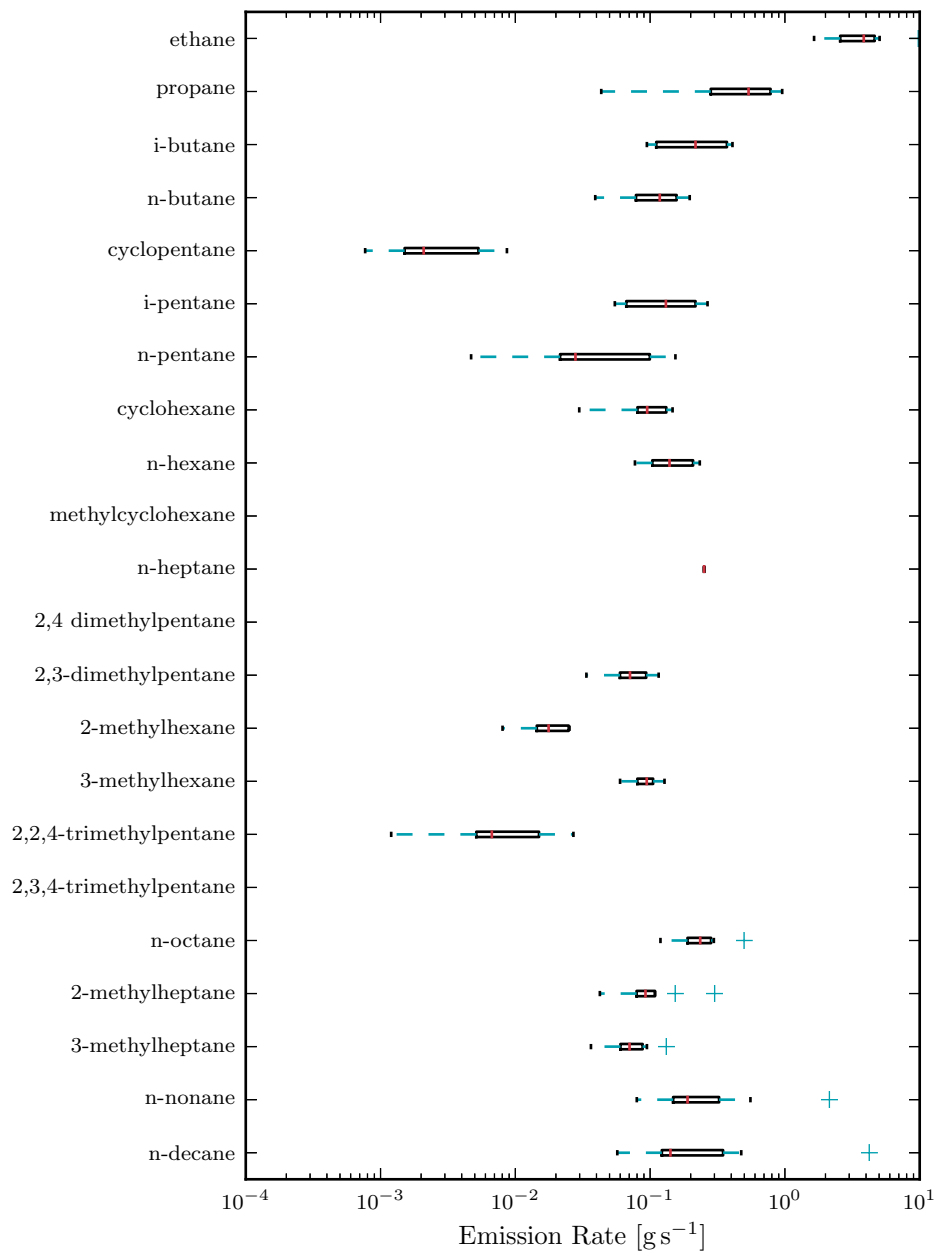


FIGURE C.3. Canister alkane emission rate distributions for flowback operations.

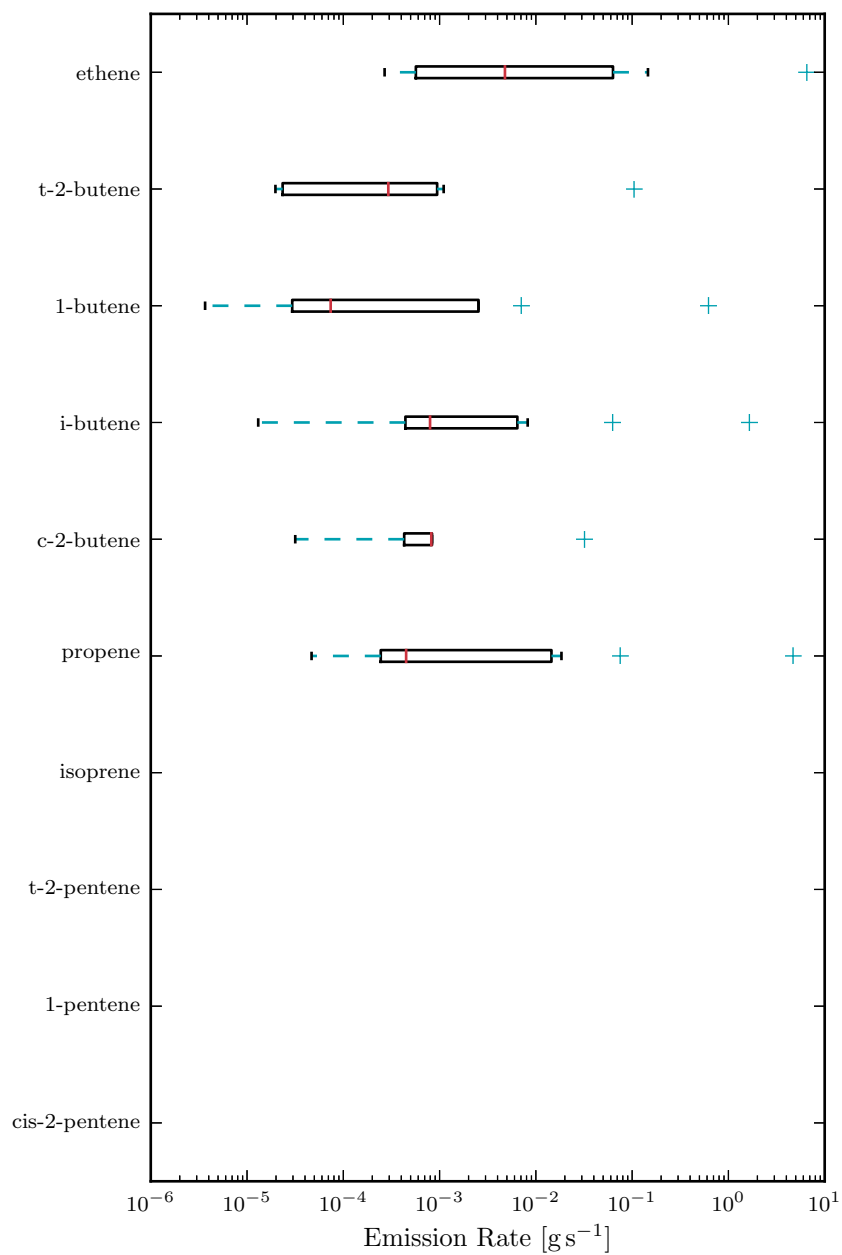


FIGURE C.4. Canister alkene emission rate distributions for drilling operations.

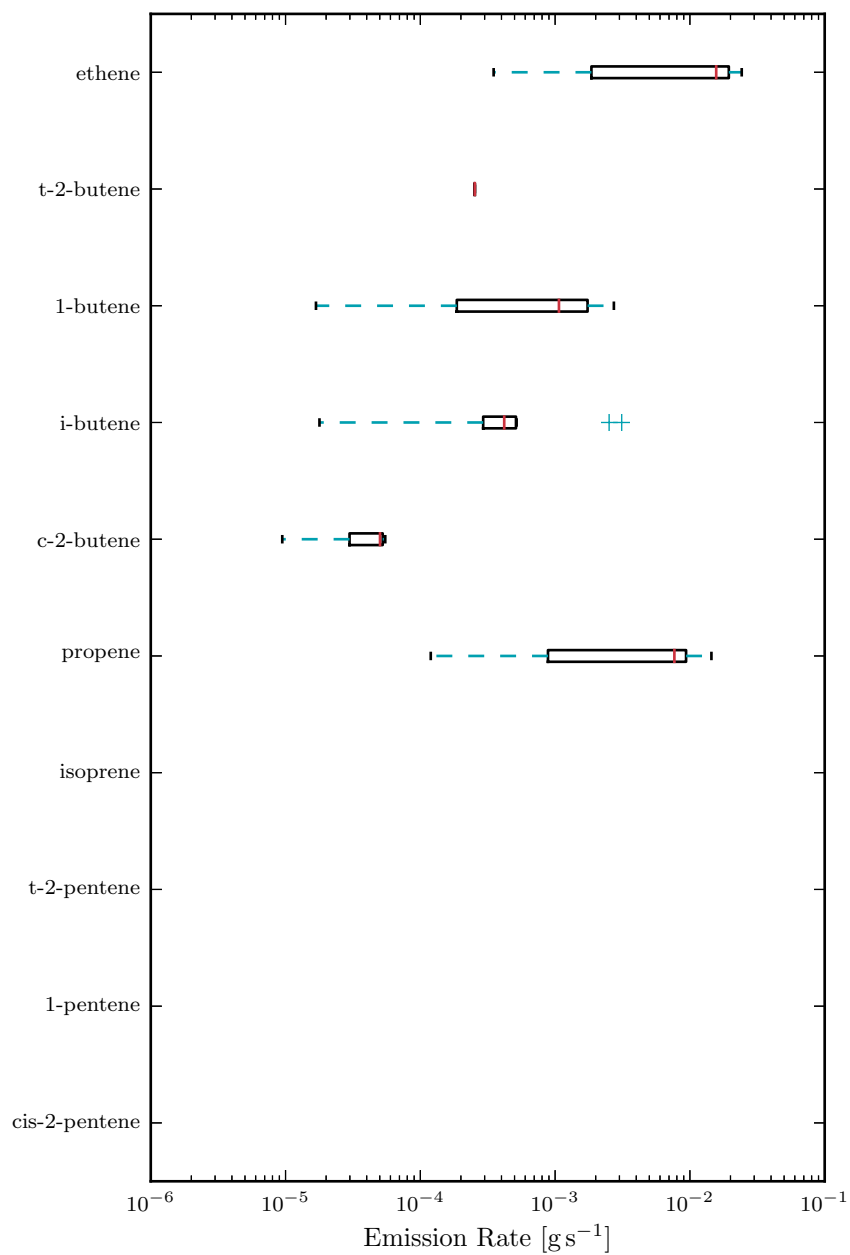


FIGURE C.5. Canister alkene emission rate distributions for hydraulic fracturing operations.

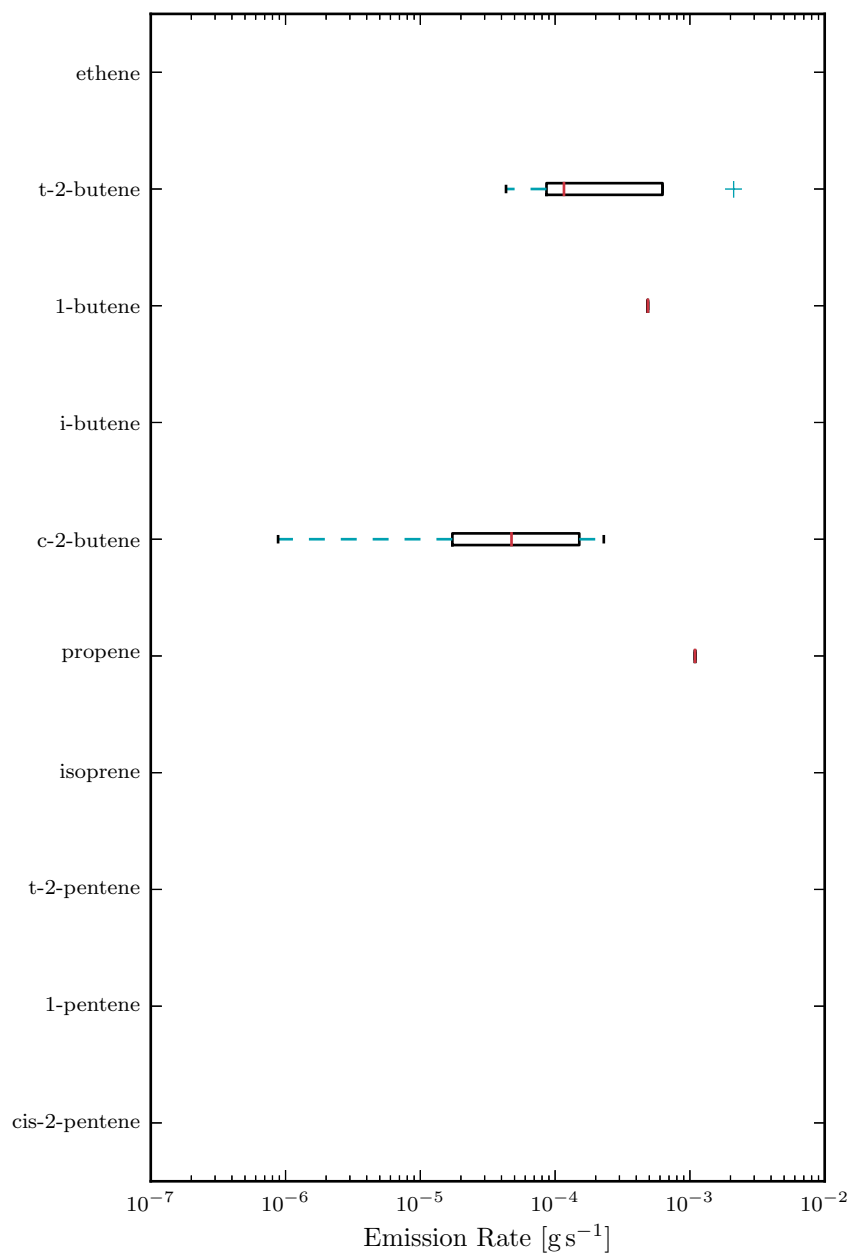


FIGURE C.6. Canister alkene emission rate distributions for flowback operations.

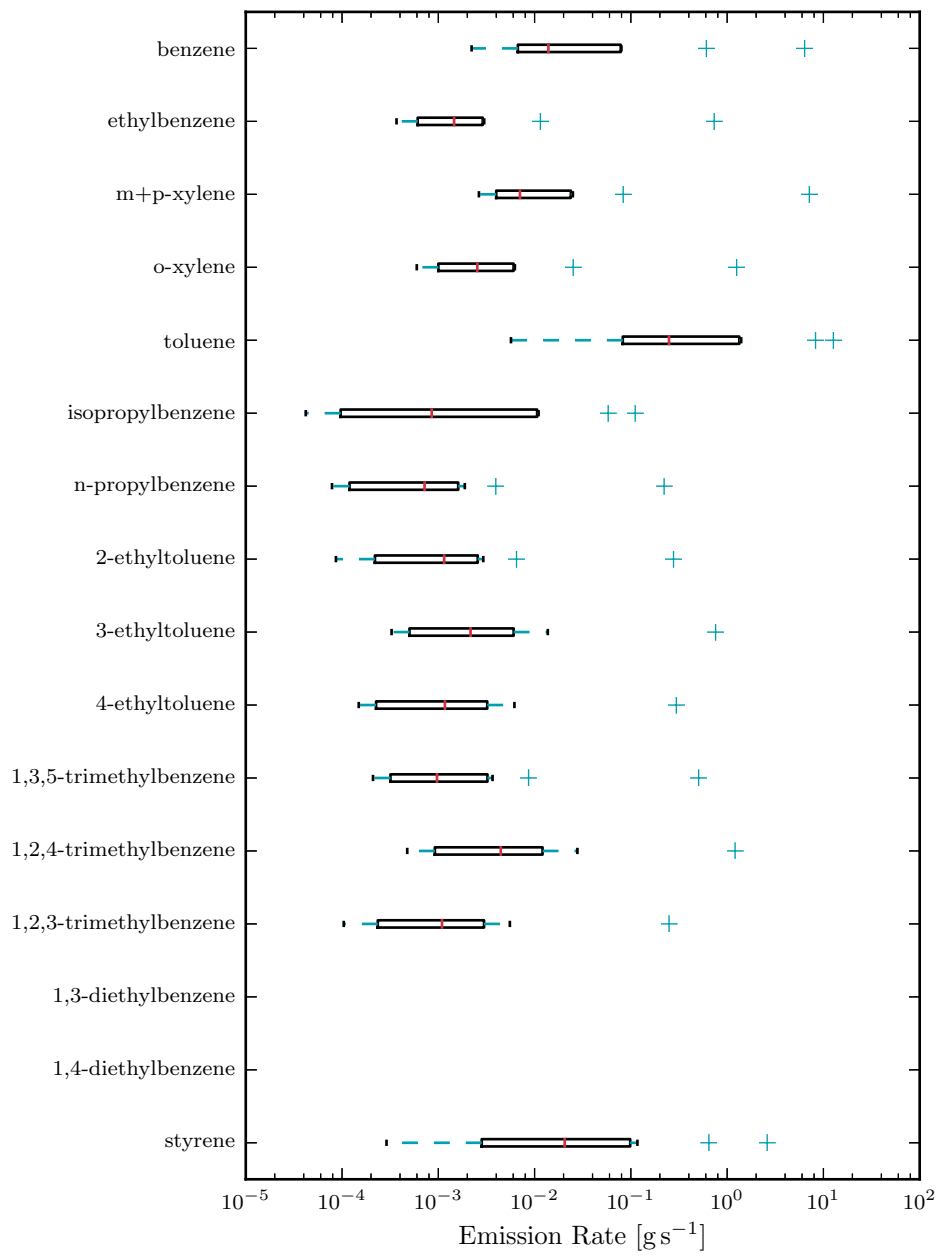


FIGURE C.7. Canister aromatic emission rate distributions for drilling operations.

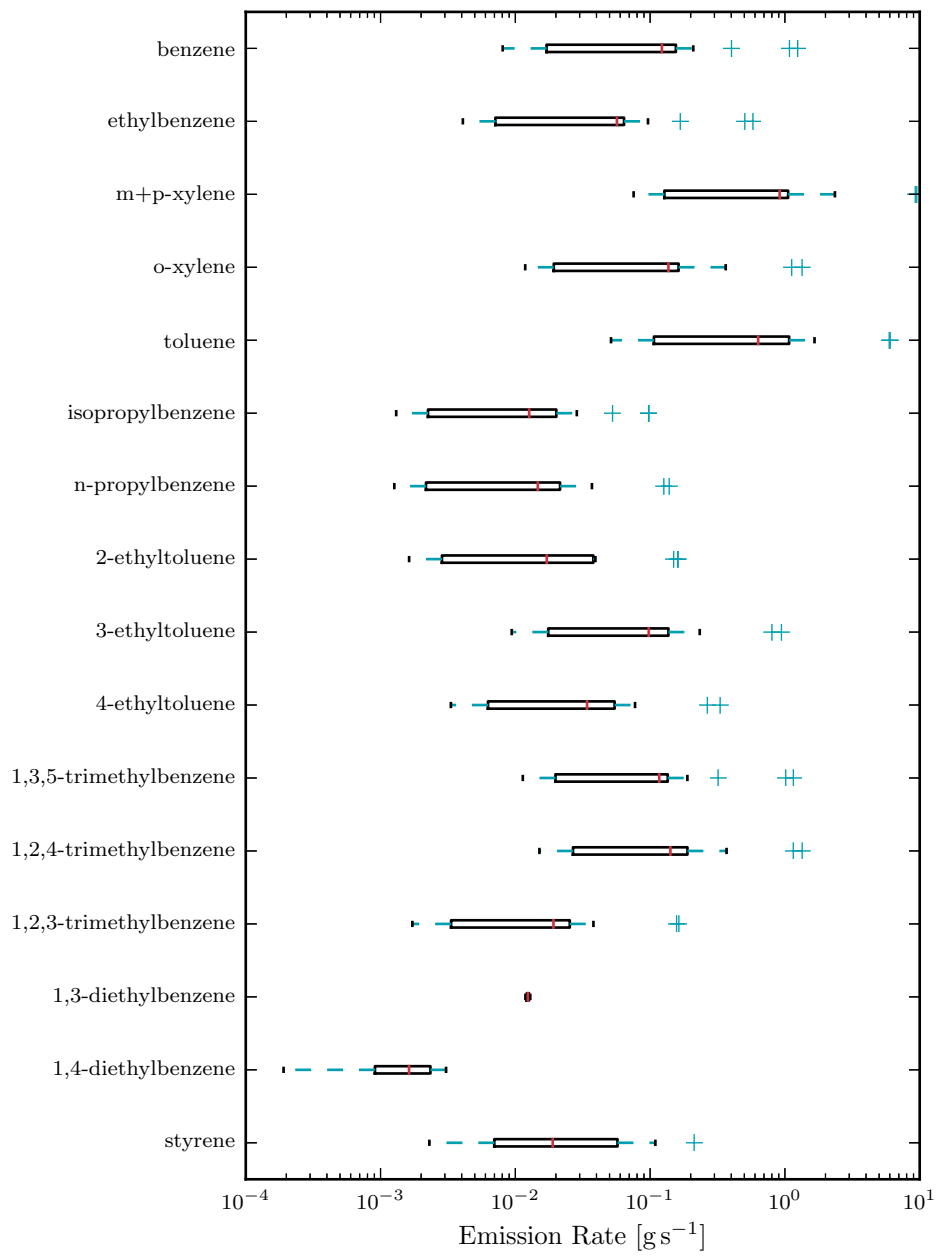


FIGURE C.8. Canister aromatic emission rate distributions for hydraulic fracturing operations.

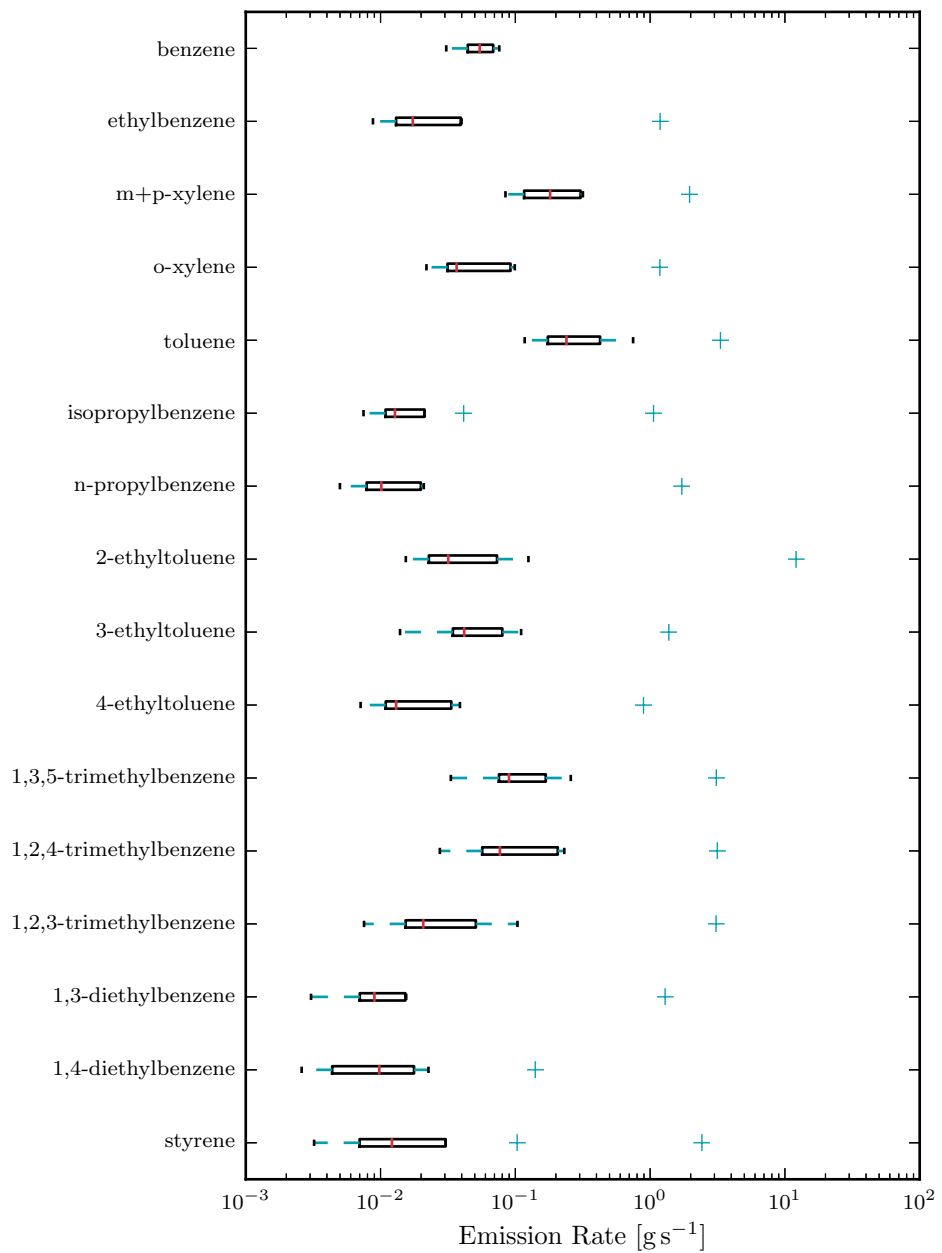


FIGURE C.9. Canister aromatic emission rate distributions for flowback operations.

APPENDIX D

CORRELATION COEFFICIENT CUTOFF

Figure D.1 shows the fraction of data points remaining for many different correlation coefficient cutoff values. Some operation types like flowback or frac/workover/flowback have identifiable change in slope as correlation coefficient increases. The drilling/flowback/frac site does not have this change in slope and appears to be very poorly correlated during the entire measurement period.

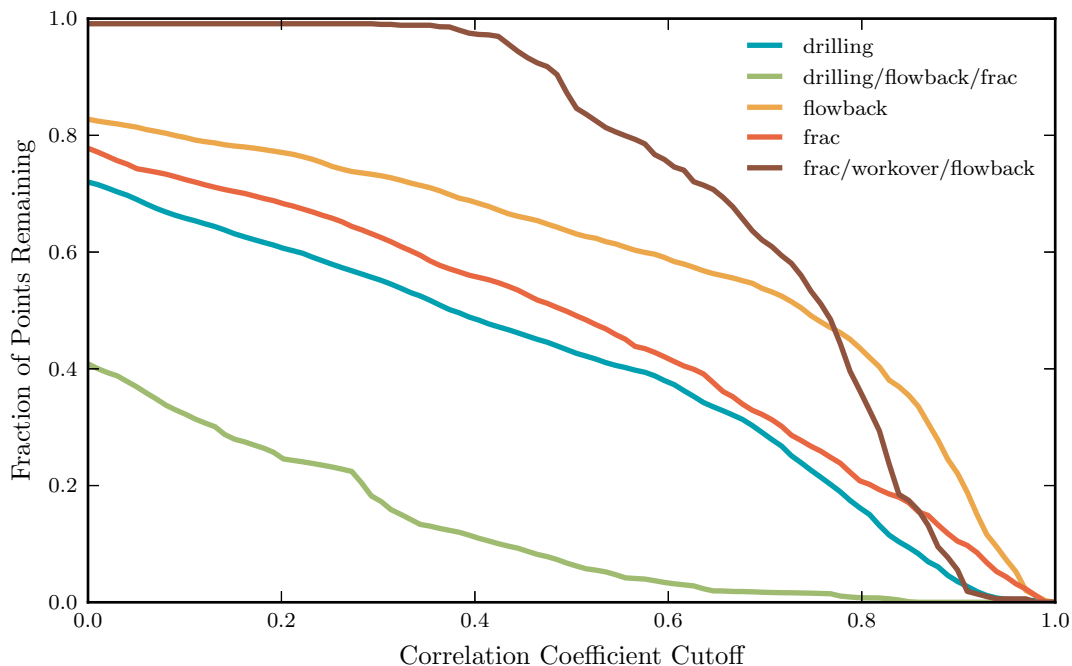


FIGURE D.1. Fraction of points remaining as a function of correlation coefficient cutoff.

It was not obvious how to chose a correlation coefficient cutoff value. Figure D.2 shows that enforcing a correlation coefficient cutoff value does not affect the overall shape of the emission rate distributions. The top panel has no correlation coefficient cut off, the middle panel has a cut off of 0.5 (used in analysis), and the bottom panel has a cut off value of 0.8.

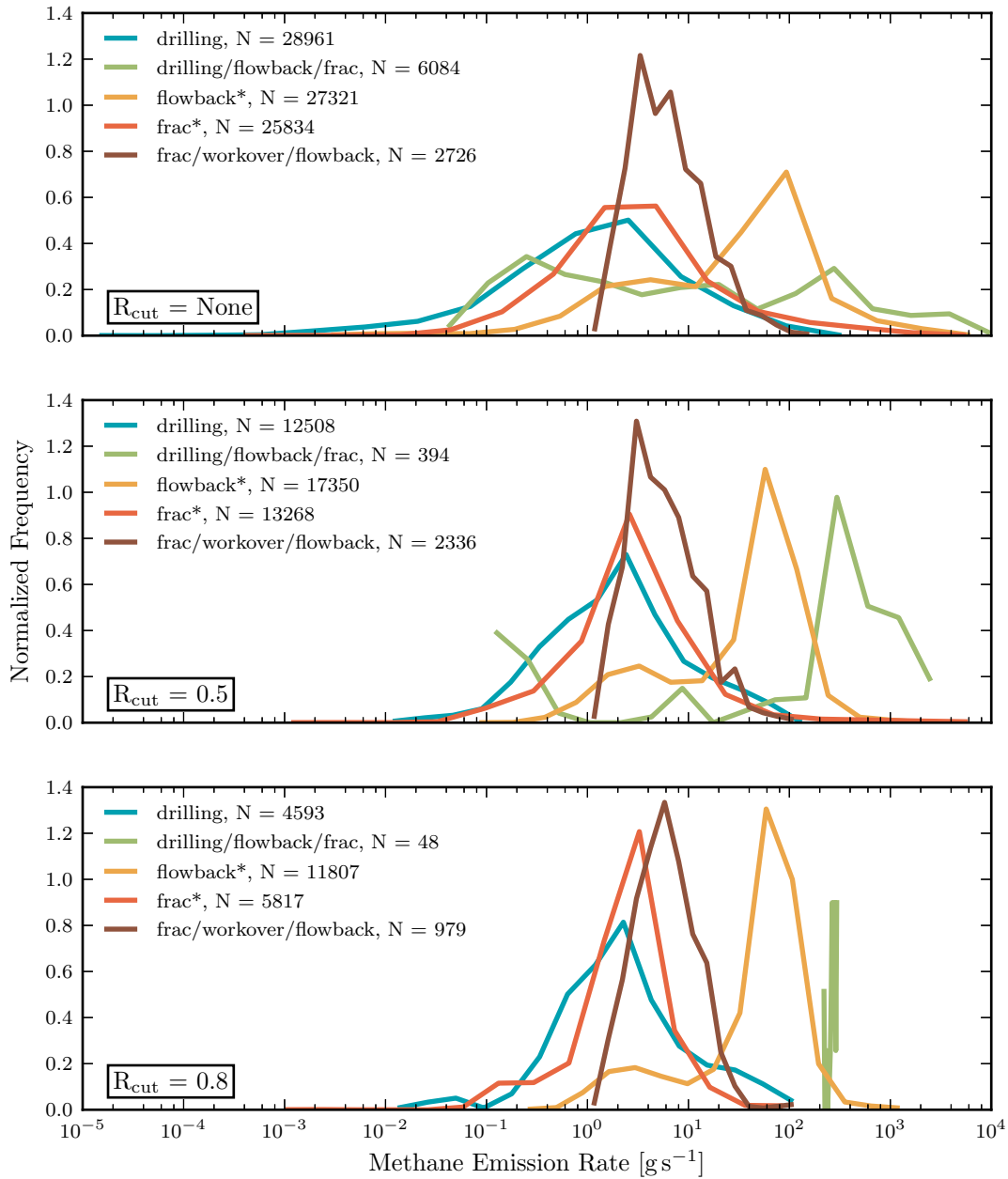


FIGURE D.2. Emission rate distribution without a correlation coefficient cut-off (top plot) and emission rate distribution with a correlation coefficient cutoff of 0.8 (bottom plot)

The positioning and shape of the distributions did not change significantly. Outliers were removed when using this correlation coefficient cut off value that were not removed when only using the acetylene cut off criteria. A correlation coefficient value of 0.5 was used in the main analysis to keep a balance of correlated plumes and enough data points to create a statistically significant distribution.

APPENDIX E

COMPARING PICARRO AND CANISTER ACETYLENE

Acetylene measured by the Picarro was used as the tracer strictly for methane emissions and acetylene from the canisters was used as the tracer for the NM-VOCs. Figure E.1 shows the mixing ratios of acetylene as measured by the GC system using the canister samples plotted against the mixing ratios measured by the Picarro. The values obtained from the Picarro device are averaged over the same three-minute period that the canister was sampling. I made this comparison for all canisters deployed in the field that have been analyzed. A one-to-one line is plotted in grey and each dot represents a three minute acetylene concentration. Three canister positions are marked: tahoe up, tahoe down, and downwind. The relative location of these canisters with respect to the Picarro can be found in Section 3. Because the tahoe up and tahoe down canisters were closest to the Picarro inlet, it was expected that these canisters would have better agreement than the downwind canister. The canisters located closest to the Picarro inlet have a correlation coefficient value of 0.57, a log-mean-bias of -0.08 , and a slope of 12.4. A negative log-mean-bias means that the canisters have lower mixing ratios compared to the Picarro measurements. Figure E.1 demonstrates the differences in measured acetylene concentrations for two sampling and measurement approaches that were within 1 meter of each other.

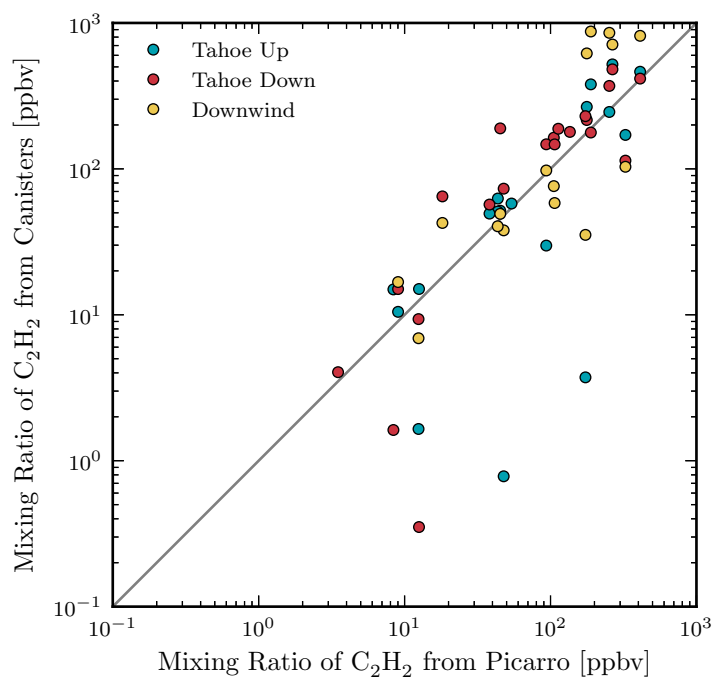


FIGURE E.1. Comparison of acetylene mixing ratios measured by the Picarro and canisters. The mixing ratios measured by the Picarro were averaged over the three minute canister sampling periods.

APPENDIX F

ATMOSPHERIC STABILITY DEPENDENCE

The concentrations of VOCs were dependent on the atmospheric conditions. In a stable atmosphere, the plume is less prone to vertical mixing and the concentrations tend to remain high downwind. In an unstable atmosphere, there is more turbulence and therefore the concentrations decrease quicker downwind compared to a stable atmosphere. For each hour of meteorology determined using the NARR database, a stability class was assigned using the Pasquill-Gifford-Turner (PG&T) scheme [78]. With this information, the cumulative distribution function (CDF) of concentrations was plotted for each different stability class. Figure F.1 shows this CDF for a setback distance of 1000 ft for site D1.

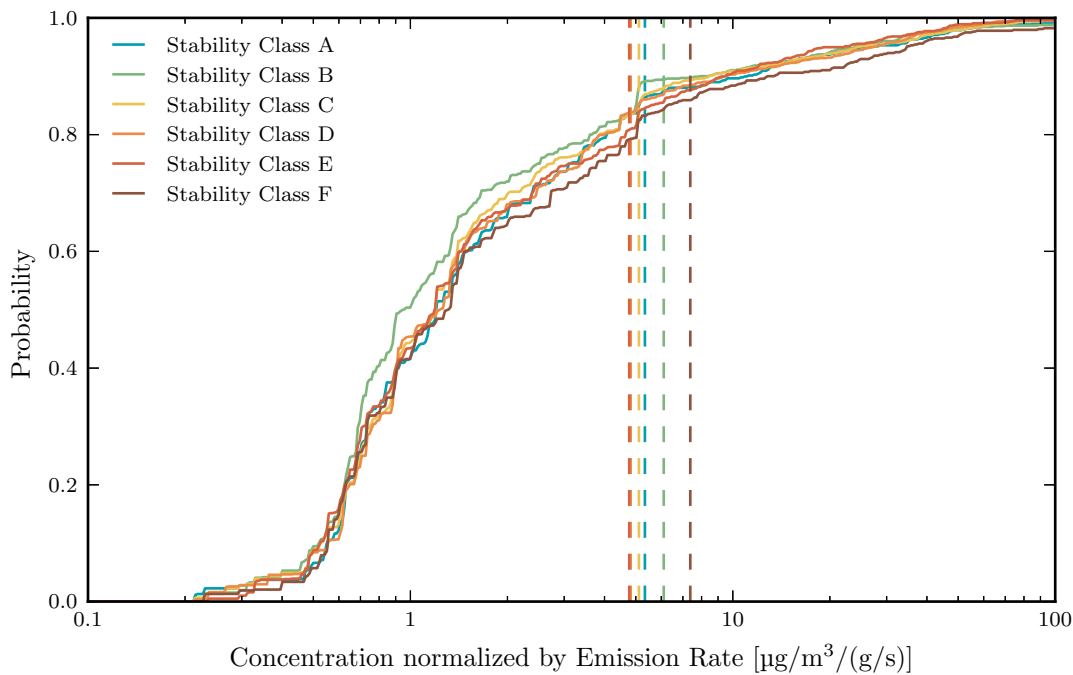


FIGURE F.1. Concentration cumulative distribution functions (CDFs) at a distance of 1000 ft away from the well. The CDFs are separated by atmospheric stability class.

The stability classes are as defined by PG&T where stability class A is extremely unstable, D is neutral and F is extremely stable. As the atmospheric stability increases, as do the mixing ratios. In a more stable atmosphere there is less mixing and therefore less entrainment of ambient air into the plume of benzene. There was a larger spread in the curves at lower concentrations. The atmospheric stability did not appear to be an important factor in predicting downwind concentrations.

APPENDIX G

COMPARISON OF METHANE EMISSION RATE DISTRIBUTIONS

Table G.1 compares the distribution details for all methane emission rates and emission rates measured while canisters were sampling.

TABLE G.1. Methane emission rate distribution details. N is the number of points, Med is the median, and SD is the standard deviation taken in log-space.

Operation Type	N	Mean [g s ⁻¹]	Med [g s ⁻¹]	25 th %ile [g s ⁻¹]	75 th %ile [g s ⁻¹]	SD
drilling	12 508	6.2	1.9	0.71	4.8	0.67
drilling (canister)	5988	14	0.94	0.33	3.3	1.0
drilling/flowback/frac	394	490	260	11	560	1.4
drilling/flowback/frac (canister)	1179	13	0.59	0.17	8.7	1.0
flowback	17 350	64	53	13	83	0.67
flowback (canister)	4722	100	52	14	98	0.73
frac	13 268	29	2.8	1.4	5.5	0.63
frac (canister)	9086	2900	8.2	2.3	37	1.1
frac/workover/flowback	2336	8.1	5.1	3.2	9.2	0.34
frac/workover/flowback (canister)	442	43	9.0	3.8	56	0.66

APPENDIX H

FLOWBACK GAUSSIAN FIT

Figure H.1 shows the methane emission rate distribution for flowback. This distribution was fit using two log-normal curves.

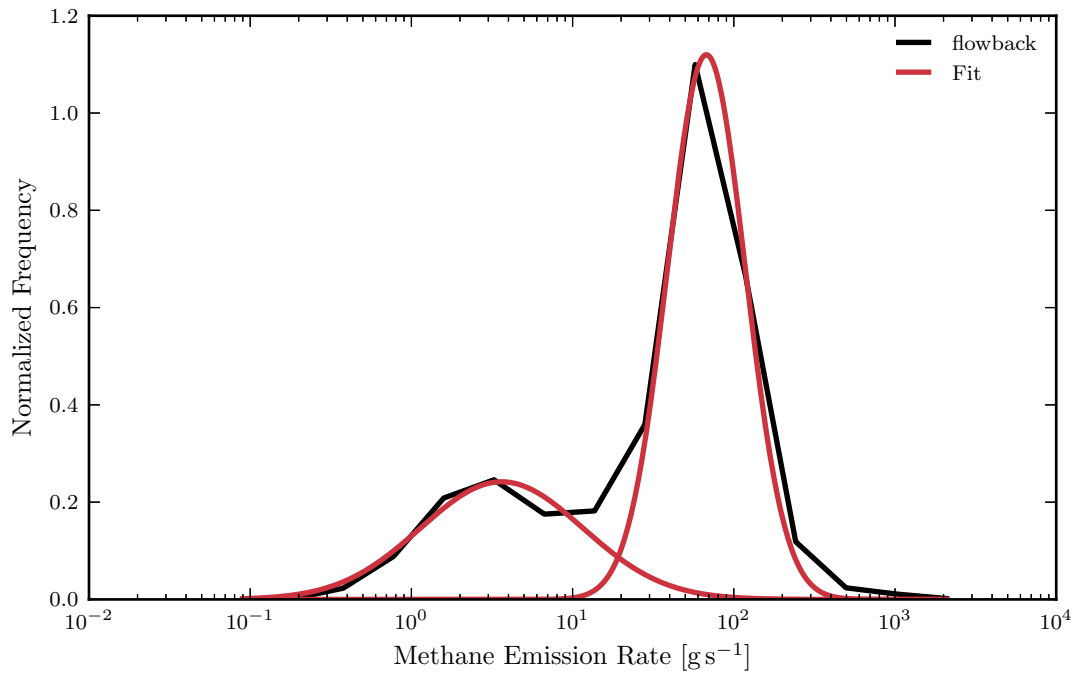


FIGURE H.1. Flowback emission rate distribution bimodal fit. The Gaussian curves are centered at 3.63 and 67.56 g s⁻¹.